`WALNUT CREEK WATERSHED

CITY OF CLIVE, IOWA

FLOOD MITIGATION ASSESSMENT – PHASE 2

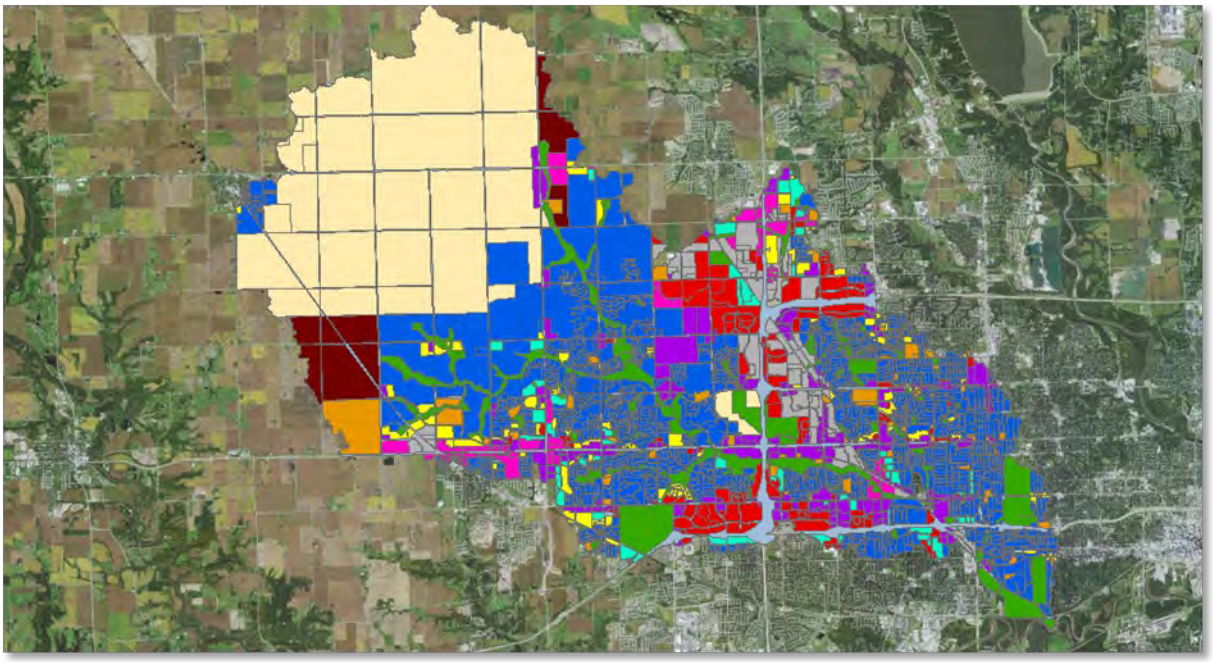

September 2022

US Army Corps of Engineers ®
Rock Island District

Table of Contents

Figures:

Tables:

1. Introduction

1.1 Study Background

The Walnut Creek watershed is a tributary of the Raccoon River, draining into the river in Des Moines, IA. The Walnut Creek watershed has a total drainage area of 82.8 square miles and is encompassed primarily by the cities of Dallas Center, Clive, Urbandale, Waukee, Grimes, Johnston, West Des Moines, and Windsor Heights, IA (Polk and Dallas counties). All eight of these local communities have experienced increased impacts from flash flooding; of these, the City of Clive has been the most impacted, as the water of the surrounding communities flows into Clive. With its history of flooding and the increasing threat, the City of Clive has an interest in looking at flood risk management.

In the last two decades, there has been a significant increase in flash flooding and smaller events such as the 10% (10-year) and 4% (25-year) annual chance exceedance events occur more throughout the year. The eastern part of Clive is comprised of Pre-FIRM and Post-FIRM sections. The Pre-FIRM section includes home that were built prior to the development of Flood Insurance Rate Maps (FIRM). Homes in the Pre-FIRM areas can be insured with “subsidized” rates. Some properties in the Post-FIRM areas that have not experienced impacts due to flooding were able to submit a Letter of Map Amendments (LOMAs) to be removed from the floodplain. A contactor created flood inundation maps to be used to create Preliminary FIRMS that will replace many of the LOMAs. Once these preliminary maps become effective, the flood insurance rates may double for some of the property owners.

There are concerns that impacts from surrounding communities could affect the flooding of Walnut Creek in Clive since the water from these communities flows into Clive. A major area of concern that experiences flooding is located on the most eastern side of Clive near University Boulevard. This is a Pre-FIRM area near the confluence of Walnut Creek and North Walnut Creek. There are different flood control measures that can be implemented in this area such as HESCO barriers or a water bladder. High water events in 2010, 2015 and 2018 have flooded the University Boulevard area.

The two main areas of focus in Clive were near University Blvd. (Pre-FIRM) (Figure 1-1, yellow star) and the Indian Hills neighborhood (Post-FIRM) (Figure 1-1, orange star). The City Manager and Community Development Department would like to generate different flood mitigation options, including elevating structures, acquisition, and basement infill.

During Phase 1 of this Silver Jackets project, USACE, FEMA, STARR and the City of Clive utilized already created hydrologic and hydraulic models to generate inundation maps. FEMA and STARR were tasked with creating inundation maps based on the Preliminary FIS discharges, and USACE was tasked with using future land use maps to calculate a future

conditions inundation map. Even though the focus was on the City of Clive, the entire Walnut Creek watershed was modeled. FEMA and STARR then used the Mitigation Benefits Estimator to determine which structures would be good candidates for mitigation options.

Phase 2 of this effort focused more on modeling the climate change impacts on the Walnut Creek watershed using data from available climate models. A new hydrologic model was developed to accomplish this using updated methods and software. Section 3 of this report outlines the development process for this model.

Along with climate change impacts, there was also interest in understanding the how streamflow would change with a fully developed watershed. This is updated from Phase 1 which only examined a partially developed watershed. The future land use maps were developed and provided by the city of Clive.

Based on impacts to streamflow due to the combined effects of climate change and land use change, these results were then used to create inundation maps of the potential changes in streamflow. Iowa Homeland Security and Emergency Management will then use the Mitigation Benefits Estimator to determine which structures would be good candidates for mitigation options.

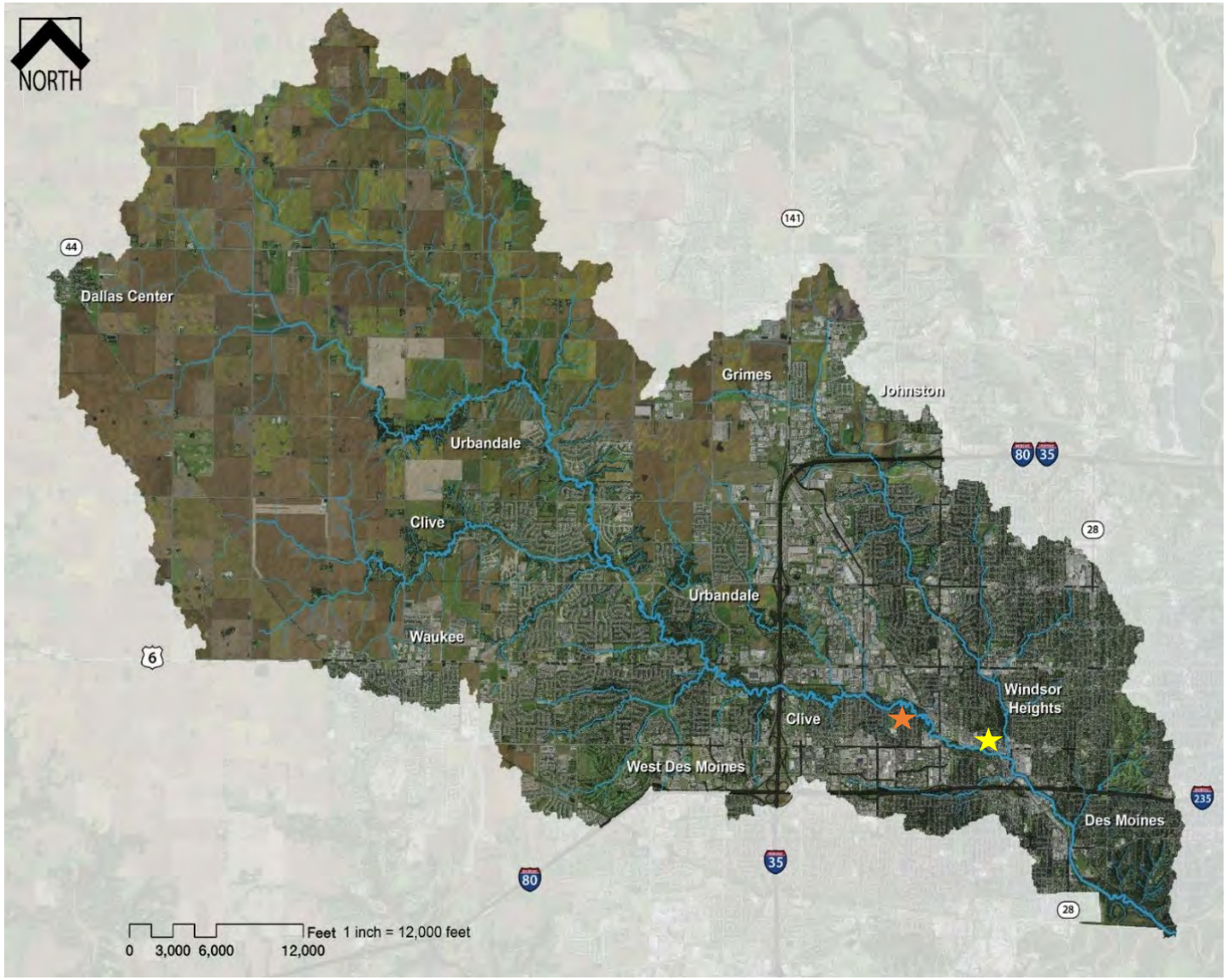

Figure 1-1: Walnut Creek Watershed (RDG, 2016)

1.2 Basin Description

The Walnut Creek Watershed is located in Dallas and Polk Counties Iowa and has a drainage area of 82.8 square miles (about 53,000 acres). This watershed drains parts of the cities of Dallas Center, Grimes, Waukee, Johnston, West Des Moines, Windsor Heights, and Des Moines, as well as the entire cities of Clive and Urbandale. The Walnut Creek Watershed consists of multiple tributaries, including three major tributary creeks and several smaller streams. North Walnut Creek (one of the three major tributaries) runs from north to south, with its sub-basin encompassing portions of Grimes, Johnston, Urbandale, Clive, Windsor Heights, and Des Moines. South Walnut Creek passes through Country Club Lake, running from southwest to northeast and crossing parts of West Des Moines, Waukee, and Clive. Little Walnut Creek flows from west to east, starting in rural land use and draining parts of Clive, Waukee, and Urbandale. For this analysis, the three major tributaries and Rocklyn Creek (which flows into North Walnut Creek), as well as the numbered streams shown in Figure 1-2 below were included in the hydrologic and hydraulic models. This was in an effort to first match and then update the preliminary FEMA study and other studies conducted in the past.

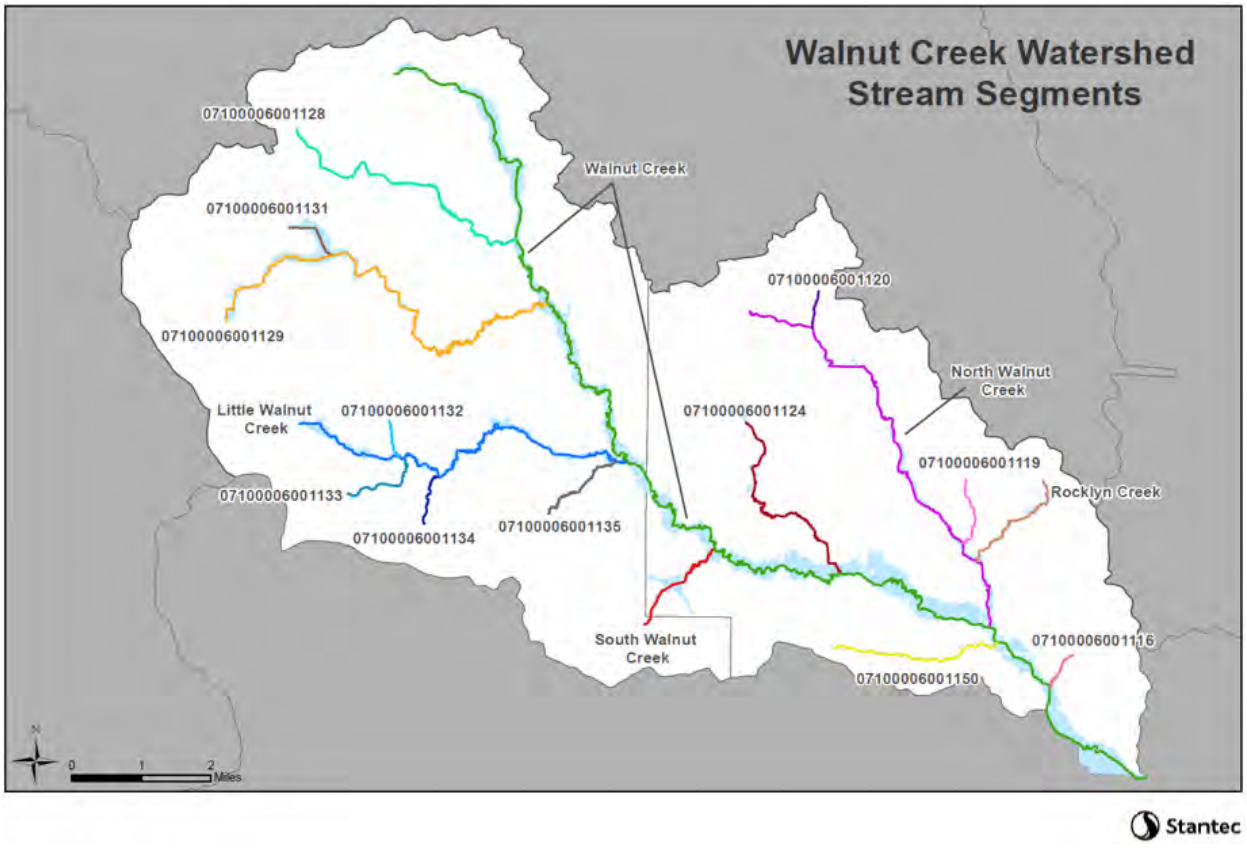

Figure 1-2: Walnut Creek Stream Segments (Stantec, 2018)

The topography of the watershed can be divided into two main regions. The upper portion of the watershed consists of typically flat land, which holds low spots and meandering streams, remnants of the prairie pothole wetlands. The lower portion of the watershed consists of steeper topography: hills and valleys with surface slopes typically between 5% and 9%. Likewise, land use of the watershed can be divided into two main regions. The upper, northwest half of the watershed is primarily rural land area, being used for agriculture or pasture with some grassland and timberland observed. The lower, southeast half of the watershed is primarily used for urban and residential use. However, rapid urban development is expected within the next ten years.

1.3 Historical Events

Below is a table of the largest events on Walnut Creek based on the gage at 63rd Street which has been in service since 1972. Major flood stage is at 17 feet and there have been nine events that have exceeded that threshold. The peak discharge for the 2018 event that place during the course of this study was 10,600 cfs which corresponds to about the 4% (25-year) annual chance exceedance event.

Table 1-1: Historical Event Peak Stage from 63RD Street Gage

Date	Stage (ft)	Discharge (cfs)
6/30/2018	19.08	10,600
6/25/2015	18.69	9,720
8/09/2010	18.59	11,700
5/10/1986	18.32	12,500
6/16/1990	18.00	7,780
7/01/1973	17.72	9,000
8/29/1993	17.56	6,460
6/09/1974	17.44	8,160
8/27/1975	17.00	5,800

1.4 Climate Change Analysis Process

Recent scientific evidence shows that in some places and for some impacts relevant to U.S. Army Corps of Engineers (Corps) operations, climate change is shifting the climatological baseline about which natural climate variability occurs and may be changing the range of variability as well. This is relevant to the Corps because the assumptions of stationary climatic baselines and fixed range of natural variability, as captured in the historic hydrologic record may no longer be appropriate for long-term projections of flood risk, drought and environmental flows. An assessment of climate change impacts, described herein, is needed to support efforts at Walnut Creek in Central Iowa.

Climate Change impacts on the hydrology of the Upper Mississippi River Basin were evaluated in accordance with the Corps' Engineering and Construction Bulletin (ECB) 2018-14, *Guidance for Incorporating Climate Change Impacts to Inland Hydrology in Civil Works Studies, Designs and Projects,* and Engineering Technical Letter (ETL) 1100-2-3 *Guidance for Detection of Nonstationarities in Annual Maximum Discharges.* In addition to the ECB and ETL protocol, quantitative measures for climate change will also be performed with HEC-HMS and HEC-RAS modeling.

The USACE's current policy is to interpret and use climate change information for hydrologic analysis through a qualitative assessment of potential climate change threats and impacts potentially relevant to the USACE project for which the hydrologic analysis is being performed. As indicated in Figure 1-3, qualitative analysis required includes consideration of both past (observed) changes as well as potential future (projected) changes to relevant hydrologic inputs.

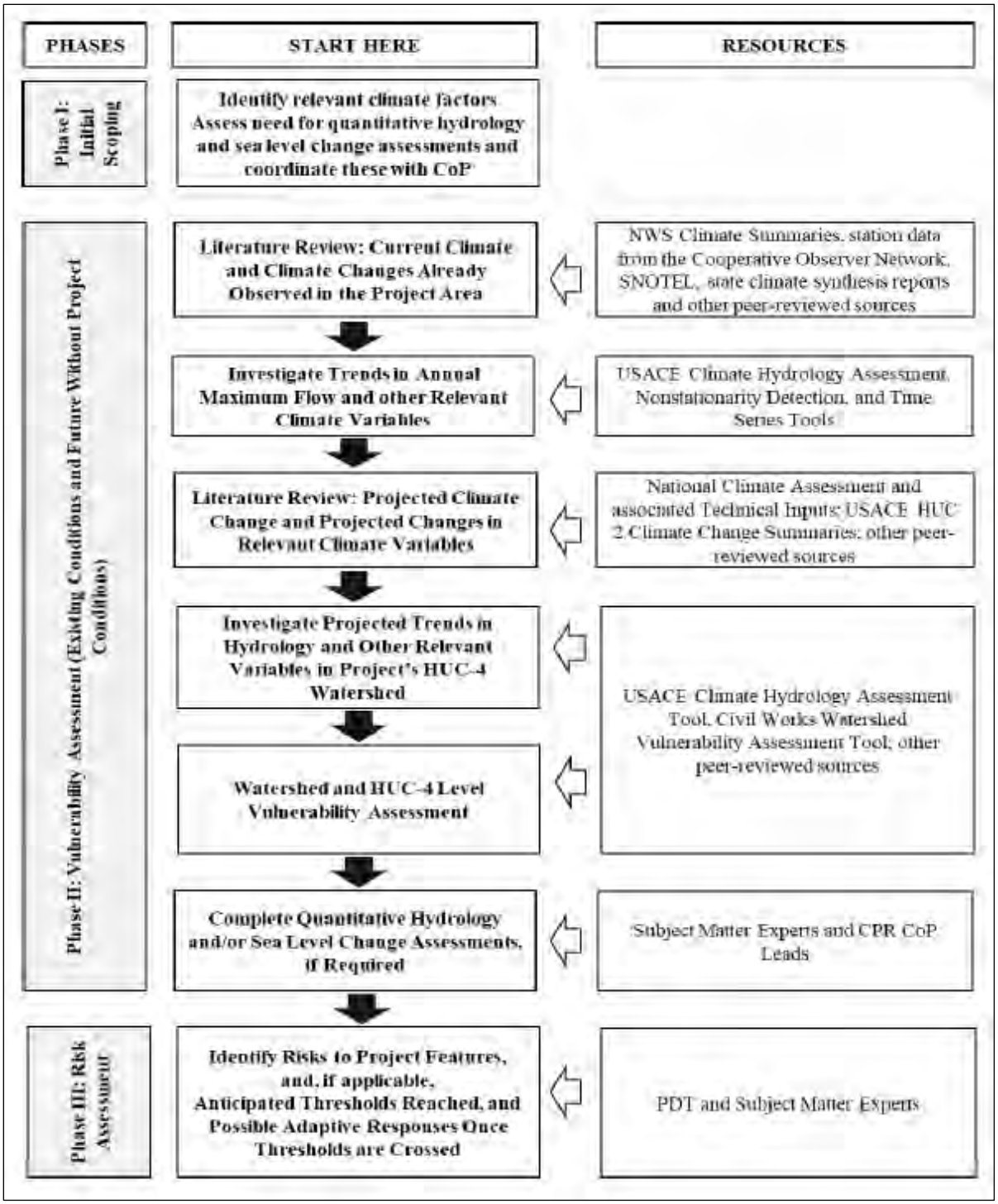

Figure 1-3: Flowchart for Conduction a Qualitative Assessment of Climate Change Impacts in Inland Hydrologic Analyses (USACE, 2018)

2. Qualitative Climate Change Analysis

The following qualitative analysis was completed using the process described in Section 1.4. It's important to note that since completion of this analysis, a few of the tools used have been updated. Therefore, some results shown in this report might have changed slightly due to these tool updates.

2.1 Regional Climate Change Trends

Observed and projected hydrometeorological data were evaluated to assess potential changes to climate over the next 50 years. Hydrometeorological variables with the potential to impact the performance of the Project were examined; including temperature, precipitation, and streamflow.

Regional summary reports prepared by the Corps in 2015 summarize observed and projected trends reported in the literature. Findings for Water Resources Region 07, the Upper Mississippi Region (UMR), which includes the Project area, include statistically significant increases in mean air temperature during winter, spring, and summer; however, a slight decreasing trend was observed for fall mean air temperatures (Wang et al., 2009). Westby et al. (2013) found during the period of 1949 to 2011, statistically significant warming occurred in the northern UMR.

In the UMR, spring onset is occurring at least a few days earlier for the current period (2001 to 2010), as compared to an earlier baseline reference decade (1951 to 1960). This denotes an apparent small shift in seasons, with spring warming occurring earlier than in the past (Schwartz et al., 2013). Increases in air and water temperature across the UMR over the past few decades have led to earlier ice-out dates and later ice-in dates for lakes and earlier spring runoff (Johnson and Stefan, 2006).

Regional results from the U.S. Global Research Program's *Third National Climate Assessment for the Upper Midwest* (NCA3) suggest the rate of warming in the Midwest has markedly accelerated over the past few decades. Between 1900 and 2010, the average Midwest air temperature increased by more than 1.5°F (Figure 2-1). However, between 1950 and 2010, the average temperature increased twice as quickly, and between 1980 and 2010, it increased three times as quickly as it did from 1900 to 2010. Warming has been more rapid at night and during winter. The literature shows consensus among authors indicating increasing trends in observed air temperatures for the Midwest and UMR.

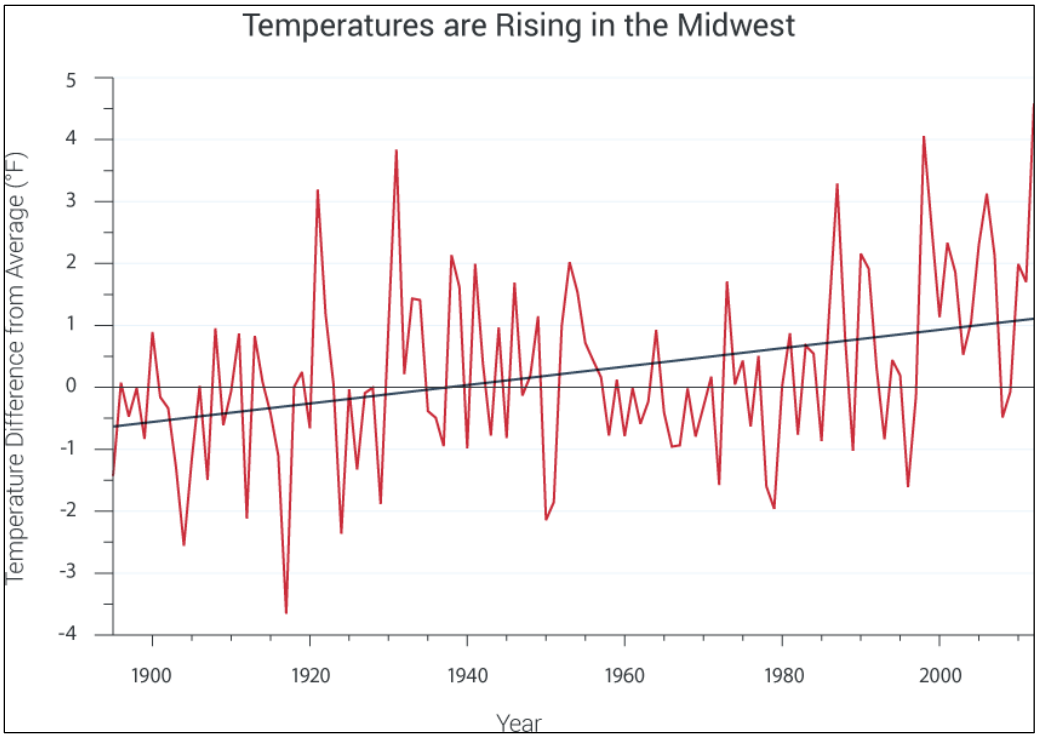

Figure 2-1: Increasing Annual Average Temperatures in Midwest (NCA3)

There is a high level of consensus across multiple Global Circulation Models (GCMs) and emissions scenarios projecting a significant warming trend across the entire UMR. Compared to the baseline time frame of 1971 to 2000, a study by Liu et al. (2013) using a single GCM and assuming an A2 greenhouse gas emissions scenario (worst case) projected an increase in maximum air temperature of 1.5 to 4.5 ºC (2.7 to 8.1 ºF) for a 2055 planning horizon in the UMR. Additionally, the study predicted an increase in the Keetch Byrum Drought Index, which is a measure of soil moisture index.

In 2014, Scherer and Diffenbaugh published a study in which they projected a steady increase in both summer and winter air temperatures throughout the whole 21st century for the UMR, using a multimember GCM and assuming an A1B emissions scenario (middle of the road). Compared to a baseline timeframe of 1980 to 2009, the study projected that by the year 2090, the air temperature would increase by 5.7°C (10.3°F) in the summer and 3.6°C (6.5°F) during the winter. Cai et al. (2009) and Wilson and Weng (2011) both produced similar results when evaluating central Illinois using GCMs and shorter planning horizons.

Using two different GCMs and assuming high greenhouse gas emissions (A2 and A1f), Kunkel et al. (2010) projected a 4.0 to 6.5 ºC (7.2 to 11.7 ºF) increase in three-day heat wave temperatures and a 15 to 50 day increase in the annual number of heat wave days for a 2090 planning horizon compared to a recent historical baseline for the UMR.

Projections of future extreme climate events were summarized in the report. Gao et al. (2012) used a planning horizon of 2058 and a single GCM with a high greenhouse gas emission assumption to project increases in heat wave intensity, duration, and frequency. Results show an increase of up to 4.0 ºC (7.2 ºF) in extreme heat wave temperatures in the UMR and the duration of heat waves is projected to increase by 2 to 4 days per event, compared to the baseline period of 2001 to 2004. The overall frequency of heat waves is projected to increase by 1 to 4 events per year. Pryor et al. (2014) used GCMs to project statistically significant increases in both annual average temperature and the number of extreme heat days over the next century for the Midwest (Figure 2-2). Additionally, projections are presented showing an increase in the frost-free season and an increase in the number of "cooling degree days," defined as the number of degrees that a day's average temperature is above 65 °F (18.3 °C).

According to the NCA3, the amount of future warming will depend on changes in the atmospheric concentration of heat-trapping gases. Projections for regionally averaged temperature increases by the middle of the century (2046-2065) relative to 1979-2000 are approximately 3.8°F for a scenario with substantial emissions reductions and 4.9°F with continued growth in global emissions. The projections for the end of the century (2081-2100) are approximately 5.6°F for the lower emissions scenario and 8.5°F for the higher emissions scenario. Statistically significant increasing trends in total annual precipitation have been reported in several studies. An increasing trend in winter storm precipitation total (1972-2002) was observed by Palecki et al. (2005), while Grundstein (2009) identified positive linear trends in both total annual precipitation and soil moisture index during the 1895-2006 period. During the 1950 to 2000 period, a significant increasing trend in precipitation, particularly in the summer and fall, was observed for the UMR (Wang et al., 2009). During the winter and spring, a mild decreasing trend was identified for the northern half of the UMR. McRoberts and Nielsen-Gammon (2011) quantified an increasing trend in annual precipitation (1895-2009) for the UMR as between 5% to 10% per century.

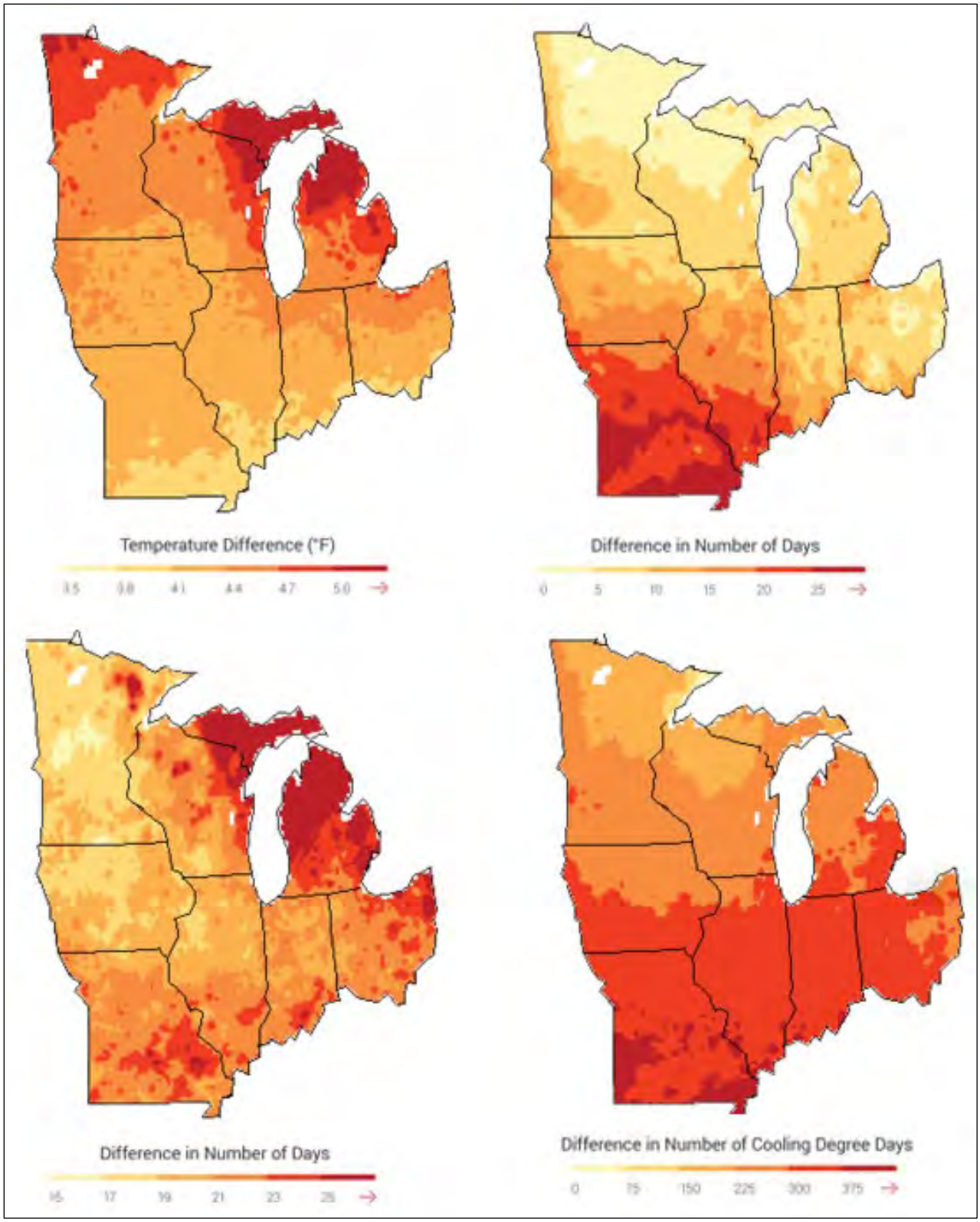

Figure 2-2: GCM Projections Showing Increasing Annual Average Temperatures, Number of Hottest Days, Length of Frost-Free Season and Cooling Degree Days (Pryor et al., 2014)

Moderate increases (33%) in the frequency of 20-year storm events in the UMR where observed by Wang and Zhang (2008) when comparing the period 1949 to 1976, to the period 1977 to 1999. Within the UMR, statistical analysis of 20th century rainfall data showed generally increasing and statistically significant trends in total annual precipitation and the number of precipitation days per year (Pryor et al., 2009). For multiple climate stations in the UMR with at least 50 years of historical record, statistically significant increasing trends in the frequency of occurrence of heavy rainfall were identified by Villarini et al. (2013).

The NCA3 report concluded that annual precipitation increased during the past century (by up to 20% in some locations), with much of the increase driven by intensification of the heaviest rainfalls. Multiple authors have identified a mild upward trend in observed precipitation for the Midwest and UMR.

Projections of future changes in precipitation in the UMR generally concur that both annual precipitation and extreme precipitation totals are going to increase. Using a planning horizon of 2055, Liu et al. (2013) projects an increase in spring, summer, and winter precipitation. Despite the projected increase in precipitation, the study also projects an increase in the severity of future droughts.

Applying a planning horizon of 2058 to a GCM, Gao et al. (2012) generally projects increases in the magnitude of annual and daily extreme (defined as 95th percentile) storm events, and in the frequency of precipitation events.

A study of the Illinois watershed by Wilson and Weng (2011) used A1B and B1 emission scenarios and a 2020 planning horizon to project changes in monthly precipitation. Results indicate a general agreement of drier summer months and wetter winter months.

Multiple studies present future projections of extreme events, which include storm events and droughts. Tebaldi (2006), Wang and Zhang (2008), Wang et al. (2011), Schuster et al. (2012), and Joetzjer et al. (2013) all generally predict increases in the number of high (>10 mm) precipitation days for the region, the number of storm events greater than the 95th percentile of the historical record, and the daily precipitation intensity index (annual total precipitation divided by number of wet days). In other words, the projections forecast small increases in the occurrence and intensity of storm events by the end of the 21st century for the general study region. Wang and Zhang (2008) used downscaled GCMs and a high emissions scenario (A2) to quantify a significant increase (50 to 100%) in the recurrence of the current 20 year 24-hour storm event for the planning horizon of 2075. In 2011, Wang et al. used multiple Regional Climate Models (RCMs) and two emissions scenarios to characterize the intensity and frequency of projected droughts in Illinois for the end of the 21st century using the Standardized Precipitation Index (SPI). Results show significant increases in the frequency and intensity of short duration (1 to 4 weeks) droughts due primarily to increased air temperatures. Joetzjeret al. (2013) did a similar study, but focused on the whole UMR, with results concurring with Wang et al.'s earlier study. These results reflect the impacts of projected temperature and

evapotranspiration increases in the basin, which appear to exceed the projected impacts of increased precipitation.

Pryor et al. (2014) studied the Midwest. Results generally support all the other studies' findings. Climate model projections presented in this study indicate a statistically significant increase in annual average precipitation (2.4 to 4.0 inches), wettest 5-day total (0.4 to 1.0 inches), and the number of heavy precipitation days by the middle of this century. Additionally, the duration of consecutive dry days is expected to increase by up to 3 days.

According to the NCA3 assessment, projections indicate increased spring precipitation (9% in 2041-2062 relative to 1979-2000) and decreased summer precipitation (by an average of about 8% in 2041-2062 relative to 1979-2000), particularly in the southern portions of the Midwest. Increases in the frequency and intensity of extreme precipitation are projected across the entire region, and these increases are generally larger than the projected changes in average precipitation. Although the total amount of water from rainfall and snowfall is projected to increase across the entire Midwest, models also indicate an increase in consecutive dry days and chances of drought.

From 1939 to 1998, the Mississippi River watershed saw an increase in river flow (Mauget, 2004). An increase in surplus flow days increased and the number of drought incidence decreased for the UMR during the same study period, with the greatest change occurring during the latter part of the century. A majority of the 42 gage stations in the UMR showed statistically positive trends in both annual streamflow and baseflow (Duan et al., 2006). Mean flow and peak flows showed the same positive trend during the period 1913 to 2002.

Statistically significant increasing trends in both annual 7-day low flow and annual mean flow were detected for multiple sites. These were based on analysis of USGS stream gage data, part of the Hydroclimatologic Data Network. Studies of surface water trends, including runoff, for the Mississippi River Region, which includes the UMR, quantified statistically increasing trends in runoff in the region for the period 1948 to 2004 (Qian et al., 2007).

The NCA3 assessment looked at climate change impacts on the water cycle. It found river flows have increased across the Midwest, however, the length of dry spells and the number of short-term droughts have also increased. The timing of peak river levels has changed in response to warming trends. Snowpack and snowmelt-fed rivers in much of the western U.S. have earlier peak flow trends since the middle of the last century, including the past decade. The change in total annual precipitation and heavy precipitation is projected to lead to an increase in the magnitude and frequency of flooding, especially flash floods.

In order to project future climate trends in hydrology, many studies of the UMR have relied upon the use of GCMs and macro-scale hydrologic models. There is no clear consensus in the literature, with some studies projecting an increase in future streamflow as a result of increased precipitation in the UMR, while others project a decrease in flows as a result of increased evapotranspiration. Seasonally, multiple studies suggest increased flows in the winter

and spring and decreased flows in the summer. An example of contradictory projections can be found in the study performed by Thomson in 2005, where two GCMs with one set of input assumptions, yielded different results. One model predicts significant decreases in water yield, the other projects significant increases in water yield. Studies by Hagemann et al. (2013) and Döll and Zhang (2010) illustrate how climate change is expected to have as much, or more, of an impact to ecologically relevant flow characteristics as dams and withdrawals over the next century. For the UMR, projections show mild (relative to global results) impacts to low and average annual flows. Results of other studies such as Jha (2006) and Wu et al. (2012) highlight the significant uncertainty associated with future hydrologic projections. However, these studies can be used to show the potential for large-scale changes in either direction.

Projected changes to streamflow are not covered in great detail for the Project area within the NCA3 report; however, the report does highlight projected changes in spring peak river flows as a result of shifts of the amount and timing of snowpack and snow melt in much of the U.S. This shift is in response to warming trends. The NCA3 notes that projecting future flooding is difficult due to variables such as river level and soil moisture prior to a rain event, yet data suggests an increase in flooding frequency.

There is strong consensus that air temperatures will increase in the UMR, with studies generally agreeing on an increase in mean annual air temperature of approximately 2 to 6 ºC (3.6 to 10.8 ºF) by the latter half of the 21st century. A reasonable consensus is also seen on projected increases in extreme temperature events. This includes more frequent, longer, and more intense summer heat waves in the long-term future compared to the recent past.

A majority of the precipitation projections in the studies forecast an increase in both annual precipitation and in the frequency of large storm events. Seasonally, though, some studies indicate a potential for drier summers despite the overall increase in annual precipitation totals. As a result of increased air temperature and evapotranspiration rates, droughts are also projected to increase in the UMR.

Regarding streamflow and hydrology projections, there is no clear consensus in the literature. Projections generated by coupling GCMs with macro scale hydrologic models in some cases indicate a reduction in future streamflow, but in other cases indicate a potential increase in streamflow. Figure 2-3 summarizes the trends and literary consensus of observed and projected primary variables of temperature, temperature extremes, precipitation, precipitation extremes, and streamflow (hydrology).

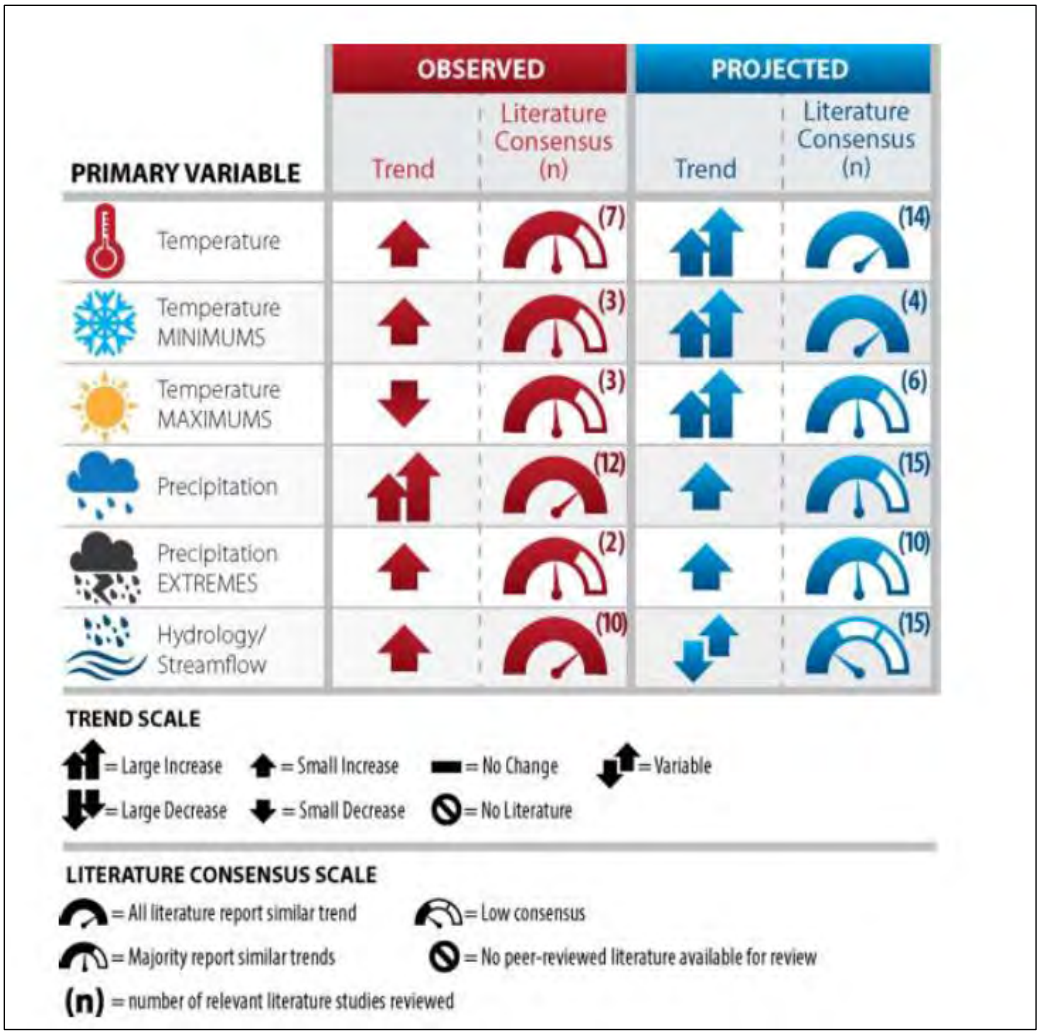

Figure 2-3: Summary and Literature Consensus of Observed and Projected Trends in Important Meteorologic Variables Potentially Impacted by Climate Change

The USGS conducted an assessment to determine if changes in flood magnitudes were consistent across certain geographic regions of the United States. The study concluded that there were changes in trends at specific locations for peak magnitude, frequency, duration and volume of frequent floods. However, the study indicated no evidence that these sites were related geographically.

The study analyzed regions of the United States based on grid cells and the stream gages located within each cell (Figure 2-4). Walnut Creek is in the green outlined cell in this analysis. This grid cell shows a statistically significant trend ($p<0.1$) for flood duration. The black outlined cells include the rest of the Upper Mississippi River Basin. For the entire basin, there is no consensus among the cells showing there is or is not statistically significant trends in flood frequency, peak magnitude, duration, or volume.

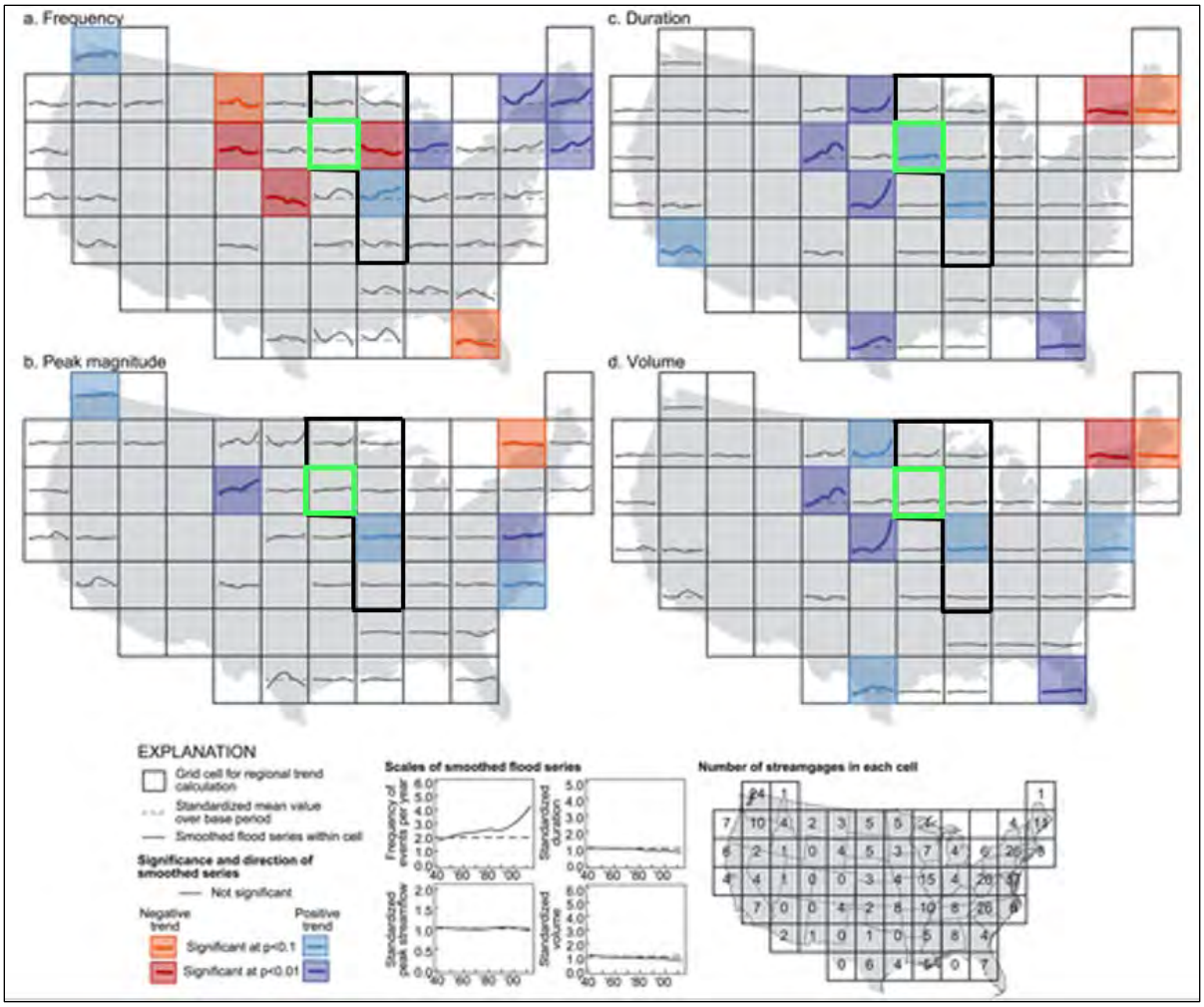

Figure 2-4: Regional Changes in Floods Across the United States (1940-1969 vs 1970-2013) (Adapted from Archfield, 2016)

2.3 Regional Scale Trends in Streamflow and Climate Change – Climate Hydrology Assessment Tool

In order to evaluate projected trends in hydrology for the Project area, the USACE Climate Hydrology Assessment Tool was used to analyze streamflow for the Des Moines watershed (HUC 0710). The Climate Hydrology Assessment Tool provides qualitative information at the HUC 4 watershed level about future climate conditions and allows the Corps to produce repeatable analytical results using consistent information.

Observed trends in annual peak instantaneous streamflow for Walnut Creek at Des Moines (USGS gage 05484800) evaluated using the USACE Climate Hydrology Assessment Tool do not indicate a statistically significant increasing trend for the period 1970-2016 (p-value =0.928064) (Figure 2-5).

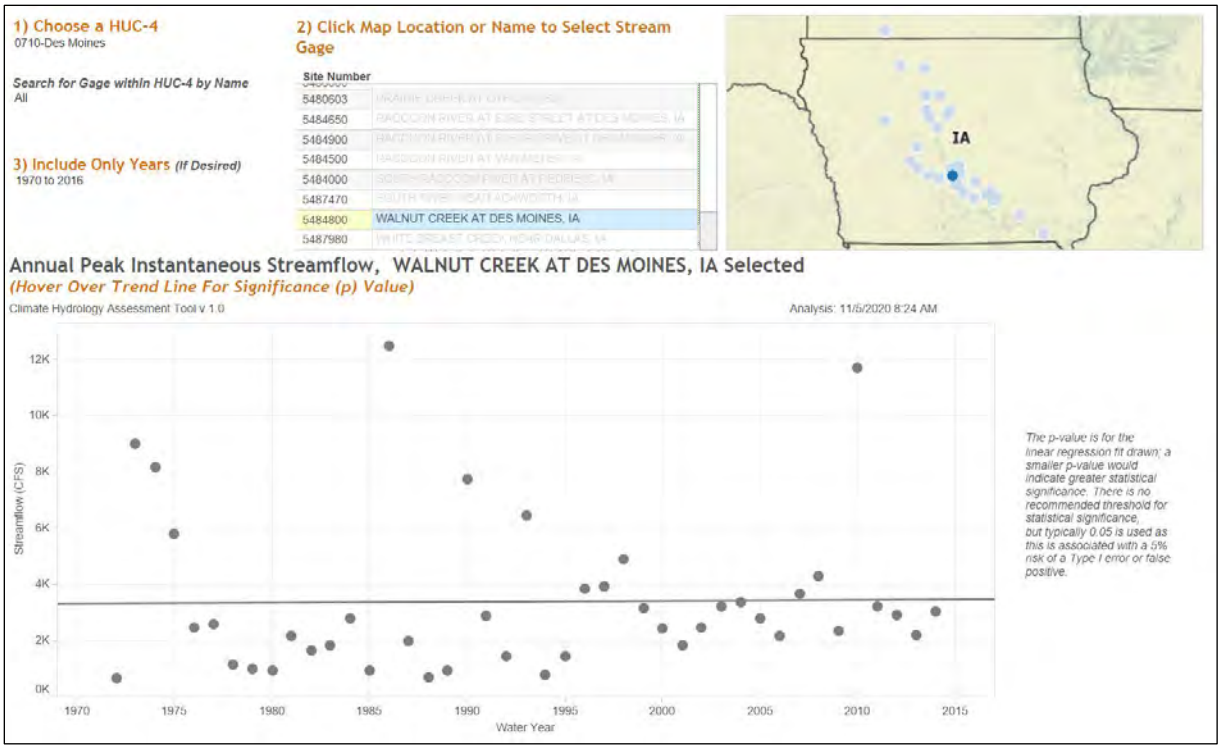

Figure 2-5: No Trend in Observed Annual Peak Instantaneous Streamflow for Walnut Creek at Des Moines, IA (p-value = 0.928064)

Projected hydrology under future climate conditions is generated using a hydrologic model with precipitation and temperature input parameters derived from GCM output. The range in projected annual maximum monthly streamflow is computed based on 93 different climate changed hydrologic model simulations for the 1950-2099 period. Results for the Des Moines watershed shown in Figure 2-6 indicate there is a lot of uncertainty in projected climate changed hydrology. Nevertheless, there is a statistically significant increasing trend in the mean projected annual maximum monthly streamflow (Figure 2-7). Based on the trendline, over a 50-year study period annual maximum monthly flows could increase by nearly 2,400 cfs (Figure 2-7). These results are qualitative only.

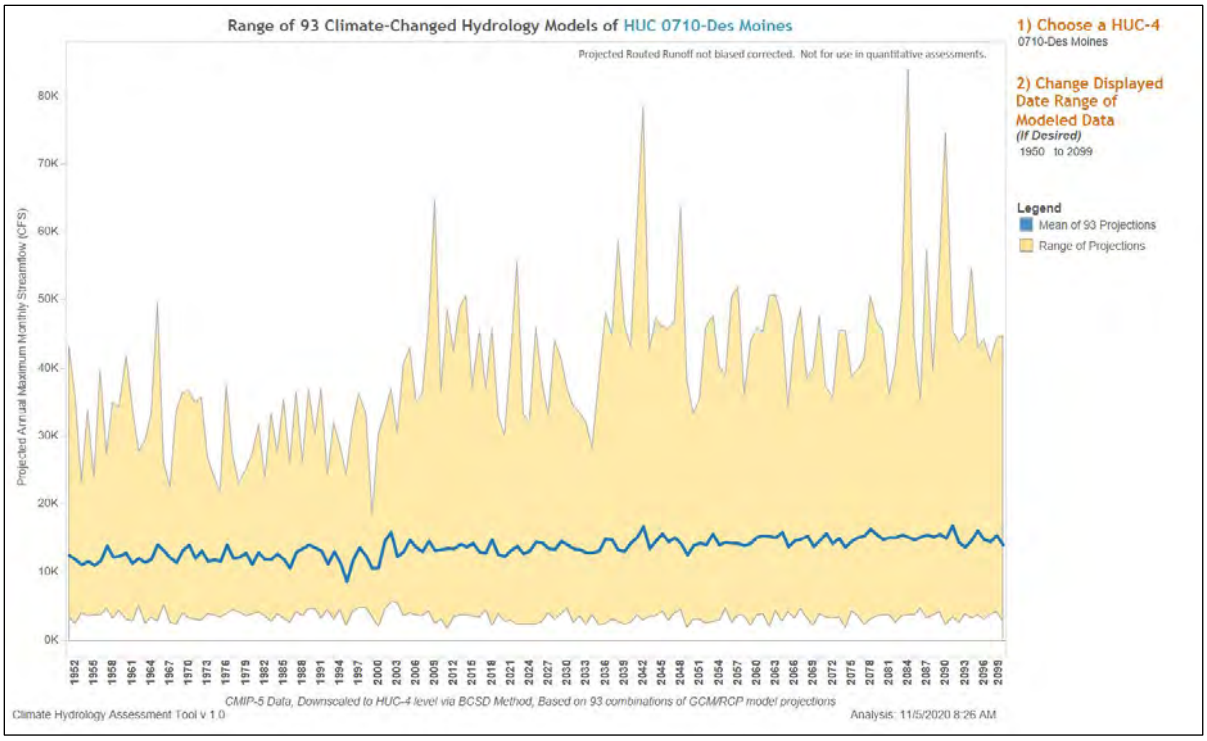

Figure 2-6: Range in Projected Annual Maximum Monthly Streamflow for the Des Moines Watershed (HUC 0710)

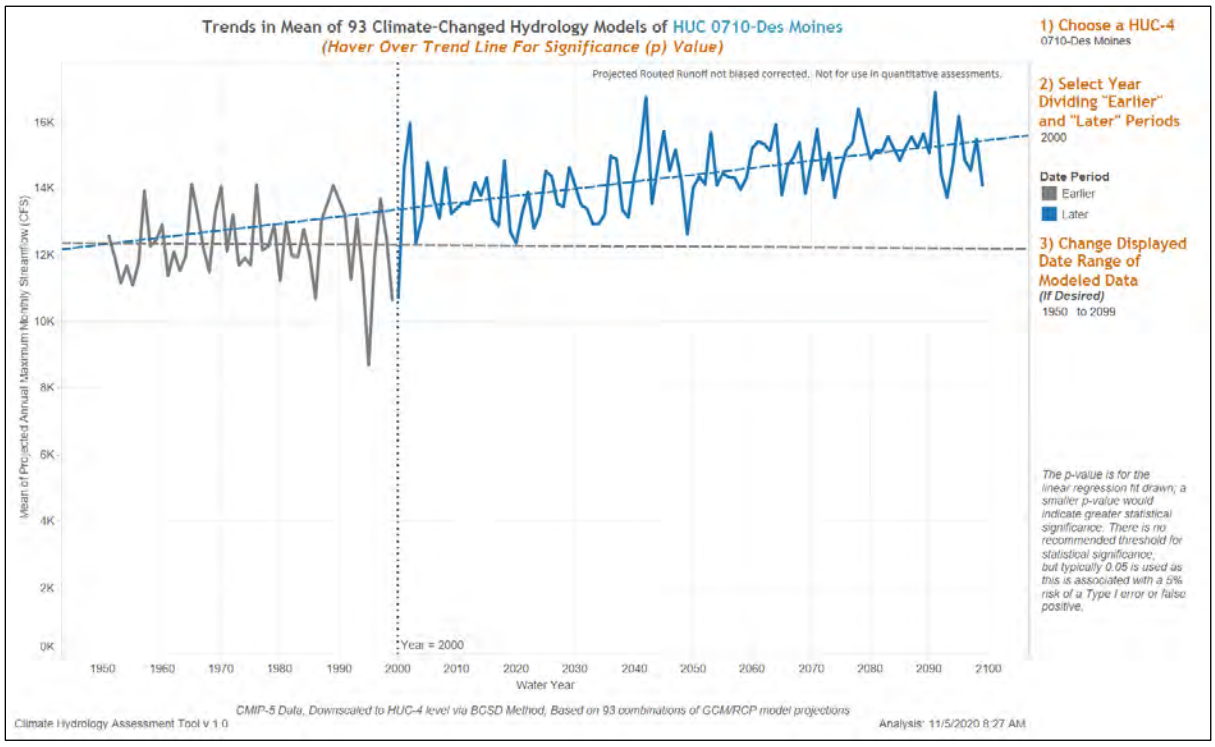

Figure 2-7: Mean Projected Annual Maximum Monthly Streamflow for the Des Moines Watershed (HUC) 0710). Trendline Equation: Q = 20.9341*[Water Year] - 28490.8, p < 0.0001

2.4 Vulnerability Assessment to Climate Change Impacts – Vulnerability Assessment Tool

The purpose of the USACE Watershed Climate Vulnerability Assessment Tool is to compare the relative vulnerability of the Project's HUC 04 watershed to climate change with that of the other 202 HUC 04 watersheds throughout the continental United States (CONUS). The tool provides a screening level comparative assessment of vulnerability to climate change according to business line. The tool is intended to identify climate threats and vulnerabilities for a specified region and business line using the Weighted Order Weighted Average (WOWA) method to calculate a composite index (Vulnerability Score).

Walnut Creek is located within HUC 0710, the Des Moines watershed and is part of the "Flood Risk Reduction" business line. Indicators including runoff elasticity (ratio of streamflow runoff to precipitation), annual variability in hydrology, two indicators of flood magnification (indicator of how much high flows are projected to change overtime), and the acres of urban area in the 500yr floodplain are used to calculate WOWA scores under Flood Risk Reduction. HUC-4 watersheds with the top 20% of WOWA scores are flagged as being vulnerable. The default National Standards setting was used when conducting this vulnerability assessment.

Results of the Vulnerability Assessment Tool suggest that Flood Risk Reduction efforts in HUC 0710, the Des Moines watershed, are relatively more vulnerable to climate change compared to the other 202 HUC 04 watersheds in the CONUS (Figure 2-8). Vulnerability scores for the two 30-year epochs indicate change between epochs and change between the wet and dry traces (Table 2-1). Contributions to the overall vulnerability score from each of the different indicators for the Flood Risk Reduction business line and the 2050 epoch are shown in Table 2-2. The dominant indicators contributing to the HUC 0710 vulnerability scores are Runoff Elasticity, and Cumulative Flood Magnification.

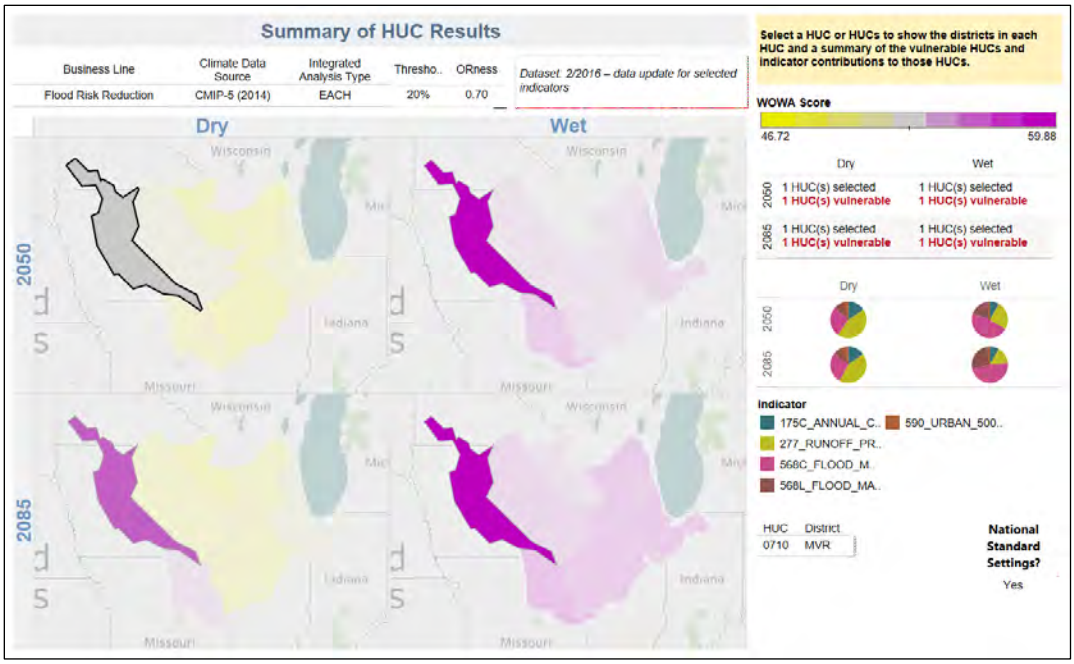

Figure 2-8: Projected Vulnerability for Flood Risk Reduction within the Des Moines Watershed (0710)

Table 2-1: Projected Ecosystem Resotration Vulnerability Scores

	Ecosystem Restoration Vulnerability Score			
HUC 04 Watershed	**2050 Dry**	**2050 Wet**	**2085 Dry**	**2085 Wet**
Des Moines River (0710)	53.804	59.878	55.654	58.884

Table 2-2: Individual Indicator Contributations Related to Flood Risk Reduction

2050 Epoch	**Mississippi River 0710**	
Indicator	**Dry**	**Wet**
	Contribution to WOWA Score	
Annual Covariance	8.329	4.961
Runoff Elasticity	23.81	15.10
Urban Area in 500yr Floodplain	2.41	2.21
Flood Magnification - Cumulative	14.499	28.311
Flood Magnification - Local	4.759	9.293

2.5 Site Specific Trend in Streamflow – Non-Stationarity Detection Tool

The Non-Stationarity Detection Tool was used to analyze the 1972-2014 period for discharge at the USGS Gage 05484800, Walnut Creek at Des Moines, Iowa using twelve different statistical tests to detect nonstationarity in the peak annual streamflow record.

The Lombard Wilcoxon Method detected a statistically significant nonstationarity in 1994 (Figure 2-9). However, a lack of consensus between the other statistical tests indicate no significant operational nonstationarities or change points in the flow record can be detected.

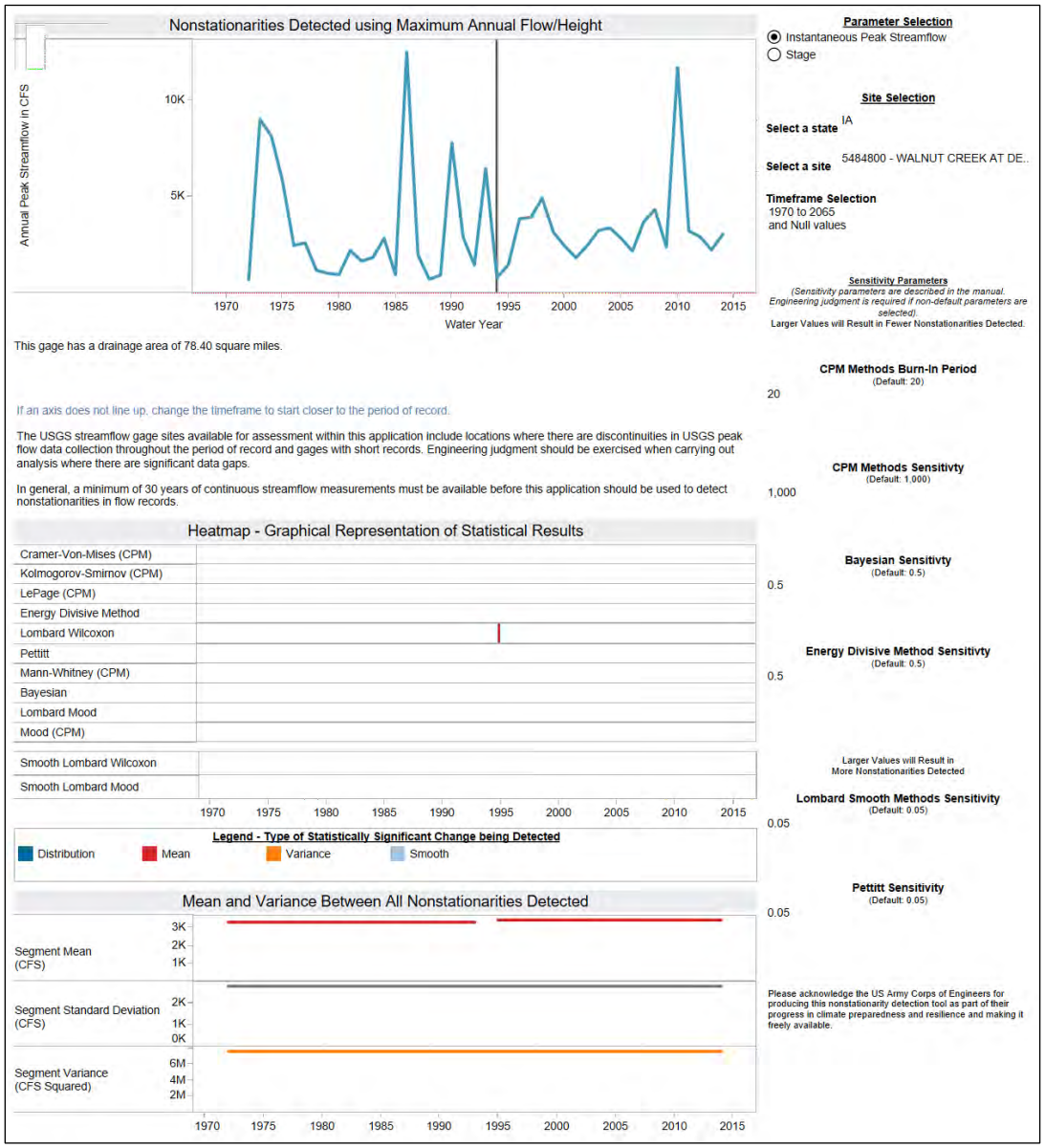

Figure 2-9: Nonstationary Analysis of Peak Annual Discharge for the Walnut Creek at Des Moines, Iowa (USGS 05484800) for 1972- 2014

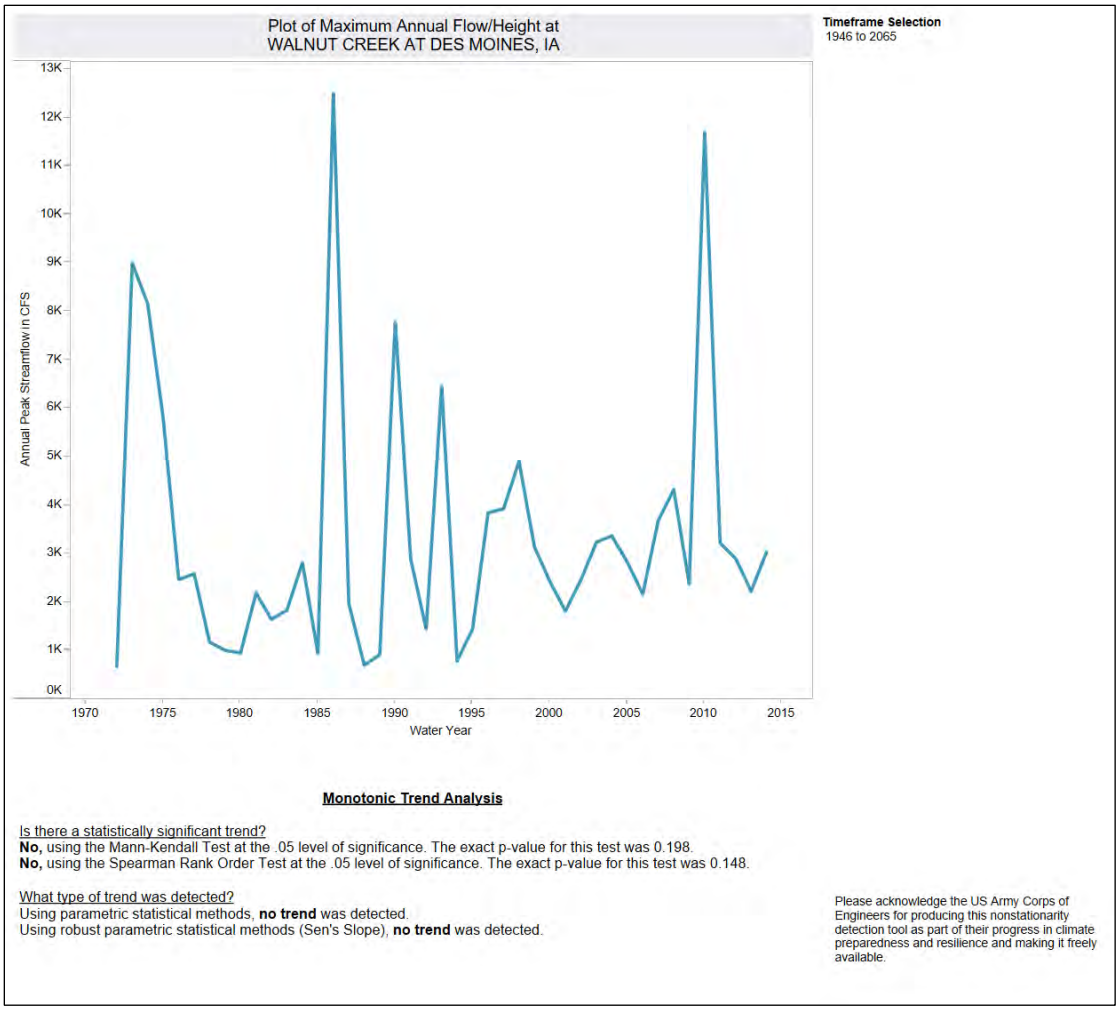

Figure 2-10: Monotonic Trend Analysis of Peak Annual Discharge for the Walnut Creek at Des Moines, Iowa (USGS Gage 05484800) for 1972-2014

Figure 2-10 shows the Monotonic Trend Analysis results which illustrate there is no statistically significant trend in peak annual discharge at the Walnut Creek gage. The Mann-Kendall and Spearman Rank Order Tests resulted in p-values of 0.198 and 0.148 respectively. The results from this analysis are qualitative.

2.6 Site Specific Trends in Streamflow – Time Series Toolbox

The Time Series Toolbox (TST) was used to evaluate mean annual flow trends on Walnut Creek for years 1990-2020. Upward trends for the time series were not significant at the α=0.05 level of significance for the simple linear regression, Mann-Kendall, and Spearman Rank-Order tests. Traditional and Sens slope fits may appear to be trending upwards but lack the evidence to definitively conclude an upward trend (Figure 2-11). Traditional and Sens slope tests also indicate that there is no trend.

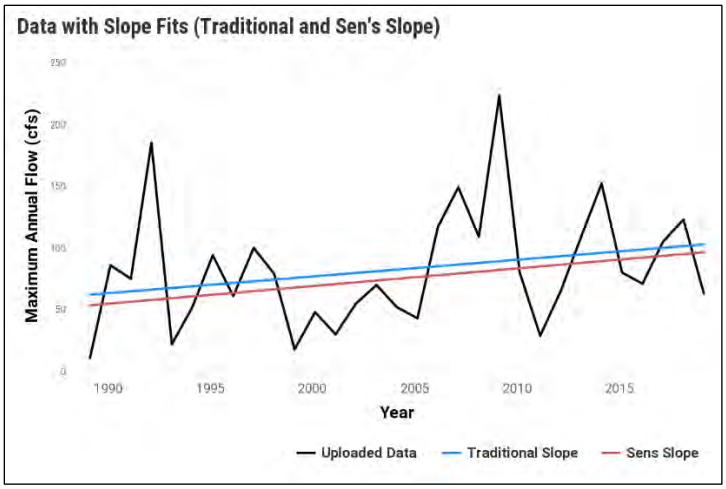

Figure 2-11: Mean Annual Flow Trends at Walnut Creek (1990-2020)

The TST also shows a single statistically significant nonstationarity (Figure 2-12). Changes in distribution took place in 2006 for the Energy Divisive method. Additionally, no breakpoints were found anywhere in the data set. With no consensus among the 12 nonstationarity tests as well as no breakpoints detected, there is no evidence to conclude any increasing or decreasing trends. The TST indicates that Walnut Creek during the study period is in fact stationary.

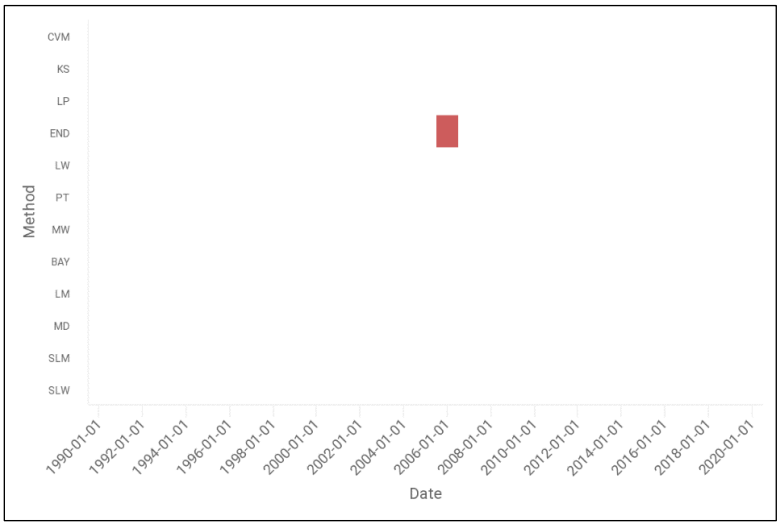

Type: Mean Distribution Variance Smooth

Abbreviation	Statistical Method	Abbreviation	Statistical Method
CVM	Cramer-von-Mises	**BAY**	Bayesian
KS	Kolmogorov-Smirnov	**LM**	Lombard Mood
LP	Lepage	**MD**	Mood
END	Energy Divisive	**SLM**	Smooth Lombard Mood
LW	Lombard Wilcoxon	**SLW**	Smooth Lombard Wilcoxon
PT	Pettitt	**MW**	Mann-Whitney

Figure 2-12: Failed Nonstationarity Tests:Mean Annual Flow at Walnut Creek (1990-2020)

2.7 Conclusions

Available literature suggests a wetter and warmer climate in the future for the Project area. Current USACE tools for the qualitative assessment of climate change indicate there have not been increases in peak streamflow in the historic record. However, peak streamflow is expected to increase in the future. The Time Series Toolbox indicated no major breakpoints or nonstationarities in annual peak flow for Walnut Creek. The Non-stationarity Detection Tool failed to identify a statistically significant trend in observed annual peak streamflow and the Climate Hydrology Assessment Tool failed to identify a statistically significant upward trend in observed annual peak instantaneous streamflow (p-value=0.928064). However, CHAT identified a significant upward trend for mean projected annual maximum monthly streamflow (p-value<0.0001).

While no significant trends in observed streamflow were detected in Walnut Creek, there are potential reasons for increasing trends in streamflow. Urbanization of the Des Moines River Basin can significantly contribute to increased streamflow. Walnut Creek lies within Polk and Dallas counties. Both of which had the largest population increases in the 2013-2017 time period (Chapman, 2018). Beyond these two counties, the Des Moines metro area is Iowa's fastest growing urban area (Norvell, 2016). Increased urbanization is indicative of expanding impervious landcover and higher runoff values which lead to larger and faster storm peak flows. Additionally, tiling also contributes to increased streamflow. A large majority of Iowa's 3,000 drainage districts lie within the Des Moines Lobe where Walnut Creek is located (Eller, 2015). In this region tiling area increased by 11% between 2012-2017 (Schmidt, 2020). Tiling contributes to increased streamflow by draining agricultural land more quickly than how it would have naturally drained. Increased urbanization and tiling in conjunction with a warmer and wetter climate are capable of causing increased streamflow in the future.

3. Hydrologic Engineering Center-Hydrologic Modeling System Model Development

3.1 Walnut Creek Model Status

During Phase 1 of this project a model for the Walnut Creek basin was created in the Hydrologic Engineering Center-Hydrologic Modeling System (HEC-HMS). However, it was determined there were limitations with the Phase 1 model that made it insufficient to meet the goals for the project in Phase 2. These limitations largely were related to climate change analysis and the need to develop a continuous simulation hydrologic model, which needed different loss, transform, and baseflow methods, as well as the addition of a canopy and surface method. Figure 3-1 shows the sub-basin boundaries used in the Phase 1 modeling.

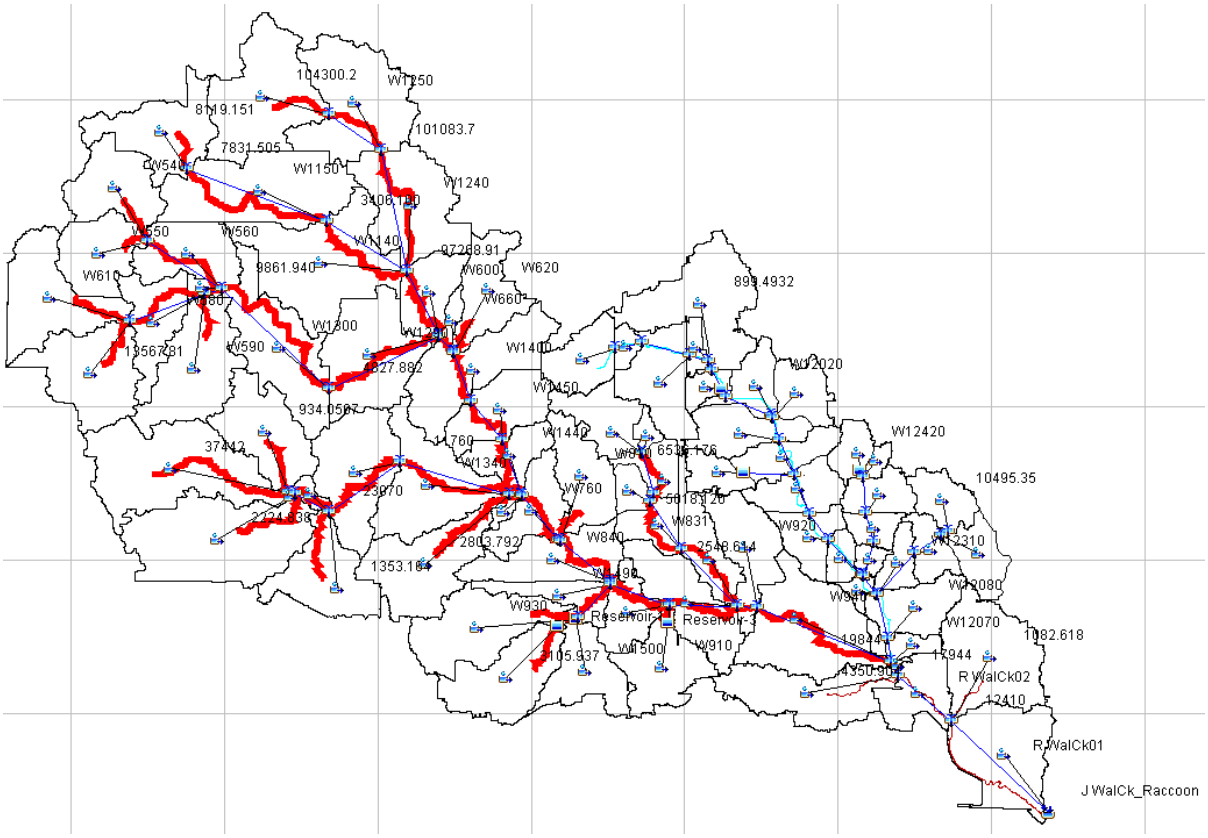

Figure 3-1: HEC-HMS Phase 1 Walnut Creek Sub-Basins

3.1.1 Modelling Concerns

The goal of this modeling effort is to look at how changes in precipitation due to climate change overtime will affect future streamflow in the Walnut Creek watershed. Future precipitation data was obtained from the Global Circulation Models (GCMs) from the fifth phase of the Coupled Model Intercomparison Project (CMIP5). The model output was downscaled using the Localized Constructed Analogs (LOCA) method which results in a resolution of 1/16. The CMIP5-LOCA daily precipitation data can be requested and then downloaded online (https://gdo-dcp.ucllnl.org/downscaled_cmip_projections/dcpInterface.html).

One of the largest limitations is due to the spatial scale of the Walnut Creek basin in comparison to the resolution of the downscaled climate data. The Walnut Creek basin only has an area of about 82 square miles and the resolution of the GCM data using the LOCA downscaling method creates pixels that are 3.7 x 3.7 miles (6 x 6 kilometers) or about 14 square miles. This makes breaking the Walnut Creek basin into smaller sub-basins difficult to do while still maintaining high accuracy.

The temporal scale is also a large limitation with this project. Due to the size of the basin, streamflow can rise and fall very quickly. However, CMIP5-LOCA data is only available at the daily scale. It's possible that small creeks within the basin can rise and fall within that timeframe resulting in lower accuracy overall.

To improve model accuracy considering both the spatial and temporal limitations, it was determined it would be necessary to use one subbasin for the modeling effort rather than splitting the Walnut Creek basin into smaller subbasins.

For Phase 2 modeling efforts, a continuous model was created which uses different methods and utilizers some other newer features in HEC-HMS. This is different from the Soil Conservation Service (SCS) Unit Hydrograph method that was used in Phase 1. The change was made because a continuous model gives a better representation of long-term climate changes. The new features used will be explained further in later sections.

3.1.2 Data Limitations

Through this work, some limitations were discovered with the CMIP5-LOCA data resulting from how the data is archived and downloaded. The CMIP5-LOCA data is downloaded as a single Network Common Data Form (NetCDF) file. Which means, when downloading output from multiple models or from multiple Representative Concentration Pathway (RCP) scenarios, it becomes necessary to break up the single file into multiple NetCDF files to be in a format that works with HEC-HMS.

During the process of preparing the gridded climate data for HMS, an unknown error was discovered resulting from how the data was formatted. After consulting with an HEC-HMS developer, no solution could be found. To accommodate with this issue, it was decided to convert the gridded data to a point dataset to represent the entire basin. This was done using the grid-to-point-convertor tool, which is available within HEC's Vortex API and converts

gridded data in an NetCDF file to a single point dataset in an HEC-Data Storage System (DSS) file (https://github.com/HydrologicEngineeringCenter/Vortex).

3.2 Watershed Delineation

The final basin boundaries and names are illustrated in Figure 3-2. The basin was developed using 3 m. LiDAR data for Polk and Dallas Counties. As discussed in section 3.1.1, only a single basin model was created to accommodate limitations due to basin size and available climate model data.

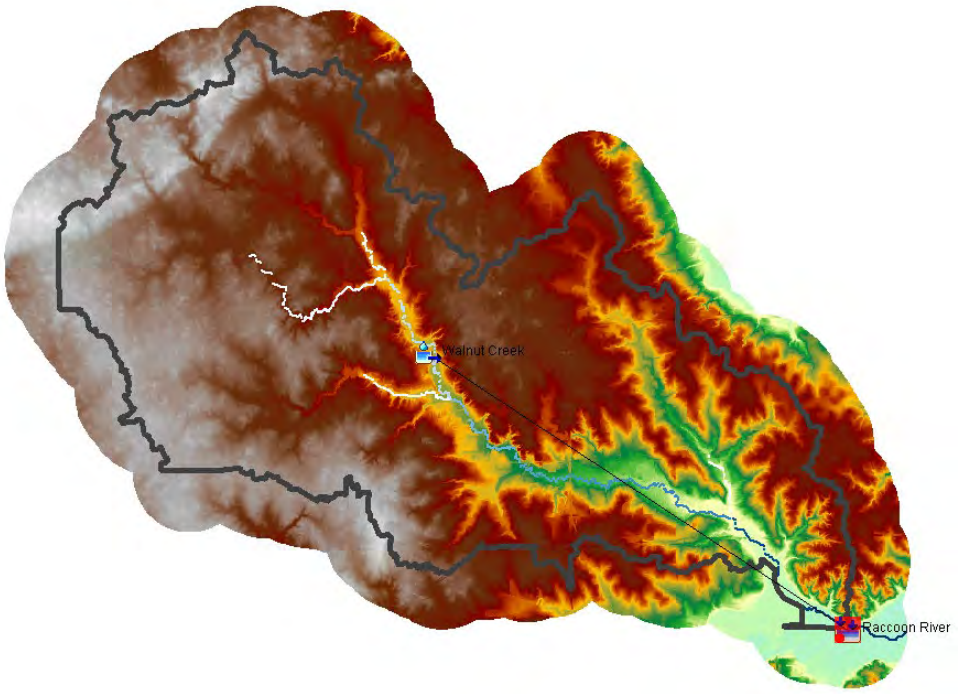

Figure 3-2: Hydrologic Engineering Center-Hydrologic Modeling System Walnut Creek Watershed Basins

3.3 Initial Basin Conditions

The following section describes how the initial model parameters were determined for the Walnut Creek watershed.

3.3.1 Loss Parameters

The Loss method used for this project was Deficit and Constant Loss. The four parameters needed for this method are initial deficit (inches), maximum deficit (inches), the constant rate (inches per hour), and percent impervious.

Typical values for the first three parameters from similar projects completed across the nation are roughly in the ranges shown in Table 3-1.

Table 3-1: HEC-HMS Model Parameter Estimation

Parameter	Typical Range of Possible Values (Estimated)
Initial Deficit (Inches)	0 – 3
Maximum Deficit (Inches)	2 – 12
Constant Rate (Inches per Hour)	0 – 0.6

Most values were at the lower end of the range for all three parameters for projects across the nation. Initial values for the Walnut Creek subbasin are shown in Table 3-2.

Table 3-2: HEC-HMS Model Initial Parameters

Parameter	Initial Values Used
Initial Deficit (Inches)	1
Maximum Deficit (Inches)	6
Constant Rate (Inches per Hour)	0.1

No attempt was made to adjust for antecedent (i.e. wet or dry) conditions for initial model parameters. These adjustments would be made as part of the normal calibration process.
The percent impervious parameter was calculated from the USGS Land Cover Land Use Percent Developed Imperviousness dataset and taking the zonal average over the watershed using the ArcGIS zonal statistics as table tool. Slightly different values were computed for each version of the dataset, as would be expected as development increases over time. The values used for calibration varied depending on each calibration event, therefore, the value was taken from the latest version of the dataset, which was within a few years of the event. A table of the dataset version (year) and percent impervious computed for the Walnut Creek basin is below (Table 3-3). Results were also plotted to show the change of percent impervious values over time (Figure 3-3).

Table 3-3: Percent Impervious from USGS LCLU Dataset

Year	% Impervious
2001	14.45%
2004	15.75%
2006	17.47%
2008	18.05%
2011	18.52%
2013	19.01%
2016	19.99%
2019	20.78%

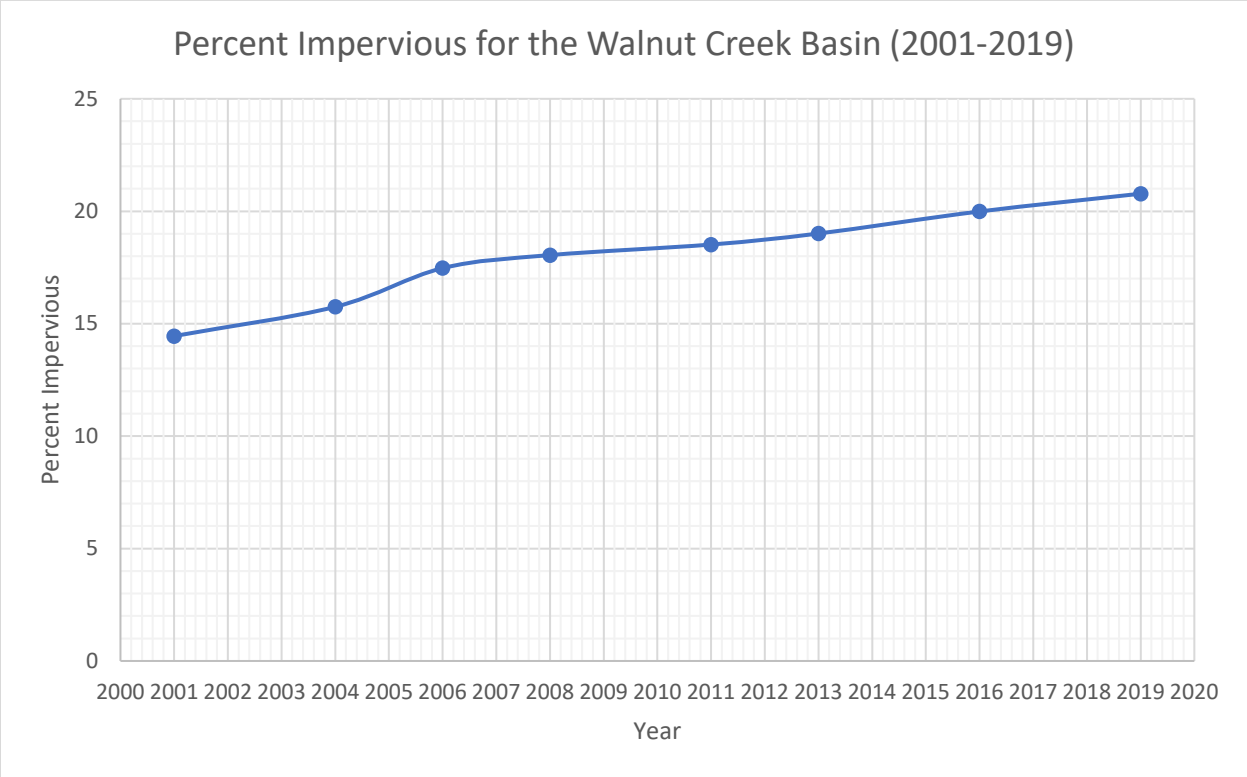

Figure 3-3: Maximum Retention Equation

3.3.2 Transform Parameters

The initial time of concentration value was estimated by first taking the basin's curve number (CN) and using it in the maximum retention equation. Maximum retention was then used in the lag time equation and finally lag time was used to find time of concentration. The three equations used are shown in Figures 3-4 to 3-7. The curve number was estimated by averaging the values obtained for each subbasin during Phase 1. This gave an average CN of 79. Putting this into the equation in Figure 3-4 results in a maximum retention of 2.66. This value was then put into the equation in Figure 3-5 and a lag time of 7.62 hours was obtained. Finally, this value was put into the equation in Figure 3-6 and was solved for time of concentration. This process gave a time of concentration of 12.71 hours. Using the time of concentration and the equation shown in Figure 3-7, an initial value for storage was estimated to be 12.71. These variables were adjusted in the calibration phase.

$$S = \frac{1000}{CN} - 10$$

CN = SCS curve number for the watershed as defined by the loss method.

Figure 3-4: Maximum Retention Equation

$$T_{LAG} = L^{0.8} \frac{(S+1)^{0.7}}{1900\sqrt{Y}}$$

where:

T_{LAG} = lag time in hours.

L = hydraulic length of watershed in feet.

Y = watershed slope in percent.

S = maximum retention in the watershed in inches

Figure 3-5: Lag Time Equation

$$T_{LAG} = 0.6 * T_c$$

where:

T_c = Time of Concentration

Figure 3-6: Time of Concentration Equation

$$0.5 = \frac{\mathrm{R}}{T_c + \mathrm{R}}$$

where:

R = Storage Coefficient

Figure 3-7: Time of Concentration and Storage Coefficient Relationship Equation

3.3.3 Baseflow Parameters

The baseflow method used was the linear reservoir method. This method, as its name implies, uses linear reservoirs to model the recession of baseflow after a storm event. It can be used with 1-3 reservoirs and partition fractions are used to split the inflow to each of the reservoirs. There are four parameters needed for each reservoir. These parameters are the initial baseflow (M^3/S), the groundwater fraction, the groundwater coefficient (hours), and the number of steps.

A standard assumption is to initially use two reservoirs and evenly split flow between them (give each reservoir a fraction of 0.5). From there, these values were adjusted to better represent the observed data. The groundwater coefficient for each reservoir is correlated to T_c. HEC recommends using a coefficient that is 3x's T_c for the top layer and 10x's T_c for the bottom layer. In this case, this gives an initial value of about 38.13 for the top layer and 127.1 for the bottom layer. From HEC recommendation, the initial baseflow was set to zero for the top layer and one for the bottom layer and the number of steps was set to two for the top layer and three for the bottom layer.

The fraction was adjusted during the calibration process to better match observations. Other variables and the number of reservoirs was kept to the recommendations from HEC.

3.3.4 Canopy Parameters

The canopy method used was the simple canopy method. This method has five variables including the initial storage, maximum storage, crop coefficient, evapotranspiration, and uptake method. The initial values for the initial storage and max storage variables were both set to 0. The crop coefficient was initially set to 1. Evapotranspiration can be set to occur only during dry periods or during wet and dry periods. Evapotranspiration was initially set to wet and dry periods. The uptake method can be set to None, Simple, or Tension Reduction. Uptake method was initially set to simple.

3.3.5 Surface Parameters

The surface method used was the simple surface method. This method has two variables including initial storage and max storage. Both were initially set to 0 and remained 0 through the calibration process.

3.4 Calibration Events

Specifics of the HEC-HMS simulated calibration events are presented in Table 3-4. These years were selected to give a general representation of streamflow in the Walnut Creek watershed during various meteorological conditions. Year selection was restricted to years prior to 2011 in order to use observation data that closely resembles the CMIP5-LOCA data. The observation data used was obtained through the National Oceanic and Atmospheric Administration's (NOAA) Physical Sciences Laboratory (PSL). This daily dataset from 1915-2011 is 1/16 resolution near-surface gridded meteorological data. Temperature and precipitation data was obtained for the calibration process (https://psl.noaa.gov/data/gridded/data.livneh.html). Similar to the CMIP5-LOCA data, the grid-to-point-convertor tool was used to covert the gridded data to a single point dataset to represent the Walnut Creek basin. Observed precipitation and observed streamflow at the Racoon River gage is shown for each scenario in Figures 3-8 through 3-13.

Table 3-4: Events Used for HEC-HMS Calibration

HEC-HMS Simulation Period					
Calibration Name	**Start Date**	**Start Time**	**End Date**	**End Time**	**Time Interval**
Dry Scenario	01Jan2002	00:00	31Dec2002	00:00	24 Hours
Mid-Range Scenario	01Jan2006	00:00	31Dec2006	00:00	24 Hours
Wet Scenario	01Jan2010	00:00	31Dec2010	00:00	24 Hours

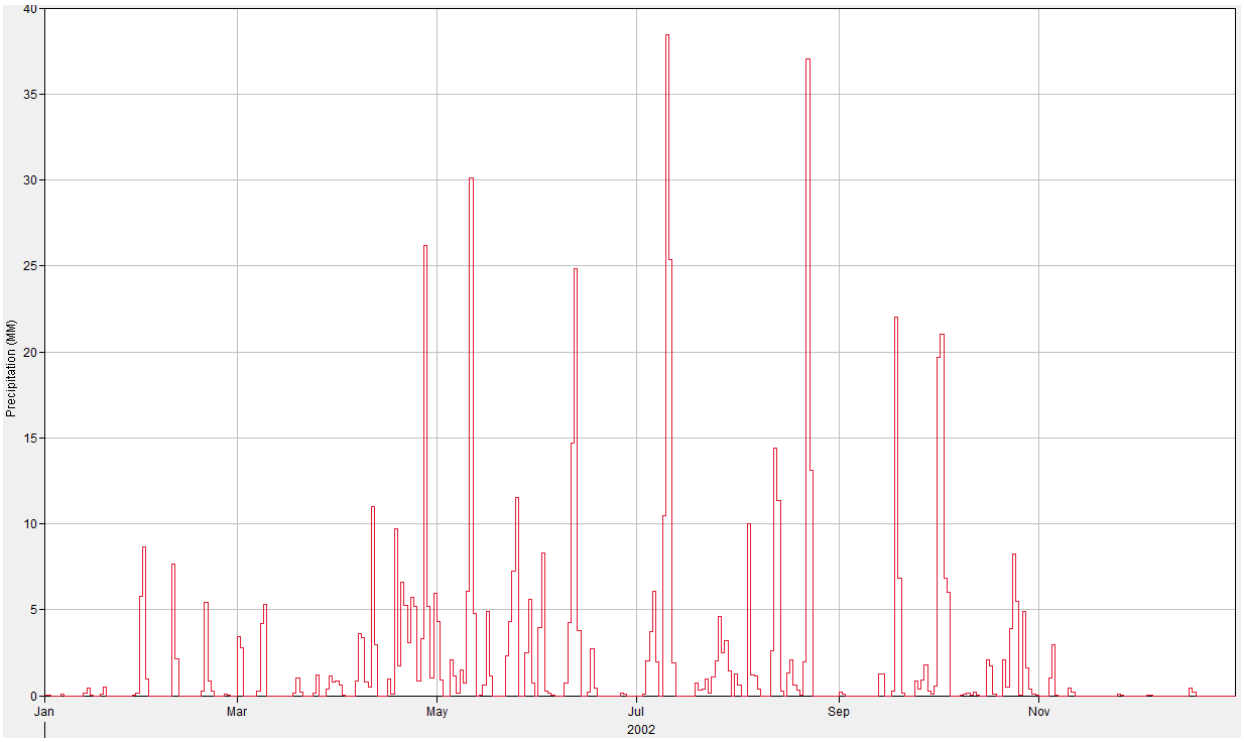

Figure 3-8: Dry Scenario Precipitation

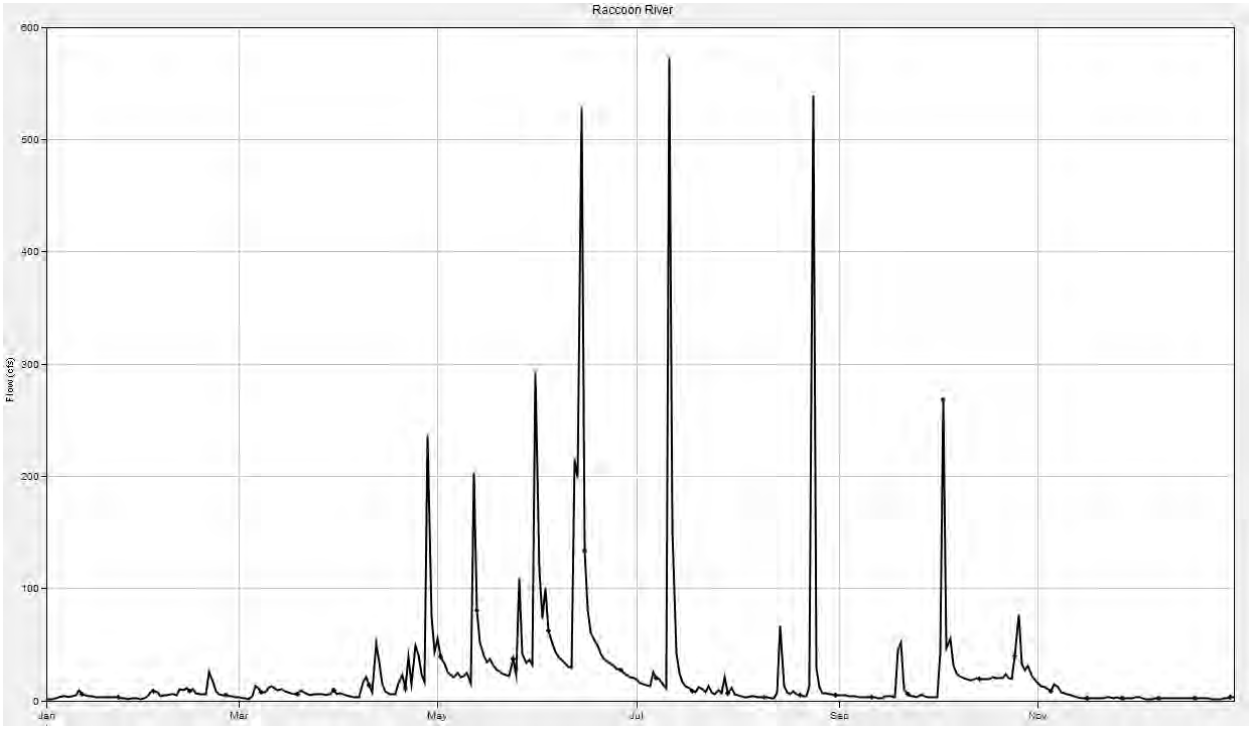

Figure 3-9: Dry Scenario Racoon River Gage Hydrograph

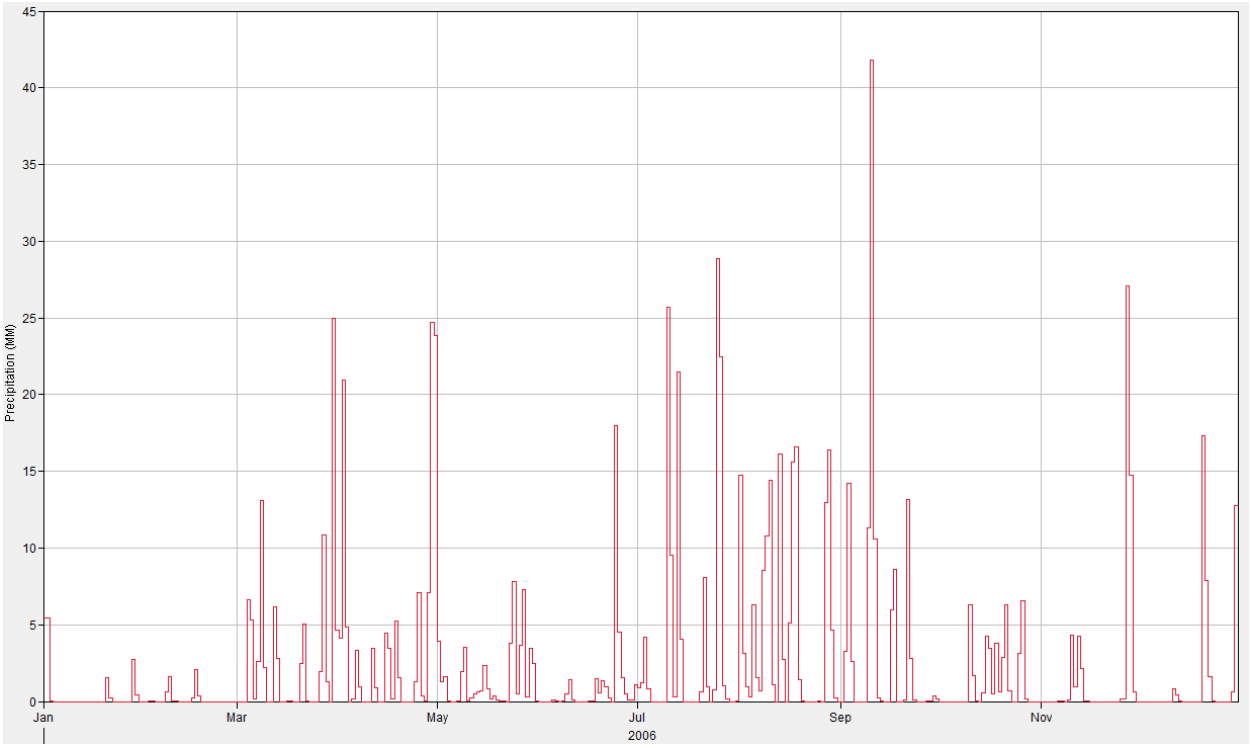

Figure 3-10: Mid-Range Scenario Precipitation

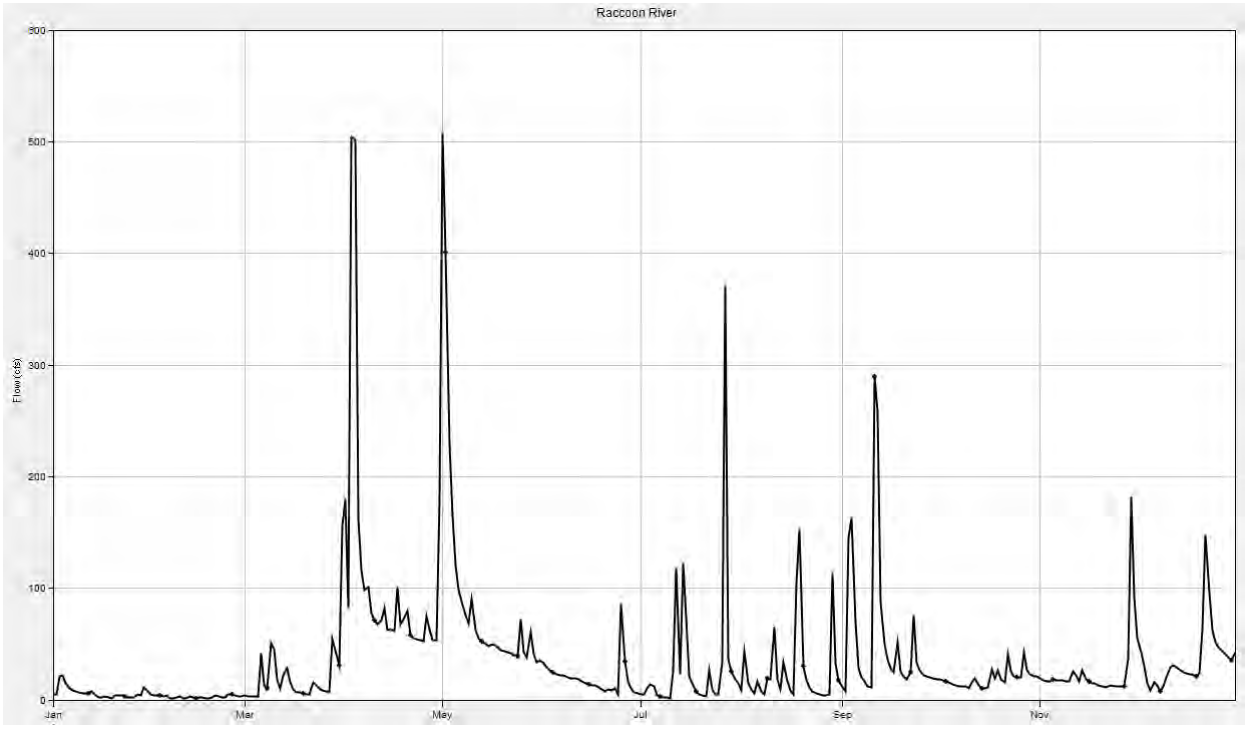

Figure 3-11: Mid-Range Scenario Racoon River Gage Hydrograph

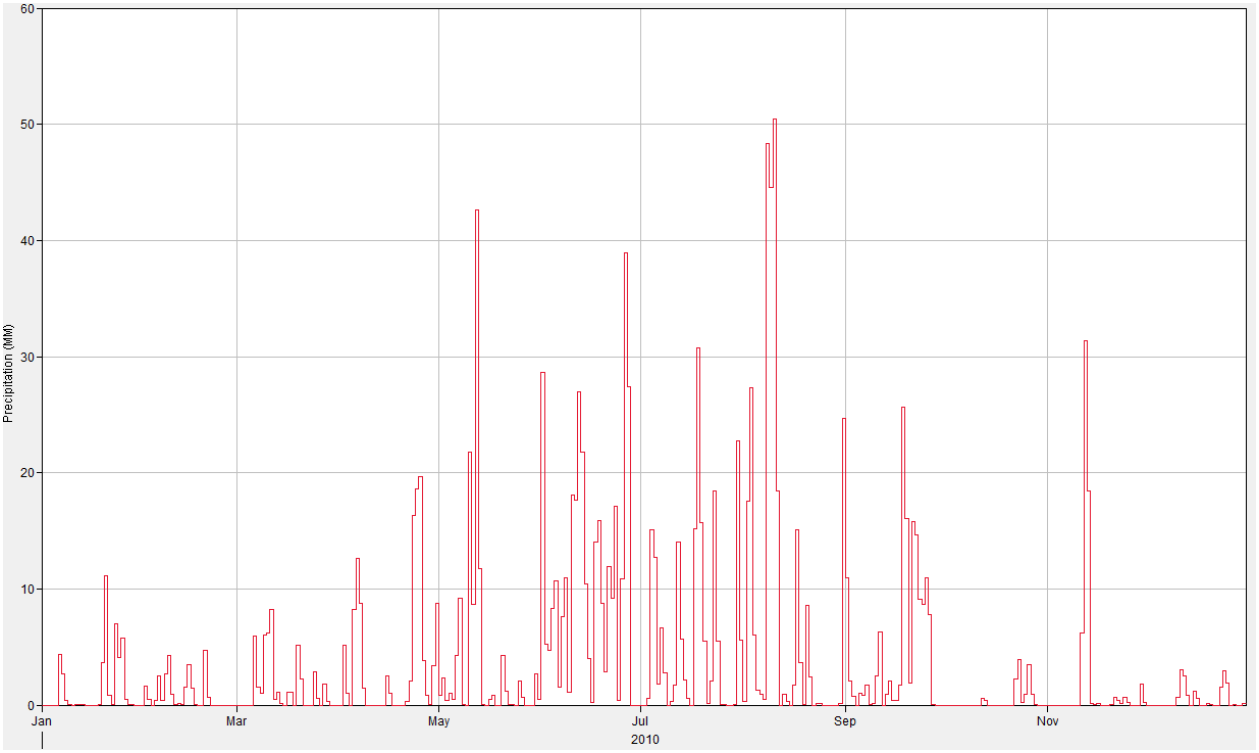

Figure 3-12: Wet Scenario Precipitation

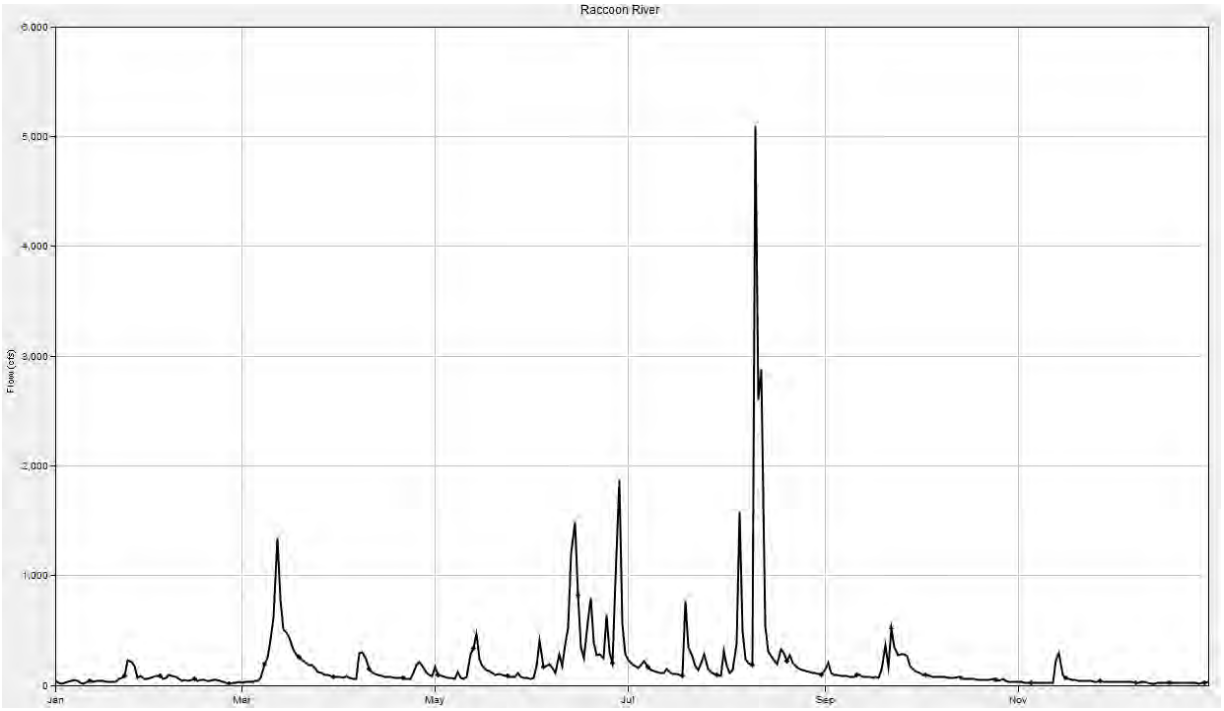

Figure 3-13: Wet Scenario Racoon River Gage Hydrograph

3.5 Single Basin Calibration Parameters and Approach

There are several potential ways to calibrate in HEC-HMS. Slider bars based on computation points and optimization are two tools that can aid calibration. Manual methods of calibration were necessary for this project. This method involved adjusting values in HEC-HMS. The following paragraphs explain how each parameter was adjusted.

During the calibration process the hydrograph flows prior to March and after about mid-November were largely ignored. This is because during these time periods it's difficult to determine how much of the flow is the result of snowmelt runoff causing complications with the accuracy of computed flow compared to the observed flow. The primary focus was model skill during the months where rain is the primary source of precipitation.

3.5.1 Initial Deficit

Initial values were set at 1. Adjusting the parameter at intervals of 0.25 produced significant difference in output. For the Wet Scenario the parameter was adjusted using an interval of 0.1 rather than 0.25 to produce a better output. Adjustments were made at these intervals between 5 and 9.5 to obtain a reasonable comparison with observed data.

3.5.2 Maximum Deficit

Initial values were set at 6 inches. This parameter was made equal to initial deficit and was adjusted at the same interval, so the two variables would remain equal. Through the calibration process it was determined this parameter was not as critical as others.

3.5.3 Constant Loss Rate

Initial values were set at 0.01. Adjusting the parameter by intervals of 0.05 produced significant difference in output. Adjustments were made at this interval between 0 and 0.1 to obtain a reasonable comparison with observed data.

3.5.4 Percent Impervious

Initial percent impervious values were maintained throughout the calibration process. Sensitivity testing demonstrated adjusting the parameter by did not significantly change the results. This variable was also calculated using observation data; therefore, it was preferred to use the initial value. Table 3-5 shows the percent impervious values for each calibration scenario.

Table 3-5: Percent Impervious for Calibraiton Events

Calibration Event	% Impervious
Dry (2002)	14.45
Mid-Range (2006)	17.47
Wet (2010)	18.5

3.5.5 Time of Concentration

Initial time of concentration values were adjusted through the calibration process. The variable was initially set to 12.71 hours, which is about half of the time step. It is important to note that HEC-HMS automatically adjusts the time of concentration to match the time interval used in the model. In this case the time interval is 24 hours, therefore HEC-HMS is also adjusting the time of concentration to 24 hours. Ultimately, a Time of Concentration of 24 hours was used.

3.5.6 Storage Coefficient

Using the equation in Figure 3-7, the storage coefficient was adjusted with time of concentration. With a time of concentration of 12.71 hours, this gave a storage coefficient of 12.71. This was adjusted to 24 hours to match T_c, as the 0.5 ratio assumption was maintained

3.5.7 Baseflow Parameters

Initial baseflow parameters were adjusted through the calibration process. As stated in section 3.3.3, the groundwater coefficient is correlated to the time of concentration. With the initially assumed time of concentration of 12.71 hours, this results in a groundwater coefficient of 38.13 for the first layer and a groundwater coefficient of 127.1 for the second layer.

The groundwater fraction was adjusted in intervals of 0.5 during the calibration process. The groundwater fractions for both layers were adjusted together to maintain a sum of 1 between them. Adjustments were made at this interval between 0 and 1 to obtain a reasonable comparison with observed data.

3.5.8 Channel Percolation

Channel Percolation was not used for this project.

3.5.9 Canopy Parameters

The initial values for the initial storage and maximum storage variables were both set to 0. The crop coefficient was initially set to 1. Max storage was adjusted at an interval of 0.01 from 0 to 0.1 during the calibration process. The other two variables were adjusted at an interval of 0.1 during the calibration process. It was determined initial storage did not have a significant impact on results and the variable remained 0 for all three scenarios. Final values for maximum storage ranges from 0.08 to 0.1. Final value for crop coefficient was 1.2 for all three scenarios. Evapotranspiration was initially set to wet and dry periods and was not changed during the calibration process. Uptake method was initially set to simple and was not changed during the calibration process.

3.5.10 Surface Parameters

The initial values for the initial storage and max storage variable were both set to 0. Sensitivity testing demonstrated adjusting the parameter did not significantly change the results. These variables were kept equal to the initial storage and max storage values used in the canopy parameters.

3.5.11 Hamon Coefficient

The Hamon Coefficient (in/g/m^3) is used in the evapotranspiration calculation in HMS. By default, this is set to 0.0065 inches, but can be adjusted as needed. In the Midwest this value typically changes throughout the year correlated to the growing season. However, in HMS a single value was needed to represent the entire basin, and this can cause some inaccuracy throughout the year. The Hamon Coefficient was adjusted during the calibration process by intervals of 0.0001. Final values for the Hamon Coefficient ranged from 0.0030 to 0.0040 for the three calibration scenarios.

3.6 Calibration Results and Discussion

The Walnut Creek Basin HEC-HMS Model was calibrated for the events listed in Table 3-6. Calibration and model refinement took place to address discrepancies in the computed HMS flow versus observed flows. Table 3-6 shows the final variables for each scenario. Values that will be used in the final model runs was calculated by averaging the values used for the three different calibration runs.

Figures 3-14 through 3-16 show the computed versus observed hydrographs for the Dry, Mid-Range, and Wet Calibration Scenarios, respectively. The following sections discuss the calibration process and what areas were focused on the most to ensure the highest accuracy for all three scenarios.

Table 3-6: Final Variables for the Dry, Mid-Range, and Wet Calibration Scenarios and the Final Values from Calibration Results

	Simple Canopy			Simple Surface		Deficit and Constant				Clark Unit Hydrograph		Linear Reservoir						Met. Models
	Initial Storage	Max Storage	Crop Coefficient	Initial Storage	Max Storage	Initial Deficit	Maximum Deficit	Constant Rate	Impervious	T_c	Storage Coefficient	GW 1 Initial	GW 1 Fraction	GW 1 Coefficient	GW2 Initial	GW 2 Fraction	GW 2 Coefficient	Hamon Coefficient
2002-Dry Calibration	0	0.1	1.2	0	0	6.8	6.8	0.1	14.45	24	24	0	0.7	38.13	1	0.3	127.1	0.0030
2006-Mid-Range Calibration	0	0.1	1.2	0	0	5	5	0.1	17.47	24	24	0	0.7	38.13	1	0.3	127.1	0.0040
2010-Wet Calibration	0	0.1	1.2	0	0	9.5	9.5	0.01	18.5	24	24	0	0.25	38.13	1	0.75	127.1	0.0035

3.6.1 Dry Calibration Discussion

The calibration for the dry scenario was largely successful. Figure 3-14 shows the comparison between the computed and observed streamflow. This scenario was largely used to determine the best variables to use for the baseflow parameters. The dry scenario was best for this because precipitation was low, therefore most of the flow seen in the hydrograph is baseflow.

It was difficult to replicate the few streamflow peaks and some compromises were necessary to get the best accuracy for a majority of the peaks in streamflow while maintaining realistic values for each parameter. One area in particular that was heavily focused on was accurately representing the fall in streamflow after the peak seen in mid-June and mid-July.

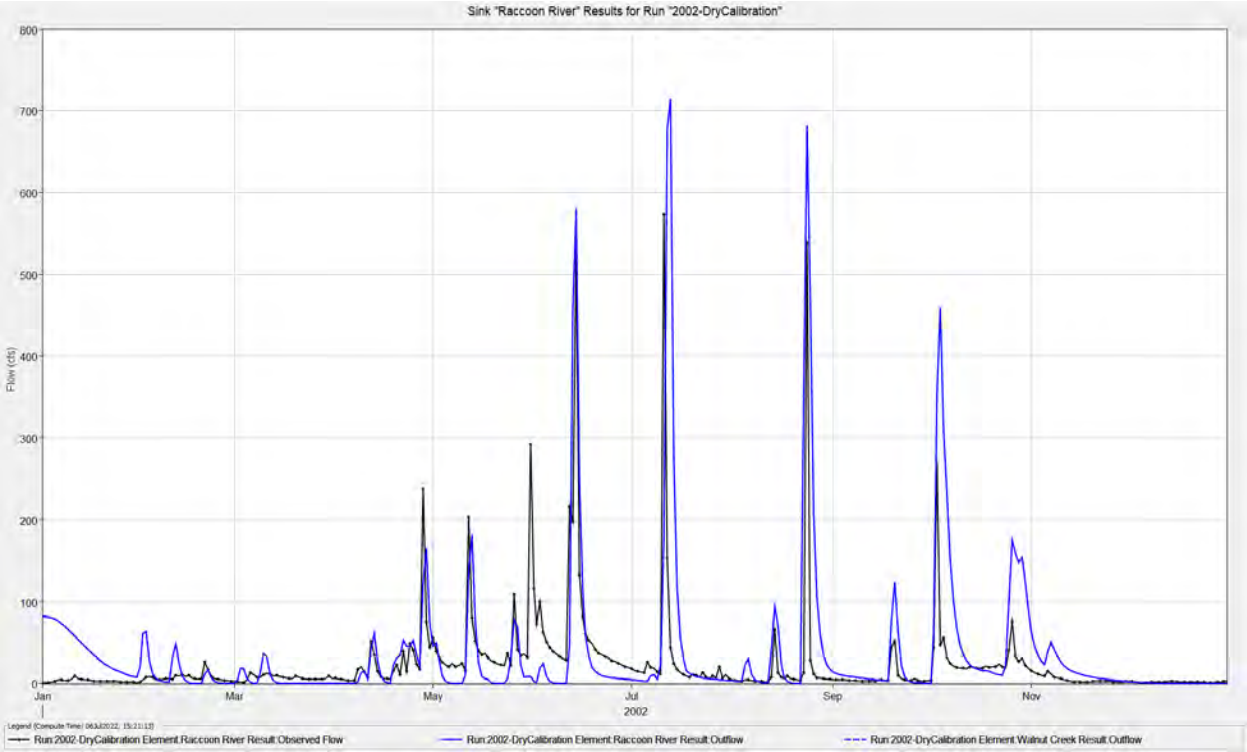

Figure 3-14: Dry Scenario Computed and Observed Hydrographs at Raccoon River Gage

3.6.2 Mid-Range Calibration Discussion

The calibration for the Mid-Range scenario was largely successful. Figure 3-15 shows the comparison between the computed and observed streamflow. This scenario was partially used to determine the best variables to use for the baseflow parameters. It also helps us understand what variables would be ideal when there aren't extreme events, either drought or flood, occurring.

The mid-range scenario was the most difficult to calibrate and some compromises needed to be made to accurately represent the observed data for a majority of the year while maintaining realistic values for each parameter. In particular there was a lot of focus in accurately representing the fall in streamflow for the events in early April and early May. There was also a

lot of focus in matching the rapid rise and fall during the events throughout late summer and into fall, but it was challenging to get an accurate representation of some of the high flow peaks while maintaining accuracy for some of the smaller flow peaks and falls in flow. This resulted in some compromises to get the most widespread accuracy.

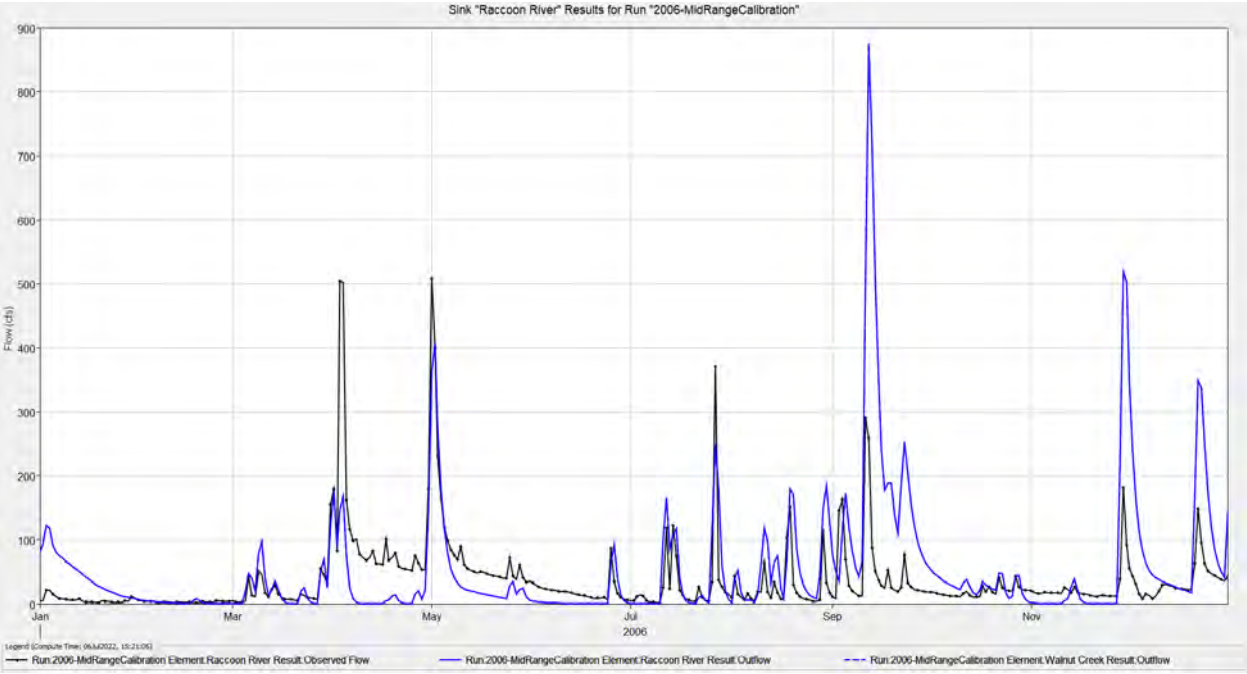

Figure 3-15: Mid-Range Scenario Computed and Observed Hydrographs at Raccoon River Gage

3.6.3 Wet Calibration Discussion

The calibration for the Wet scenario was largely successful. Figure 3-16 shows the comparison between the computed and observed streamflow. This scenario was largely used to determine the best variables to use for the loss parameters. Of the three scenarios this was considered to be the most critical because based on climate change trends precipitation is expected to increase in this region and a wet scenario will be more frequent than the other scenarios.

A large focus was put on representing the peak flow shown in August. However, there was difficulty getting the computed flow up to the observed peak without causing significant inaccuracy for other smaller peaks throughout the year. The other primary area of focus was the quick rise and falls shown in June. There was a lot of success in accurately representing these flows.

Based on these results, it was ultimately determined that the variables for the Wet Calibration would be used for the final HEC-HMS model. This is because it best represents the observed streamflow and this study is primarily interested on extreme flow events, where a wet scenario for the basin characteristics would make the most sense.

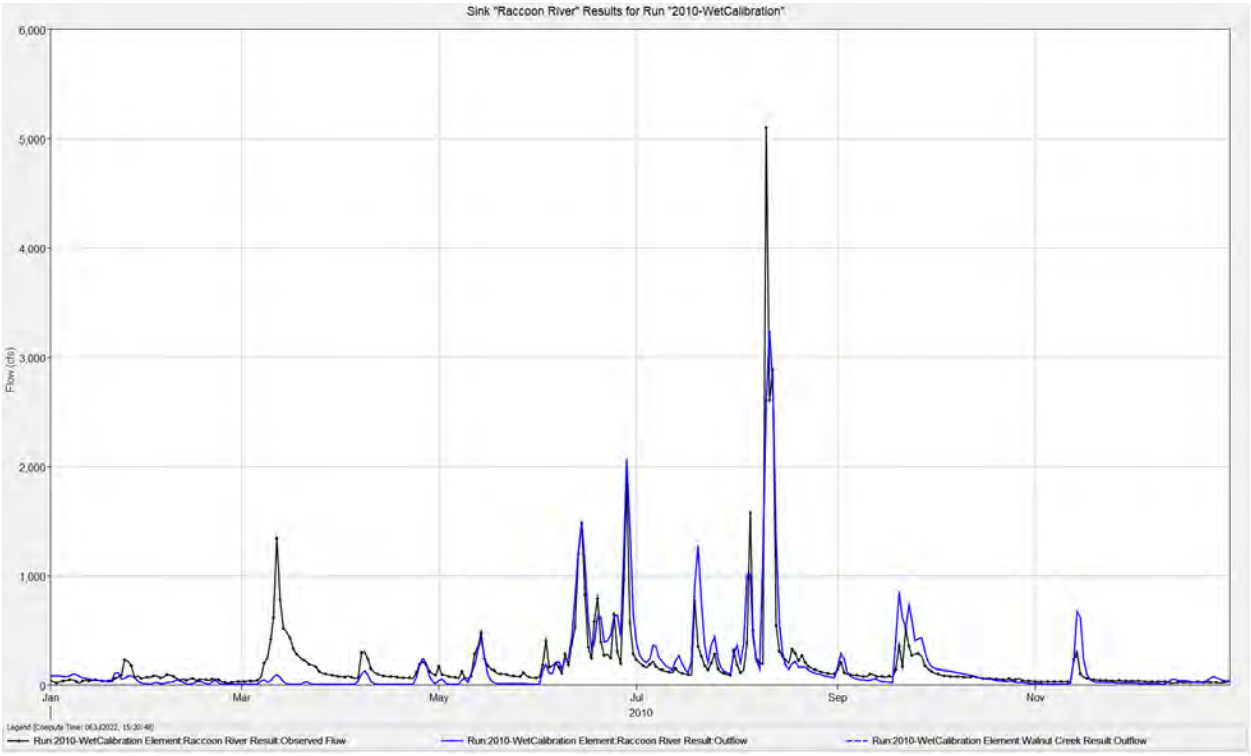

Figure 3-16: Wet Scenario Computed and Observed Hydrographs at Raccoon River Gage

3.7 Phase 1 Model Comparison

To further calibrate and verify model accuracy, flow results were compared to calibration results used during Phase 1. Phase 1 of this project utilized a weather radar gridded dataset from a precipitation event in August of 2010. Section 3.4 discusses the datasets used for calibration for Phase 2 of the project. The results from the Wet Scenario (2010) were compared to the results from Phase 1.

The two different datasets result in flows that are fairly comparable. Figure 3-17 shows the results from both datasets with the observed flow also plotted (blue). Although the results are similar, they do not accurately represent the observed data. Due to how the model is set up in Phase 2, model performance improves when a longer dataset is used. To show this, the results using the Phase 2 dataset with the full year of data is also plotted (dashed green). Model accuracy improves significantly for this event when the entire year of data is included in the analysis.

Based on these results, it was concluded that the Phase 2 model is a reasonable representation of the basin and an effective continuation of the work from Phase 1 of this project. However, due to the nature of the model, it's difficult to see accuracy compared to observed flows with limited datasets such as these.

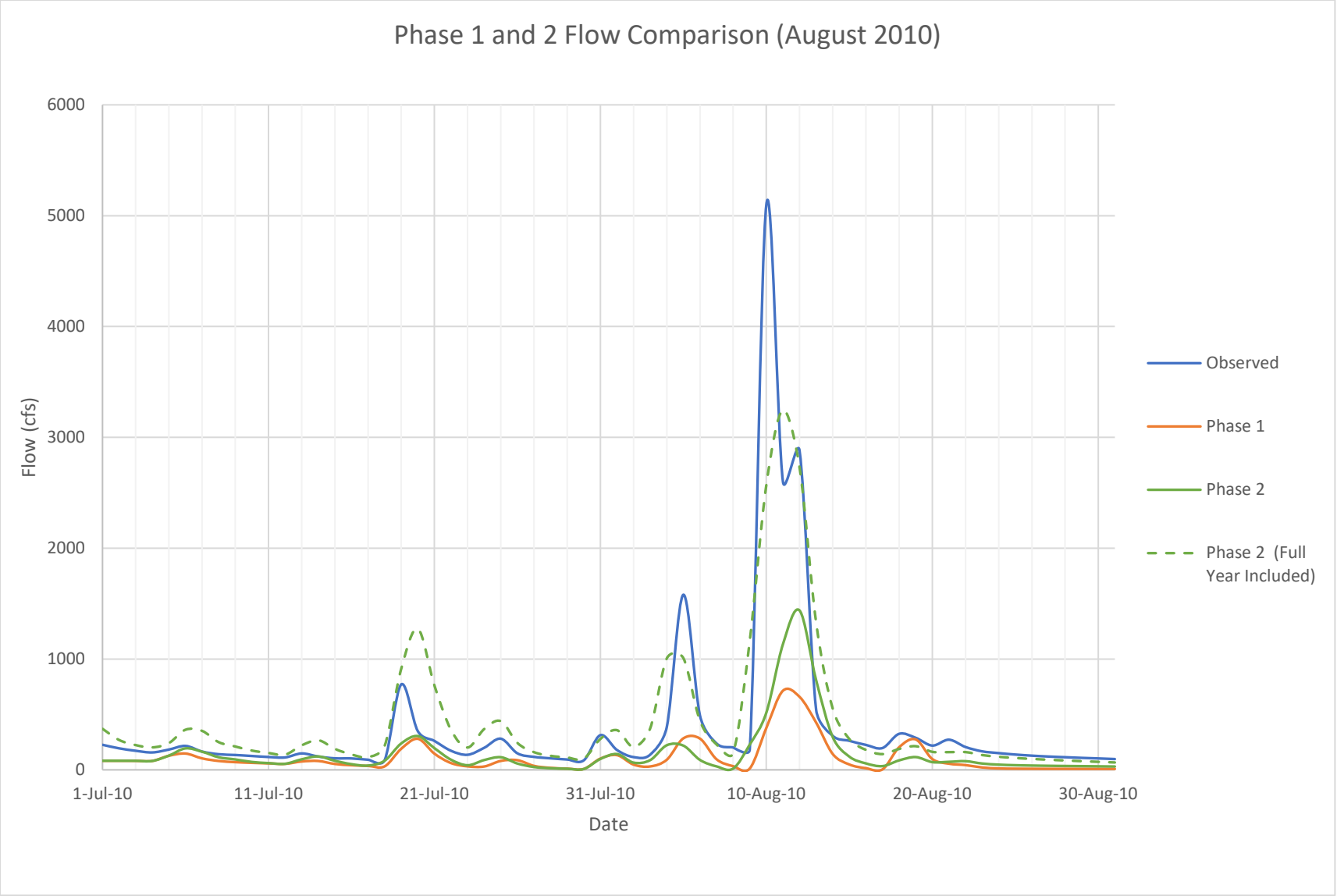

Figure 3-17: Model Result Comparison for the Phase 1 Dataset (Orange), the Phase 2 Dataset (Green), the Phase 2 Dataset with Full Year of Data Included (Green Dashed), and Observed Streamflow (Blue).

4. HEC-HMS Climate Change Analysis

4.1 Introduction

The goal of this modeling effort is to look at how changes in precipitation due to climate change overtime will affect future streamflow in the Walnut Creek watershed. The City of Clive is located within the Walnut Creek Basin and other communities are developing watershed planning documents to assist with identifying and potentially reducing future flood damages. Many climate change documents state that the future condition could result in more variability in weather, but it is difficult to place a quantitative estimate on how communities can plan for the variability. Communities and regulators often use Atlas 14 precipitation frequency relationship which would then be simulated in hydrologic and hydraulic models to assess future risks. However, for this work modeling was done utilizing downscaled GCM data modeled in HEC-HMS. The following sections will discuss the data used and modeling results.

4.2 Climate Models

For this work, precipitation data was obtained from the GCMs from CMIP5. The model output was downscaled using the LOCA method, which results in a resolution of 1/16. This data was then simulated in HEC-HMS to obtain changes in streamflow in the Walnut Creek watershed. Some of the modeling concerns and data limitations were discussed in Sections 3.1.1 and 3.1.2.

Data was taken from 32 GCMs (Table 4-1). These GCMs utilize Representative Concentration Pathways (RCPs) to calculate the projected changes in precipitation. An RCP is a greenhouse gas concentration (not emission) trajectory adopted by the Intergovernmental Panel on Climate Change (IPCC). Four pathways (RCP 2.6, RCP 4.5, RCP 6.0, and RCP 8.5) are used to describe different climate futures. As of now, RCP 2.6 is no longer possible without advancements in carbon capture technology. The other three scenarios are still possible depending on the volume of greenhouse gases emitted in the years to come. These pathways can be seen in Figure 4-1.

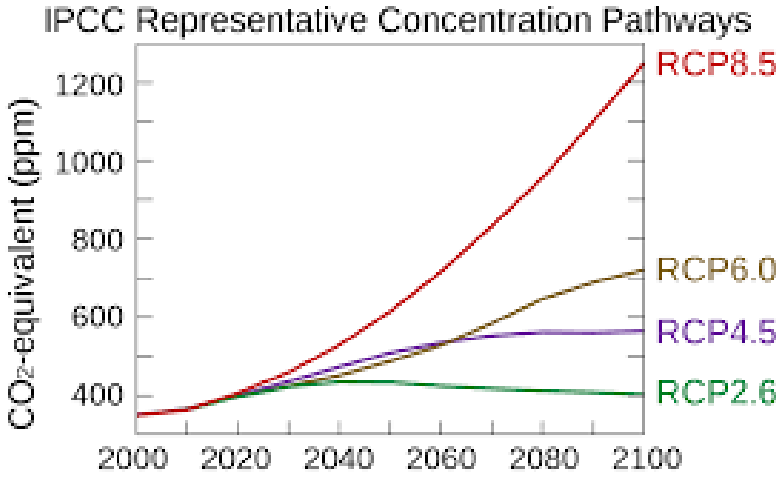

Figure 4-1: IPCC Representative Concentration Pathways

Table 4-1: A list of the CMIP5 models used in this study and the corresponding RCP output avaiable for each model. ("Y" indicates the RCP was available for the model and "N" indicates the RCP was not available).

	Research Center	Country	Reference	Available RCPs			
Models	-	-	-	2.6	4.5	6	8.5
ACCESS1-0	Research Organization/Bureau of Meteorology	Australia	http://www.bom.gov.au	N	Y	N	Y
ACCESS1-3				N	Y	N	Y
BCC-CSM1-1	Beijing Climate Center	China	http://bcc.ncc-cma.net/	N	Y	N	Y
BCC-CSM1M1				N	Y	N	Y
CanESM2	Canadian Centre for Climate Modelling and Analysis of Environment and Climate Change Canada	Canada	https://climate-scenarios.canada.ca/?page=pred-canesm2	N	Y	N	Y
CCSM4	National Center for Atmospheric Research	United States	https://www.cesm.ucar.edu/models/ccsm4.0/ccsm/	N	Y	N	Y
CESM1-BGC	National Science Foundation, Department of Energy, National Center for Atmospheric Research	United States	https://journals.ametsoc.org/view/journals/clim/26/18/jcli-d-12-00184.1.xml	N	Y	N	Y
CESM1-CAM5				N	Y	N	Y
CMCC-CM	Centro Euro-Mediterraneo sui Cambiamenti Climatici	Italy	https://www.cmcc.it/models/cmcc-cm	N	Y	N	Y
CMCC-CMS				N	Y	N	Y
CNRM-CM5	Centre National de Recherches Meteorologiques	France	https://www.umr- cnrm.fr/?lang=fr	N	Y	N	Y
CSIRO-mk3-6-0	Queensland Climate Change Centre of Excellence and the Commonwealth Scientific and Industrial Research Organization	Australia	https://confluence.csiro.au/public/CSIROMk360	N	Y	N	Y
EC-Earth	European EC-Earth Consortium and Swedish Meteorological and Hydrological Institute	Sweden	http://www.ec-earth.org/	N	Y	N	Y
FGOALS-g2	State Key Laboratory of Numerical Modeling for Atmospheric Sciences and Geophysical Fluid Dynamics	China	http://www.lasg.ac.cn/english/	N	Y	N	Y
GFDL-CM3	Geophysical Fluid Dynamic Laboratory (NOAA)	United States	https://www.gfdl.noaa.gov/	N	Y	N	Y
GFDL-ESM2G				N	Y	N	Y
GFDL-ESM2M				N	Y	N	Y
GISS-E2-H	National Aeronautics and Space Administration: Goddard Institute for Space Studies	United States	https://data.giss.nasa.gov/modelE/cmip5/	N	Y	N	Y
GISS-E2-R				N	Y	N	Y
HadGEM2-AO	Hadley Centre: Met Office	United Kingdom	https://www.metoffice.gov.uk/research/approach/modelling-systems/unified-model/climate-models/hadgem2	N	Y	N	Y
HadGEM2-CC				N	Y	N	Y
Had-GEM2-ES				N	Y	N	Y
INMCM4	Institute of Numerical Mathematics	Russia	https://link.springer.com/article/10.1134/S000143381004002X	N	Y	N	Y
IPSL-CM5A-LR	Institute Pierre Simon Laplace	France	https://www.ipsl.fr/en/	N	Y	N	Y
IPSL-CM5A-MR				N	Y	N	Y
MIROC5	Atmosphere and Ocean Research Institute and Japan Agency for	Japan	https://www.jamstec.go.jp/e/	N	Y	N	Y
MIROC-ESM				N	Y	N	Y
MIROC-ESM- CHEM				N	Y	N	Y
MPI-ESM-LR	Meteorological Research Institute Japan Meteorological Agency	Germany	https://mpimet.mpg.de/en/science/models/mpi-esm.html	N	Y	N	Y
MPI-ESM-MR				N	Y	N	Y
MRI-CGCM3	Meteorological Research Institute	Japan	http://www.mri- jma.go.jp/index_en.html	N	Y	N	Y
NorESM1-M	Norwegian Climate Center	Norway	https://cicero.oslo.no/no	N	Y	N	Y

For all 32 models, only RCP 4.5 and RCP 8.5 (also labeled as RCP45 and RCP85) were available on the online database. RCP 4.5 is currently described by the IPCC as a reasonable lower bound with emissions peaking around 2040 and then declining. In the RCP 8.5 scenario, emissions continue to rise throughout the 21st century and is generally taken as the basis for a reasonable high bound for atmospheric CO_2 concentration scenarios.

4.3 Precipitation Data

The precipitation data from the GCMs is at a daily time scale and ranges from 1950-2099. Due to limitations from the spatial scale difference, projected precipitation for the Walnut Creek basin varies greatly between models. Figures 4-2 and 4-3 show the composite plots for daily precipitation output. For both RCP 4.5 and RCP 8.5, it's difficult to discern any pattern, but generally models indicate precipitation will slightly increase across the basin.

More details on the climate model precipitation data used for streamflow calculations can be found in Appendix B.

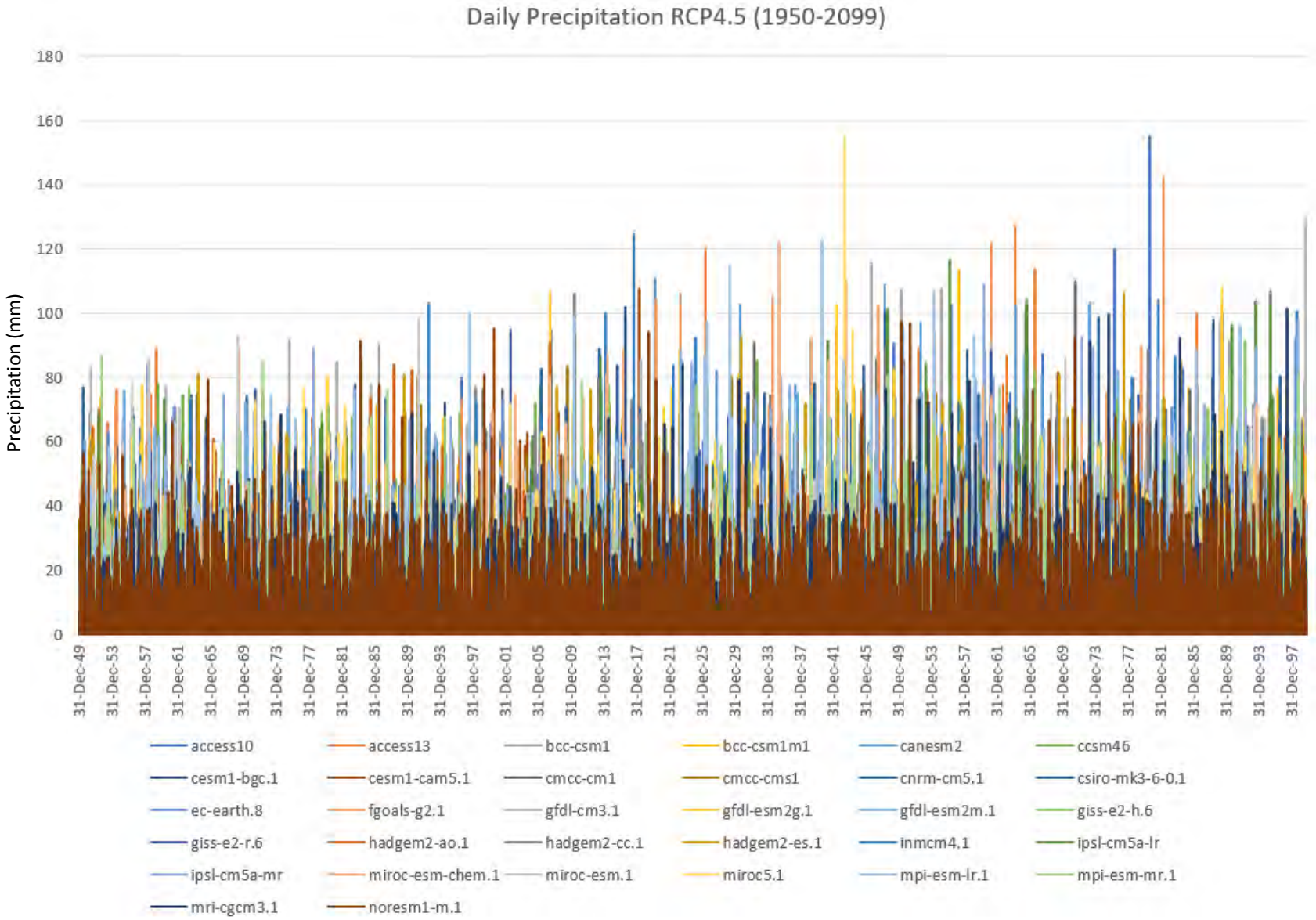

Figure 4-2: Daily Precipitation Plot RCP45 (1950-2099)

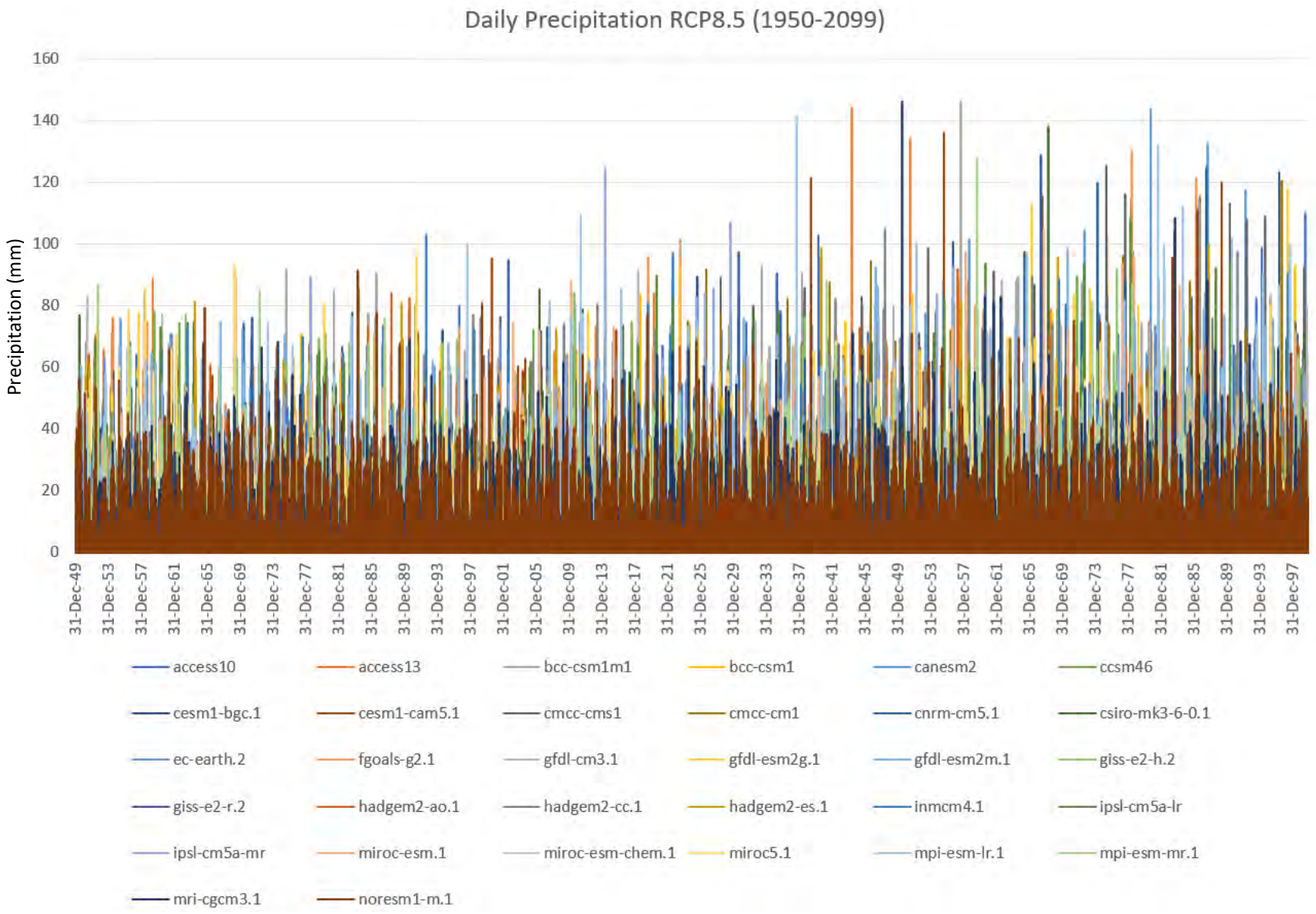

Figure 4-3: Daily Precipitation Plot RCP 8.5 (1950-2099)

4.4 Peak Streamflow Event Comparison

For this project, there is particular interest in how peak streamflow events will change over time within the Walnut Creek basin. The daily streamflow results were analyzed for each model and most indicated the number of peak events will increase and the magnitude of these events will also increase through the end of the century. This was done for RCP 4.5 and RCP 8.5 results. The following section summarize these results.

4.4.1 RCP 4.5 Peak Event Results

A boxplot was created for the RCP 4.5 percent change in peak streamflow to determine the most likely change in streamflow that should be expected for the basin (Figure 4-4). Out of the 32 models examined, 24 showed an increase in peak streamflow. The models show a wide range of percent increase in streamflow ranging from 2.2% to 112.4%, with a median of 17.4%. The first quartile, the lower boundary of the boxed area, is 2.2%. The third quartile, the upper boundary of the boxed area, is 42.6%. A majority of models, 18, have a percent increase within 10-50%. Eight models show a decrease in percent change and six show an increase greater than 50%. Based on this plot, the 112.4% increase is an outlier in the data and is not considered in the calculations of the median, first quartile, and third quartile.

4.4.2 RCP 8.5 Peak Event Results

A boxplot was also created for the RCP 8.5 percent change in peak streamflow to determine the most likely change in streamflow that should be expected for the basin (Figure 4-4). Out of the 32 models examined, 26 showed an increase in peak streamflow. The models show a wide range of percent increase in streamflow ranging from 3.9% to 133.8%, with a median of 34.8%. The first quartile is 7.1% and the third quartile is 61.8%. A majority of models, 14, have a percent increase within 10-50%. Five models show a decrease in percent change and 13 show an increase greater than 50%.

Between RCP 4.5 and RCP 8.5, the percent changes in peak streamflow are generally larger for RCP 8.5. There is also a larger amount of variability for RCP 8.5. Both scenarios result in primarily an increase in streamflow with only a few models showing a decrease. However, the magnitude of the change varies significantly.

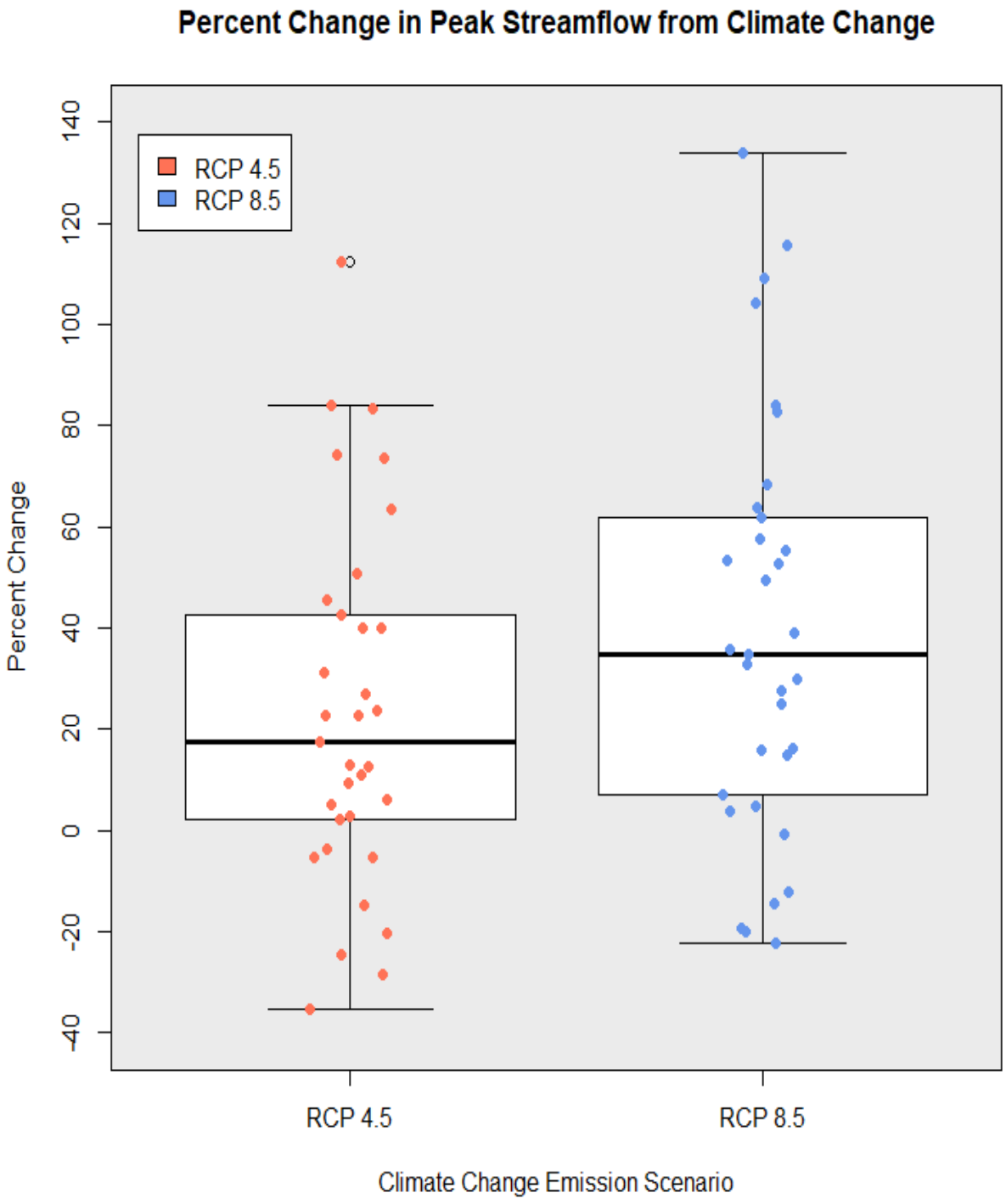

Figure 4-4: Boxplots of Percent Change in Peak Streamflow due to Climate Change Only

4.5 Future Land-Use Effects

Future land-use across the Walnut Creek basin was estimated collaboratively by the communities and was endorsed by the full Walnut Creek Watershed Management Authority (WMA). This is an updated version from the land-use dataset that was created during Phase 1 of the project. The future land-use map (Figure 4-5) was created to represent a fully developed scenario for the region, instead of reflecting a specific year like was done in Phase 1 of the project. Phase 1 land use represented development in 2050 and used a percent impervious of 43.44%.

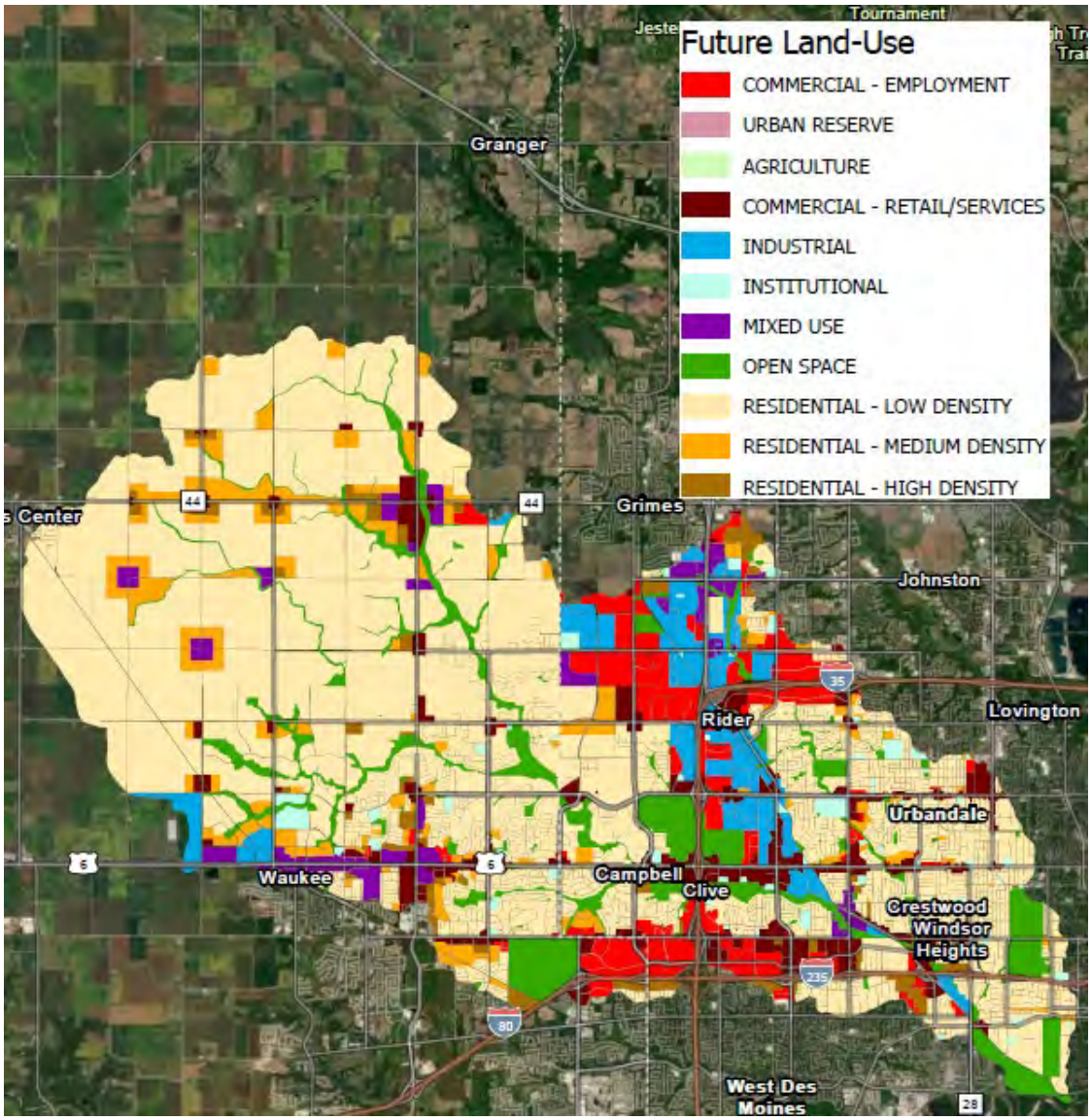

Figure 4-5: Phase 2 Future Land-Use for the Walnut Creek Basin

The percent impervious for the entire basin was calculated from this land-use map and it was then used in HMS to estimate impact future land-use would have on streamflow in Walnut Creek. This was calculated using Impervious Surface Coefficients (ISC) that were developed by the Office of Environmental Health Hazard Assessment and the Center for Water & Land Use, UC Davis (https://oehha.ca.gov/media/downloads/ecotoxicology/fact-sheet/iscfacts072208_0.pdf). Table 4-2 shows the ISC used for each land-use type, the total acreage for each, the impervious acreage for each, and the resulting percentage of the total area that is impervious. This gives a total impervious area of 56.66%.

From communication with Doug Ollendike, the Community Development Director from Clive, the Walnut Creek watershed had been developing at a rate of about 400 acres per year. Based on this and the assumption that the land-use dataset used in Phase 1 is the condition for 2050 (43.44%), Doug indicated this fully developed watershed dataset would represent the condition for 2090/2100. It was therefore assumed the 56.66% would be representative of the total percent impervious for the watershed in 2099.

The calculated impervious area was compared to the calculated values used during calibration and what was used in Phase 1 (Figure 4-6). Based on the historical trend and what was used in Phase 1, this confirms that the assumed year of 2099 and calculated percent impervious area of 56.66% makes sense for the Walnut Creek basin.

Table 4-2: Walnut Creek Basin Land-Use and Percent Impervious Calculations

Land-Use	Area (Acres)	ISC	% Impervious
RESIDENTIAL - LOW DENSITY SUM	19080.61	0.50	9633.37
RESIDENTIAL - MEDIUM DENSITY SUM	11709.15	0.63	7327.18
RESIDENTIAL - HIGH DENSITY SUM	774.62	0.77	593.76
INDUSTRIAL	1632.74	0.91	1485.79
MIXED USE	2167.88	0.80	1734.31
OPEN SPACE	3966.70	0.02	79.33
COMMERCIAL - RETAIL/SERVICES	2849.63	0.86	2450.68
COMMERCIAL - EMPLOYMENT	2744.74	0.80	2195.79
INSTITUTIONAL	706.17	0.50	353.08
Total Area	45632.22	-	25853.29
-	-	-	56.66%

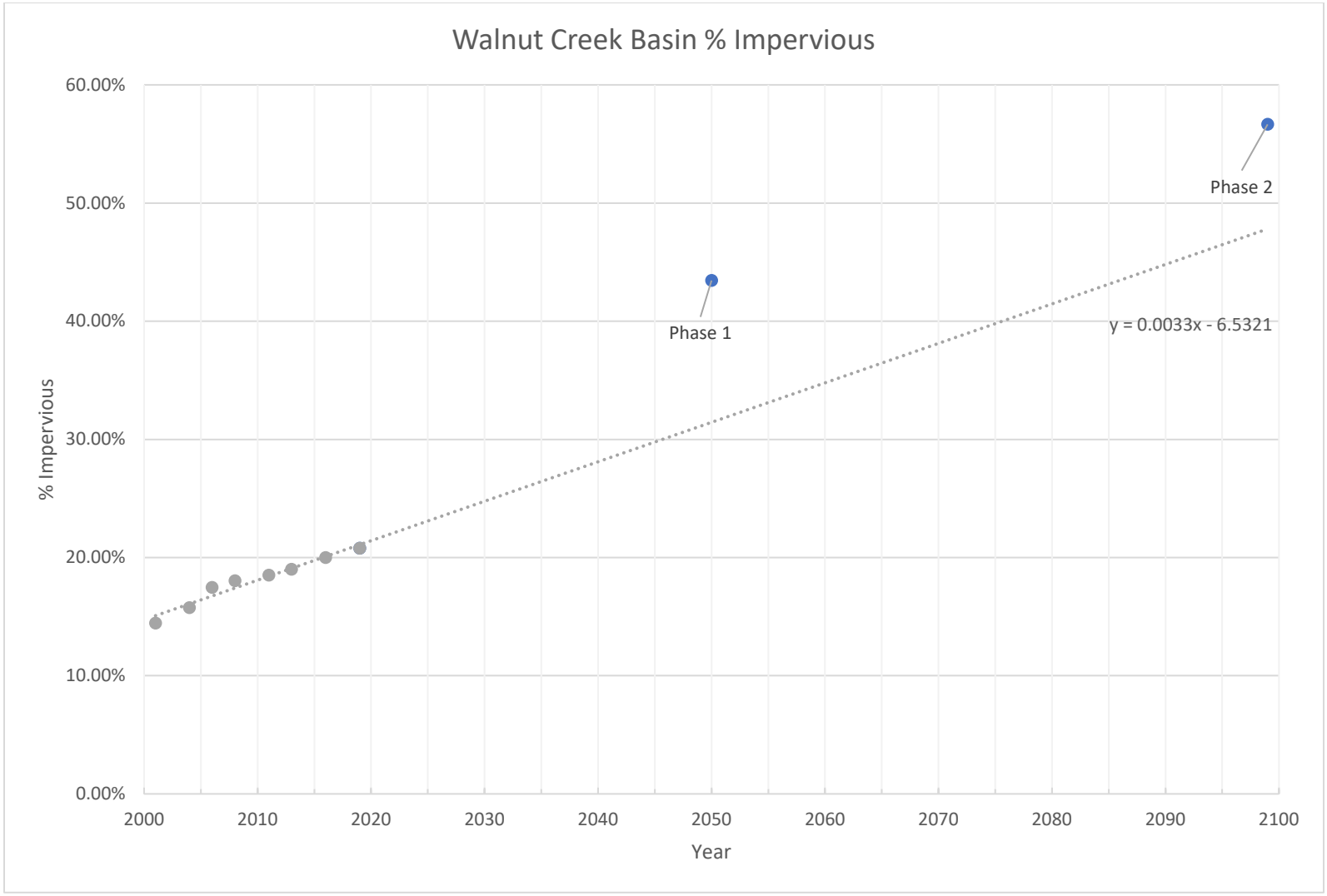

Figure 4-6: Walnut Creek Basin Percent (%) Impervious

4.5.1 Future Land-Use Modeling Results

For the land-use model runs, parameters were kept the same as the previous modeling, but with the updated percent impervious. The primary interest is on how the increase in the percent impervious impacts peaks in streamflow. The same models from the previous sections for the climate change analysis were examined for this analysis.

For this analysis the peak flows for each model using the historical percent impervious (18.5%) and the future percent impervious calculated from the future land-use dataset (56.6%) were compared. Peak flows were taken from the time period 1950-2005. This was because prior to 2006 climate change doesn't have an influence on the resulting streamflow. Starting in 2006, streamflow results vary between the RCP 4.5 and RCP 8.5 for each model. Therefore, to determine the influence land-use change has on streamflow without the influence of climate change, peak flows need to be taken from prior to 2006. The percent increase was calculated from these peak flows and a boxplot was created of the resulting percent change in peak streamflow (Figure 4-7).

A majority of models have an increase of 1-6% due to land use change with a median of 4.5%. The first quartile is 3.0% and the third quartile is 5.8%. Based on this plot, there are two outliers at 27.1% and 17.1% and they are not considered in the calculations of the median, first quartile, and third quartile. Compared to the percent change due to climate change, there's more confidence in the percent change due to land use change. However, climate change is likely to have a larger impact on peak streamflow than land use change alone.

4.5.2 Future Land-Use and Climate Change Combine Impacts

To determine the combined impacts of land-use change and climate change, the peak flow for the time period 1950-2005 using the historical percent impervious (18.5%) was found for each model and then compared to the peak streamflow for the time period 2021-2099 using the future percent impervious calculated from the future land-use dataset (56.6%). This was done for every model for both RCP 4.5 and RCP 8.5 climate change scenarios.

Two boxplots of the percent change were created for both RCP 4.5 and RCP 8.5 (Figures 4-8). The majority of the models for both climate change scenarios show an increase of 10-50% with 15 of the 32 models within this range for RCP 4.5 and 12 of the 32 model within this range for RCP 8.5. The median percent change for RCP 4.5 has increased from 17.4% to 26.2% and the median percent change for RCP 8.5 has increase from 34.8% to 38.3%. These changes are reasonable based on the results discussed in section 4.5.1.

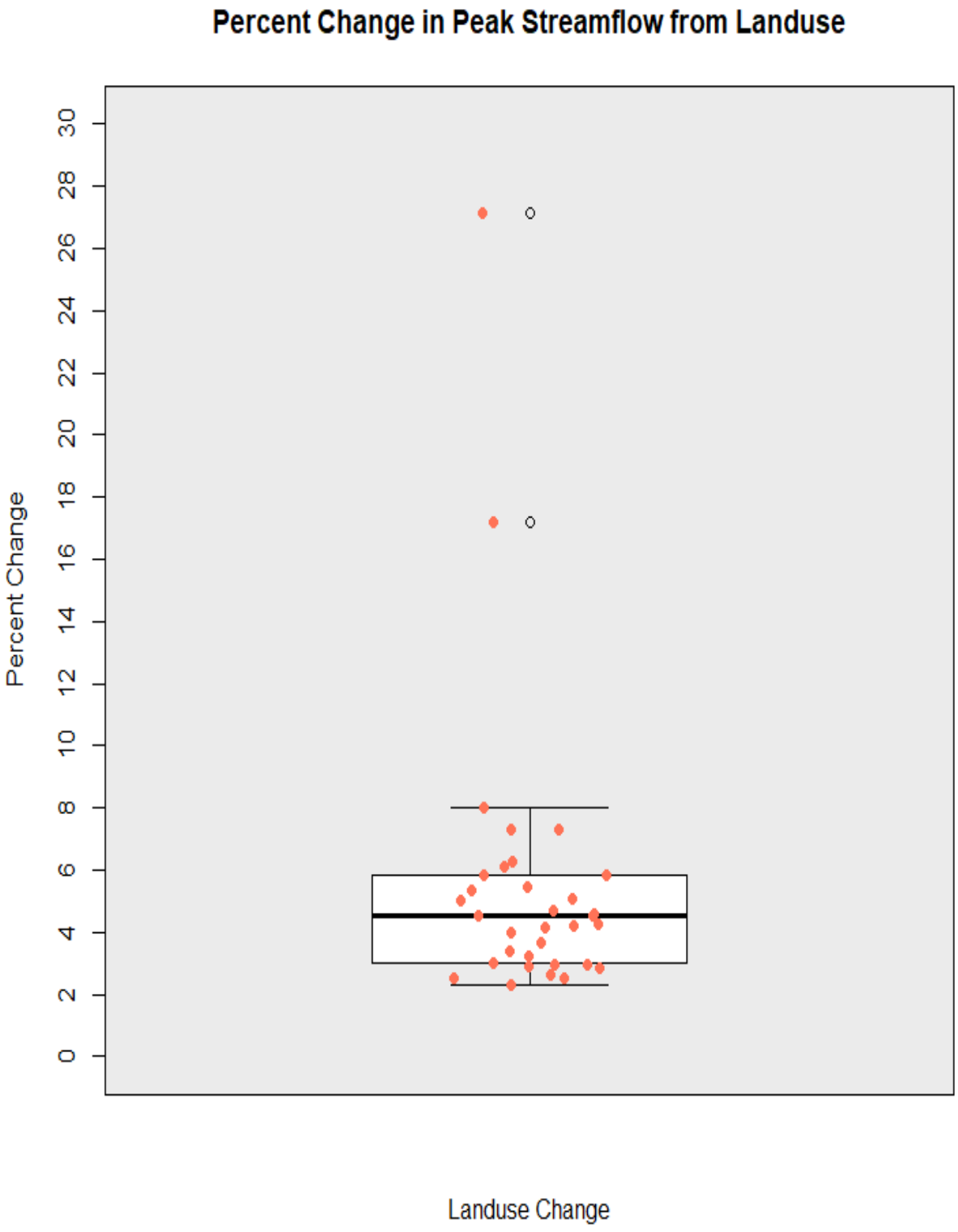

Figure 4-7: Boxplot of Percent Change in Peak Streamflow due to Landuse Change Only

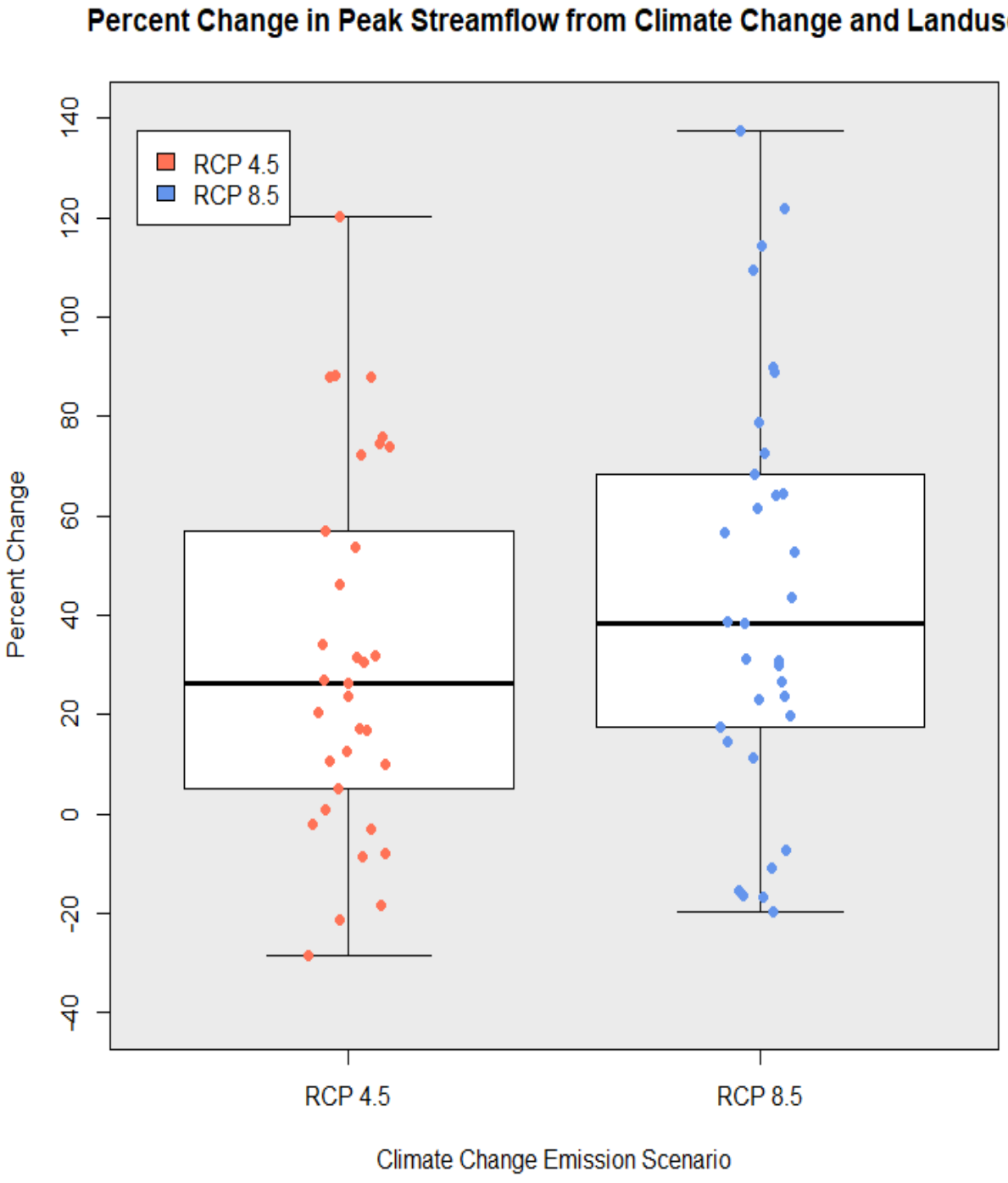

Figure 4-8: Boxplots of Percent Change in Peak Streamflow due to Climate Change and Landuse Change

4.6 Discussion and Considerations

From these modelling results it evident that there is some uncertainty of how climate change will impact future precipitation and streamflow across the Walnut Creek basin. There is a large amount of variability between models for projected precipitation at the daily time scale. The composite plots of the models show an increase in precipitation across the region for both RCP 4.5 and RCP 8.5 scenarios.

Due to the high variability between models for precipitation, this in turn results in a high amount of variability between models for streamflow. Due to this inconsistency, it's difficult to discern a clear trend in the models for daily streamflow and this needs to be considered when interpreting results.

Although there is quite a bit of variability in the percent increase of peak streamflow, over half of the models show an increase in the magnitude of peak events for both RCP 4.5 and RCP 8.5 scenarios, when just climate change influences are considered. Models have a median increase of 17.4% for RCP4.5 and 34.8% for RCP8.5. This indicates that, higher concentrations of CO_2 in the atmosphere will result in higher streamflow within the Walnut Creek basin. This is comparable to similar climate change studies.

Land-use change on its own has a smaller impact on changes in streamflow with a median percent increase of 4.5% shown through this modeling effort. This indicates climate change impacts should be a primary concern for future planning and land-use change will have less of an impact on changes in streamflow.

As it's expected, when both land-use change and climate change are incorporated into the modeling, there is more of an increase in streamflow. Models have a median increase of 26.2% for RCP4.5 and 38.3% for RCP8.5. The increases shown are reasonable considering the results from the percent change in streamflow due to land-use only.

With these results it's still important to remember there is quite a bit of uncertainty. This is largely due to limitations with the climate data itself in relation to the size of the Walnut Creek basin. These results give some idea of what general trends in streamflow will be like for the basin because of climate change and land-use change, but they're less useful for determining specific values. In order to get more refined results, improvements in downscaled climate data is necessary.

5. Hydrologic Engineering Center-River Analysis System Inundation Mapping

5.1 Introduction

In Phase 1 on the project, streamflow frequency charts were developed using Atlas 14 precipitation frequency charts. To create the inundation maps for this phase of the project, these streamflow charts were taken, and streamflow was increased based on the percent changes calculated in sections 4.4.6 and 4.4.7. Streamflow for the 5, 10, 25, 50, 100, 200, 500, 1000-year floods were increased at increments of 10% from 10-60%. It's assumed that these percent increases being tested are a representation of combined effects due to climate change and land-use change.

5.2 Inundation Maps

Figures 5-1 through 5-27 compare the existing inundation extents (in blue), to the future inundation extents (in red). These figures show the results for a 10%, 30%, and 60% increase in streamflow. Generally, there is a farther inundation extent as streamflow increases. There is also a farther extent in more urban areas closer to the Racoon Creek confluence. Only the results for the 5-year (20% chance exceedance), 100-year (1% chance exceedance), and 1000-year (0.1% chance exceedance) streamflow are shown.

5.3 Streamflow Percent Change

Streamflow at specific locations along Walnut Creek were examined as part of Phase 1 and have been reexamined here based on the updated results. Table 5-1 shows the Existing Atlas-14 and Future Atlas-14 for the 100-year (1% change exceedance) event that were used in Phase 1. For the Phase 2 results, the percent change was applied to the Existing Atlas-14 from Phase 2. This was done for 10-50% increase. Table 5-1 has been color coded based on the percent change results from land-use change, climate change, and the combination of land-use change and climate change. The median percent change due to land use is 4.5%. The largest percent change, excluding outliers, is 8.0%. For simplicity for the HEC-RAS modeling, this was rounded up to 10% (yellow). A 20-40% increase (orange), is what can be expected due to climate change alone, as supported by the median increase for RCP 4.5 and RCP 8.5 (17.4% and 34.8%). A 50% increase (red) is on the higher range and it's reasonable to assume that the combined impacts of land use change and climate change could result in this level of change.

Table 5-1: Percent Increase in Streamflow Based on Locations Along Walnut Creek

		1% (100-yr) Event							
		Phase 1		Phase 2					
Location Description	**RAS XS**	**Existing Atlas-14**	**Future Atlas-14**	**10% Increase**	**20% Increase**	**30% Increase**	**40% Increase**	**50% Increase**	**60% Increase**
DS of Meadow Drive	95580	7235.8	7325.1	7959.3	8682.9	9406.5	10130.1	10853.6	11577.2
DS of Trib 07100006001129	91535	14026.3	14191.0	15429.0	16831.6	18234.2	19636.9	21039.5	22442.1
US of Waterford Drive	88931	14326.8	14474.8	15759.5	17192.2	18624.8	20057.5	21490.2	22922.9
DS of NW 156th Street	82896	14798.7	14936.3	16278.5	17758.4	19238.3	20718.1	22198.0	23677.9
DS of Meredith Drive	76555	14821.8	14955.3	16304.0	17786.1	19268.3	20750.5	22232.7	23714.8
US of Douglas Pkwy/DS Little Walnut Conf.	68099	19813.8	20497.2	21795.2	23776.6	25758.0	27739.3	29720.7	31702.1
DS of NW 142nd Street	62251	19813.8	20497.2	21795.2	23776.6	25758.0	27739.3	29720.7	31702.1
US of NW 128th Street	52575	21564.1	22325.5	23720.5	25877.0	28033.4	30189.8	32346.2	34502.6
US of I-80	45199	21663.7	22443.3	23830.1	25996.5	28162.9	30329.2	32495.6	34662.0
US of NW 100th Street	36532	21743.3	22559.4	23917.7	26092.0	28266.3	30440.7	32615.0	34789.3
DS of NW 100th Street	35156	22238.5	23021.1	24462.3	26686.2	28910.0	31133.9	33357.7	35581.6
73rd Street	19844	25885.0	27204.6	28473.5	31062.1	33650.6	36239.1	38827.6	41416.1

*Phase 2 Percent Increase from Existing Atlas-14 from Phase 1.
*Yellow – Landuse Change Only
*Green – Climate Change Only
*Blue – Landuse and Climate Change

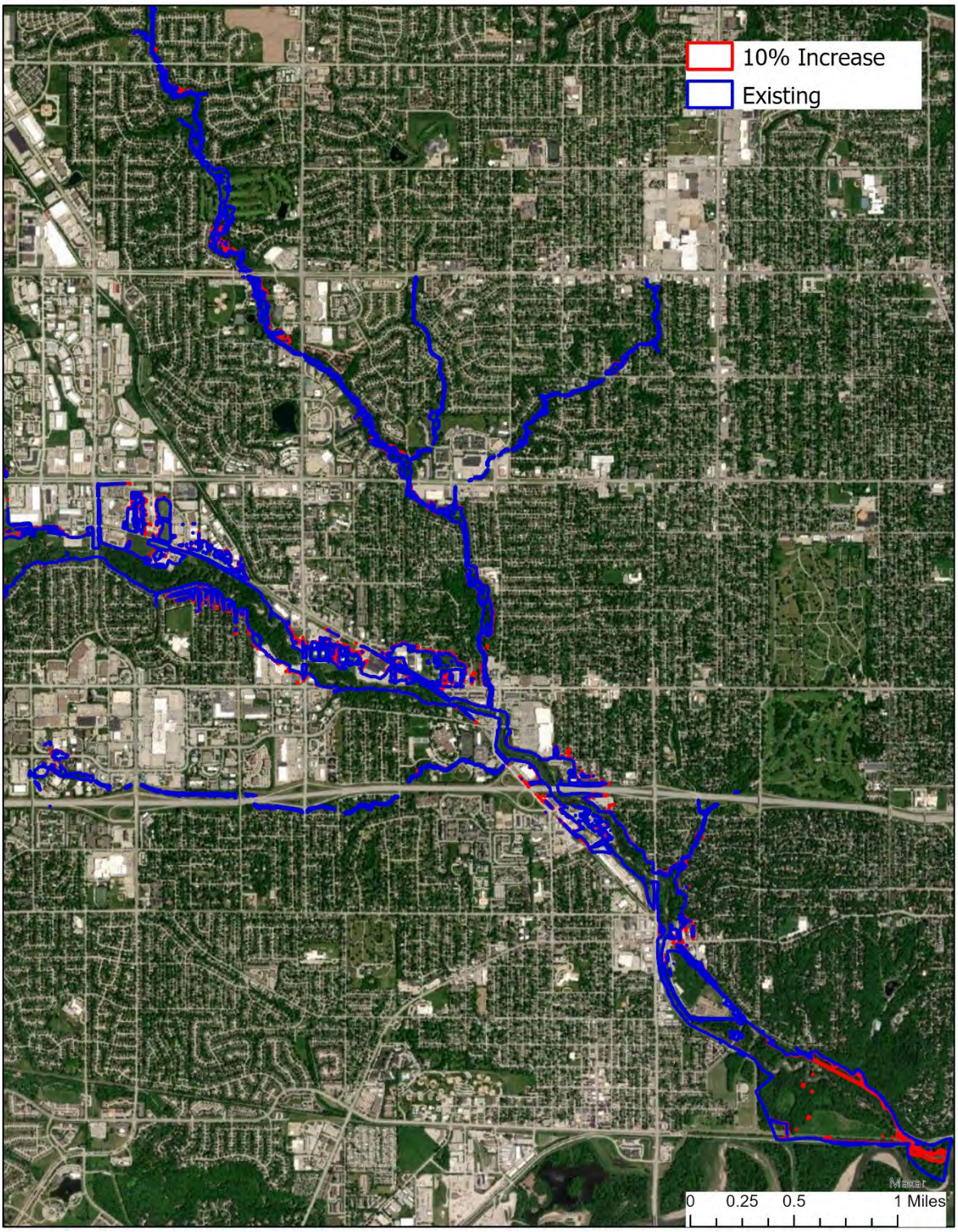

Figure 5-1: 10% Increase vs. Existing 5-Year Streamflow Southern Section

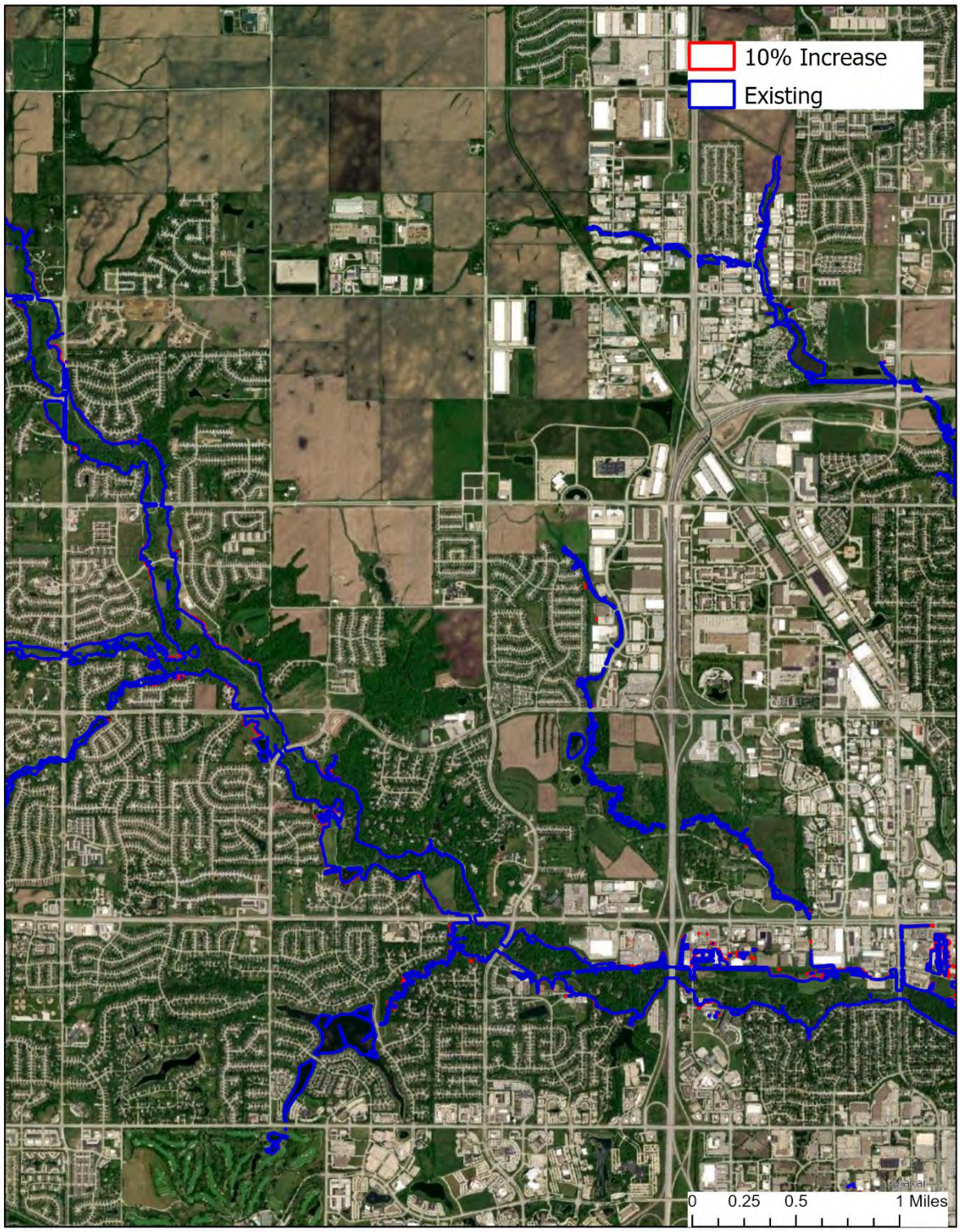

Figure 5-2: 10% Increase vs. Existing 5-Year Streamflow Middle Section

Figure 5-3: 10% Increase vs. Existing 5-Year Streamflow Western Section

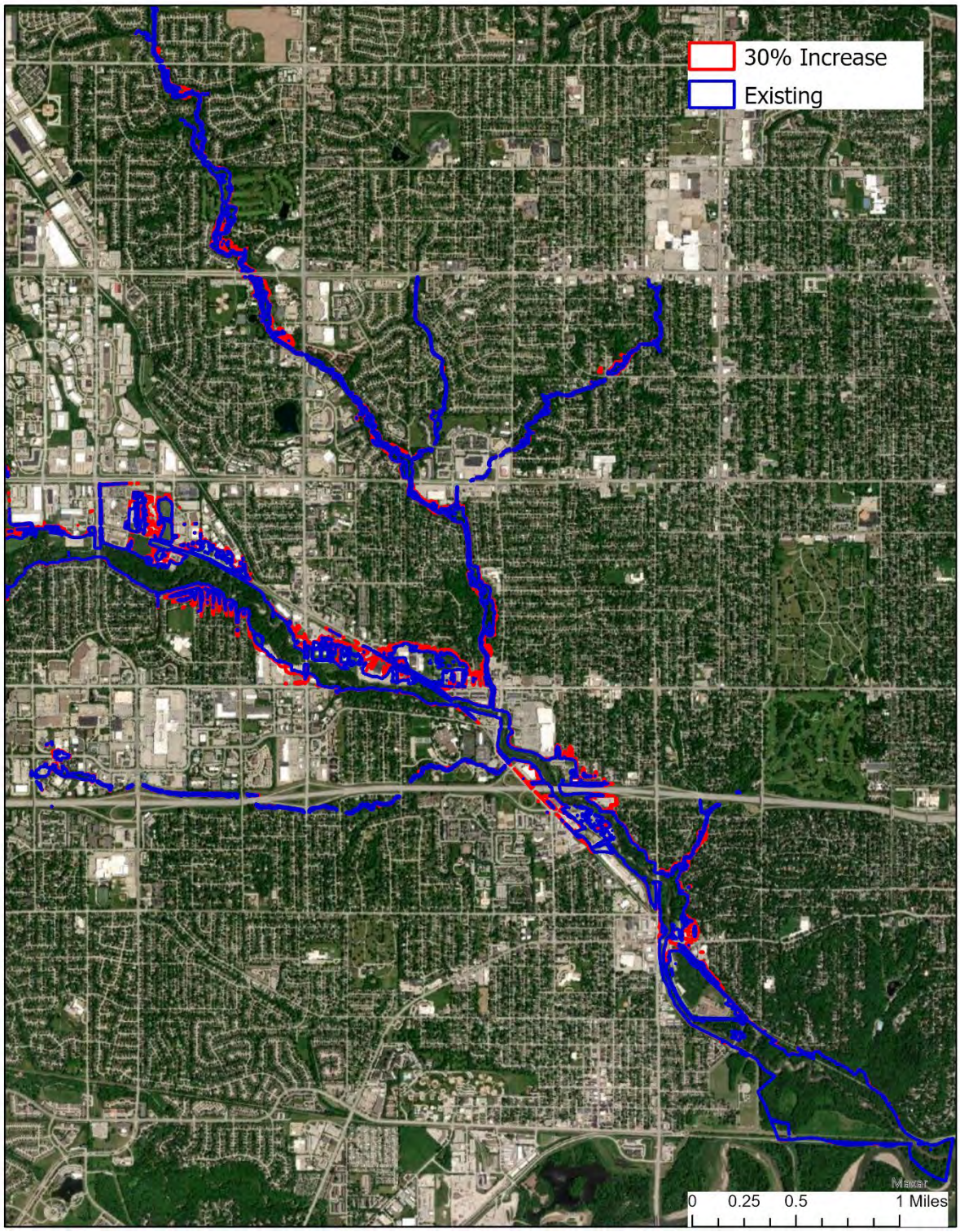

Figure 5-4: 30% Increase vs. Existing 5-Year Streamflow Southern Section

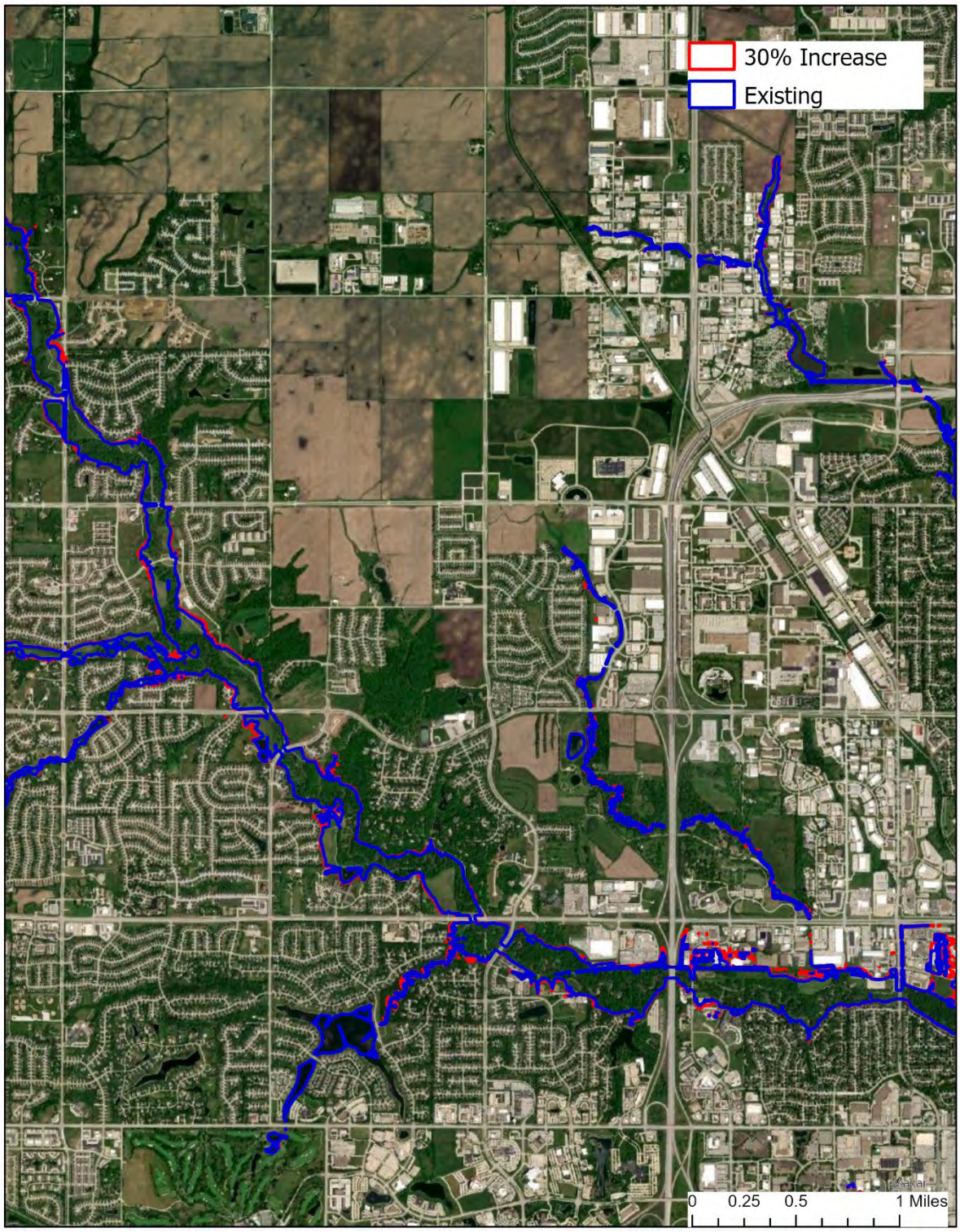

Figure 5-5: 30% Increase vs. Existing 5-Year Streamflow Middle Section

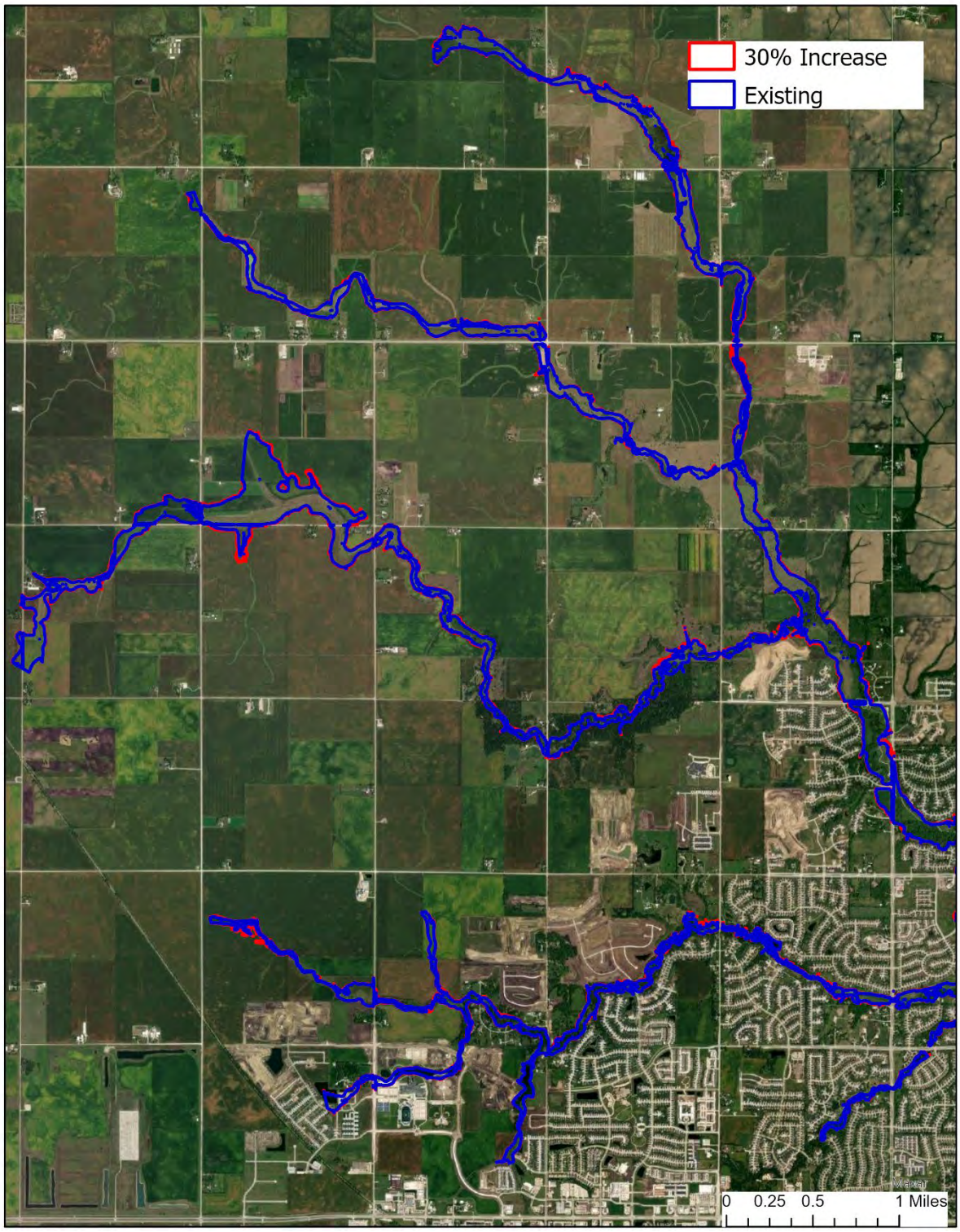

Figure 5-6: 30% Increase vs. Existing 5-Year Streamflow Western Section

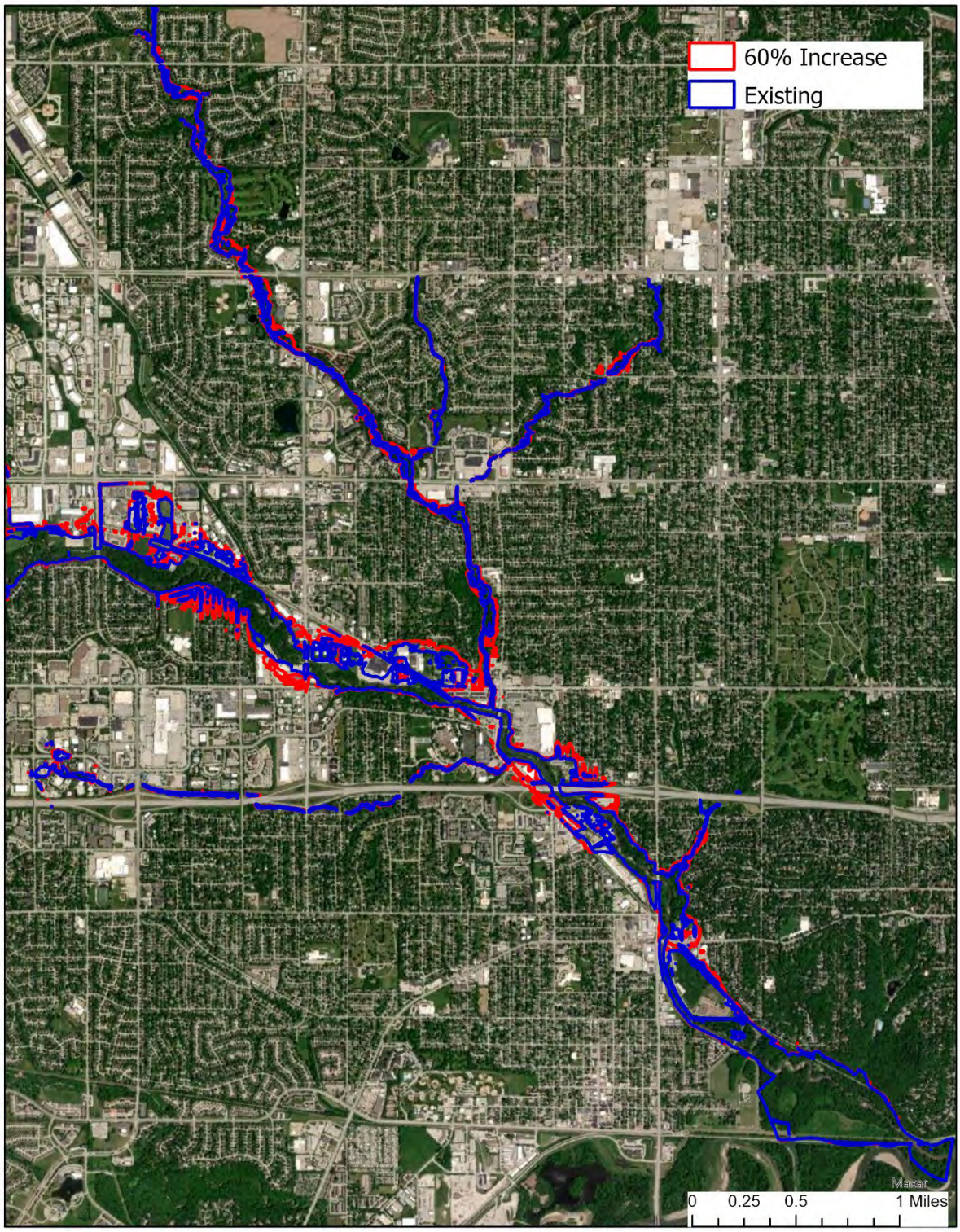

Figure 5-7: 60% Increase vs. Existing 5-Year Streamflow Southern Section

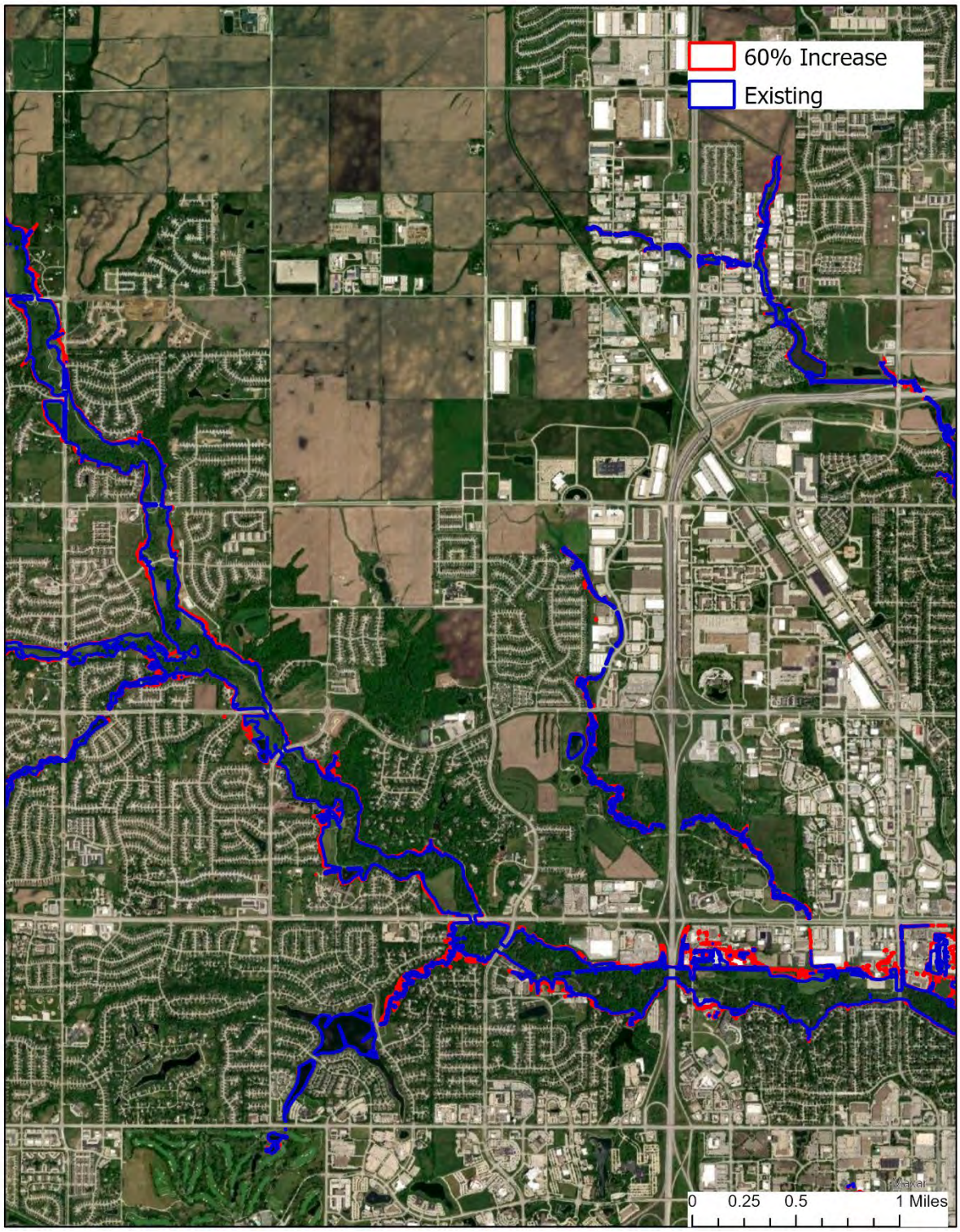

Figure 5-8: 60% Increase vs. Existing 5-Year Streamflow Middle Section

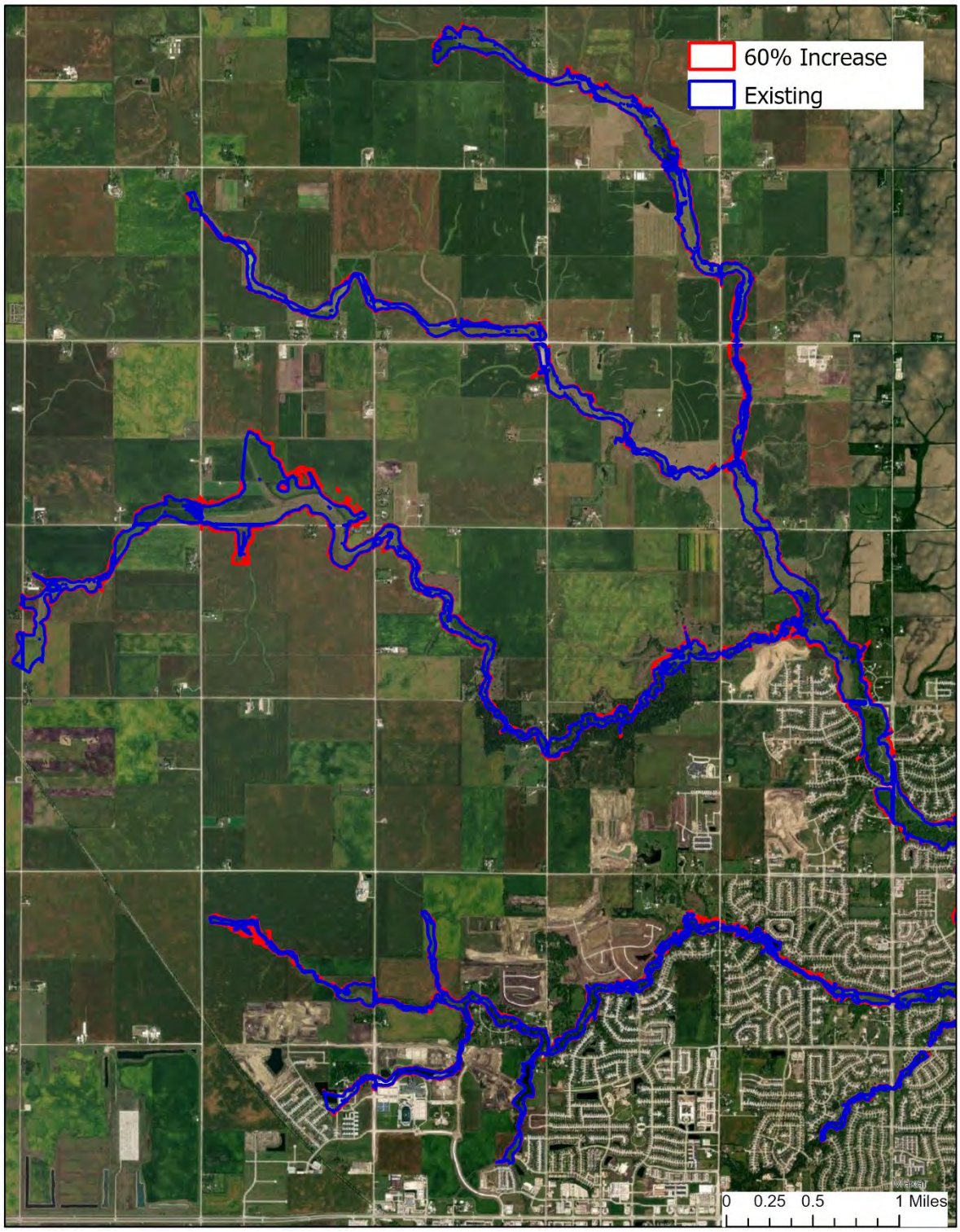

Figure 5-9: 60% Increase vs. Existing 5-Year Streamflow Western Section

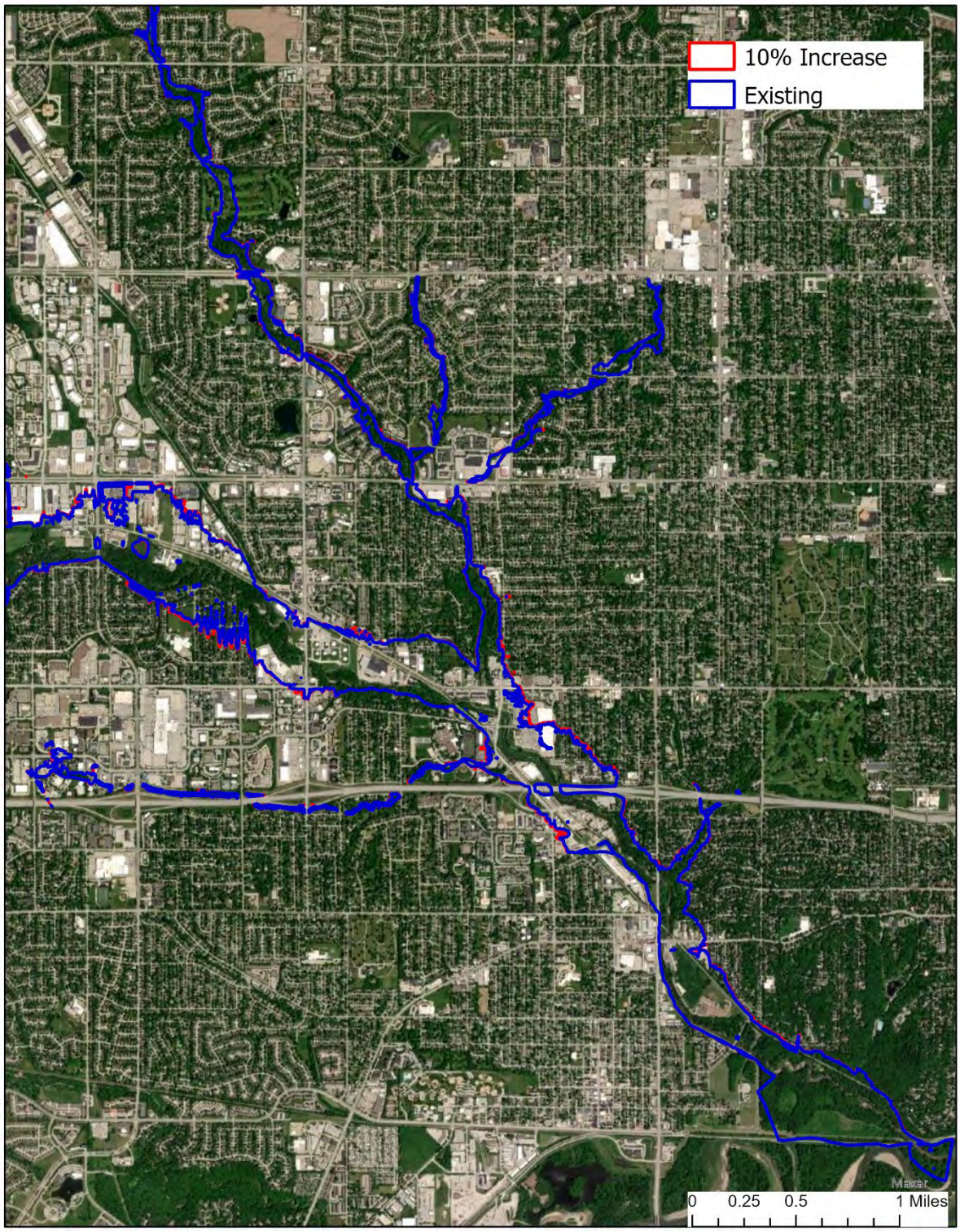

Figure 5-10: 10% Increase vs. Existing 100-Year Streamflow Southern Section

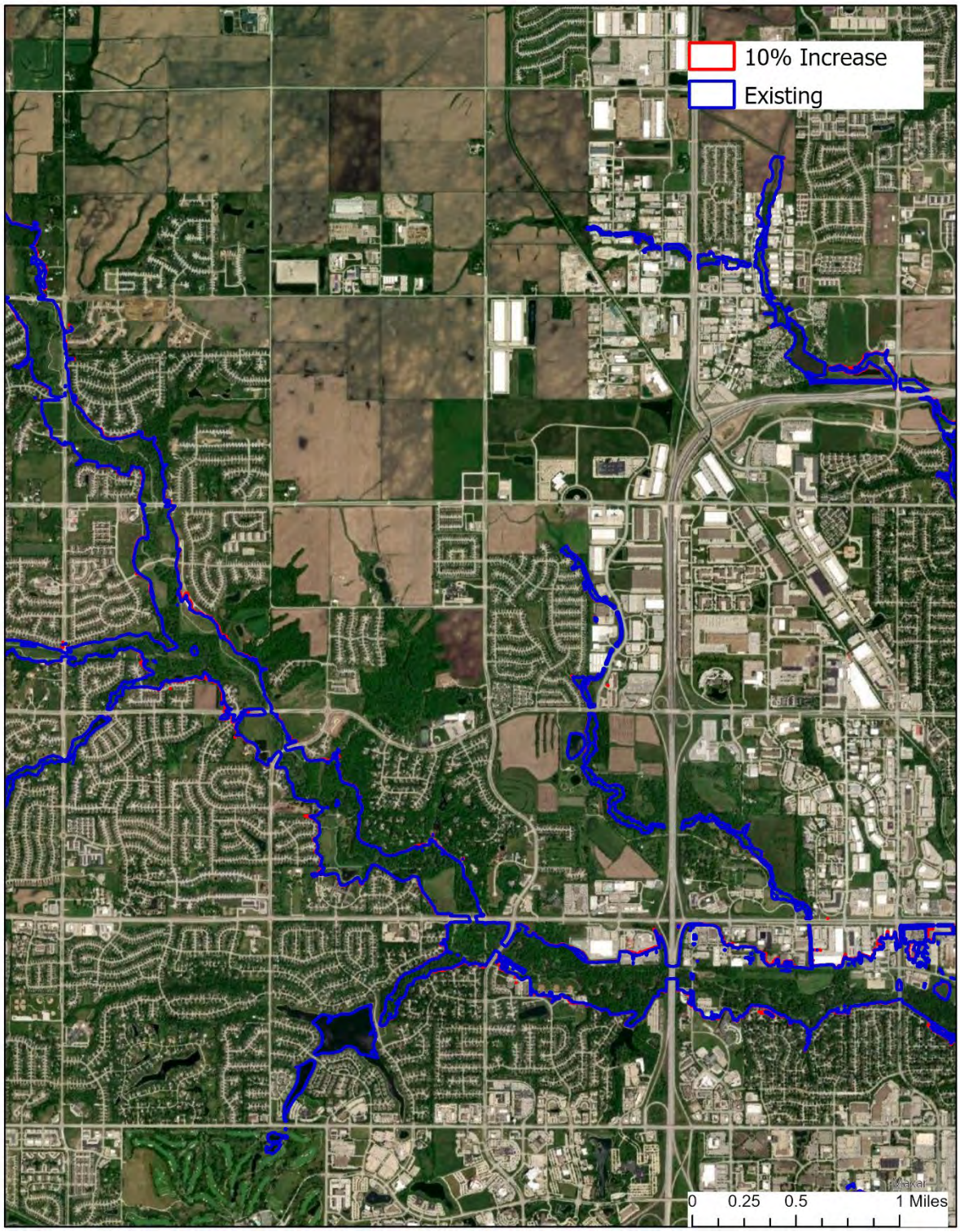

Figure 5-11: 10% Increase vs. Existing 100-Year Streamflow Middle Section

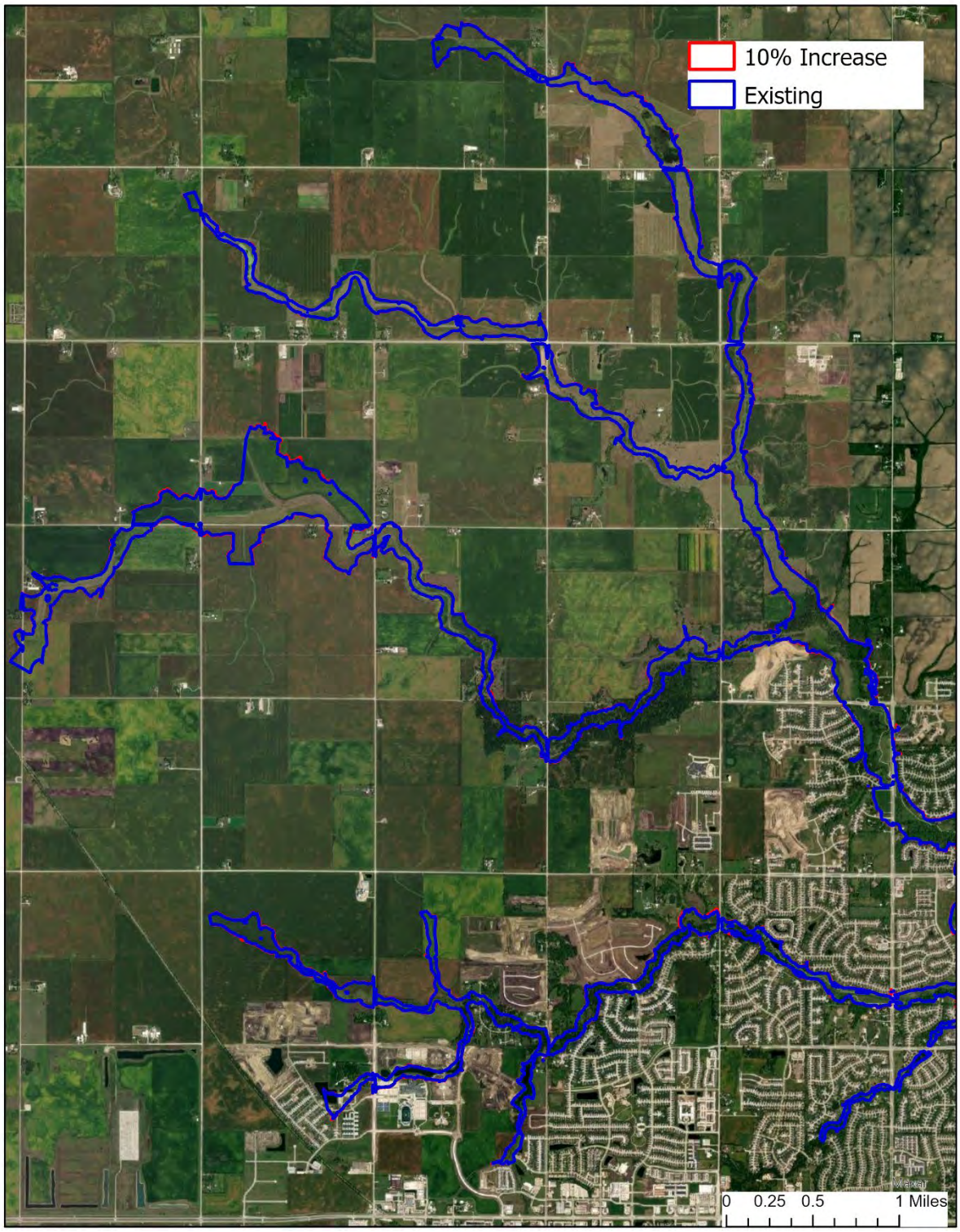

Figure 5-12: 10% Increase vs. Existing 100-Year Streamflow Western Section

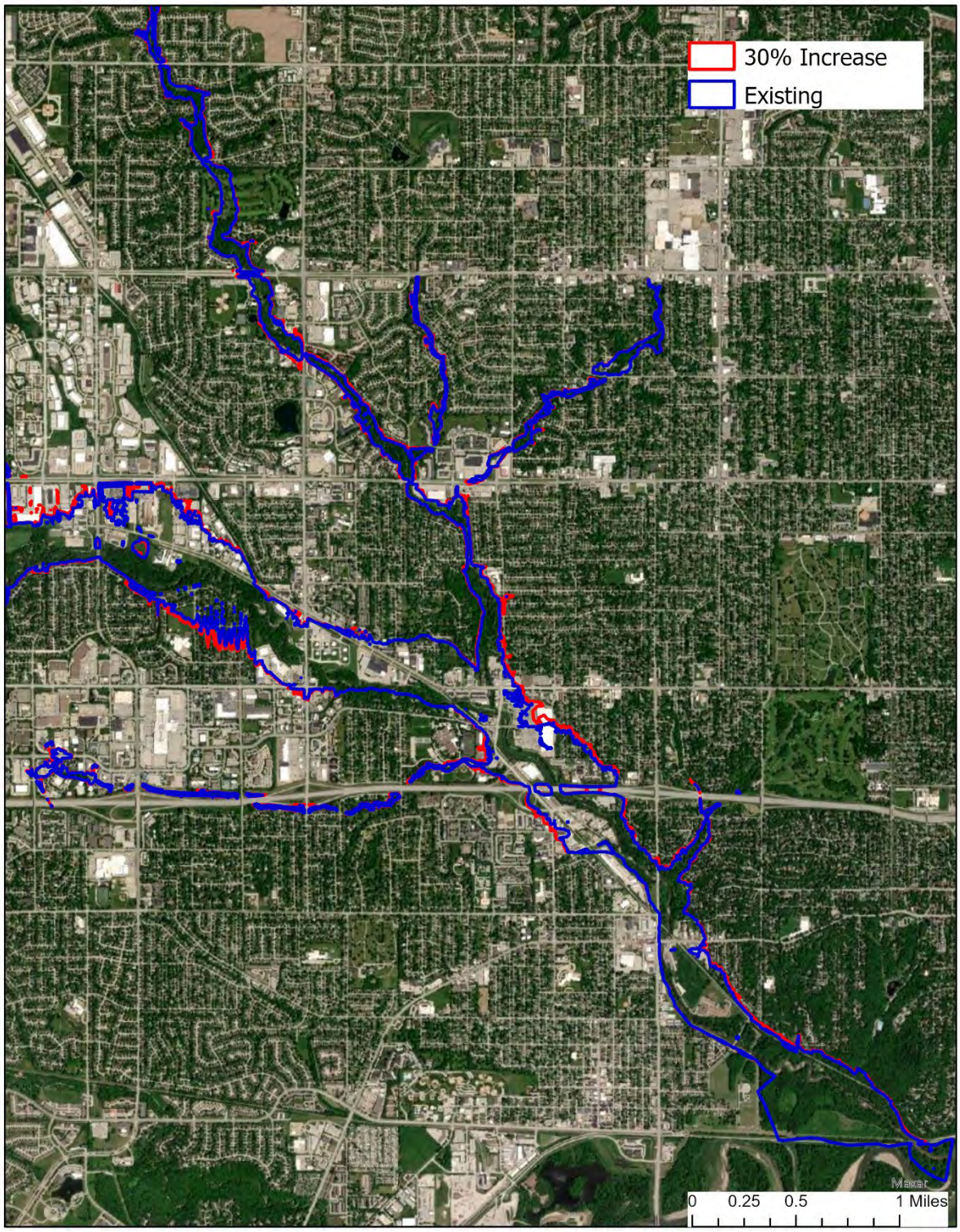

Figure 5-13: 30% Increase vs. Existing 100-Year Streamflow Southern Section

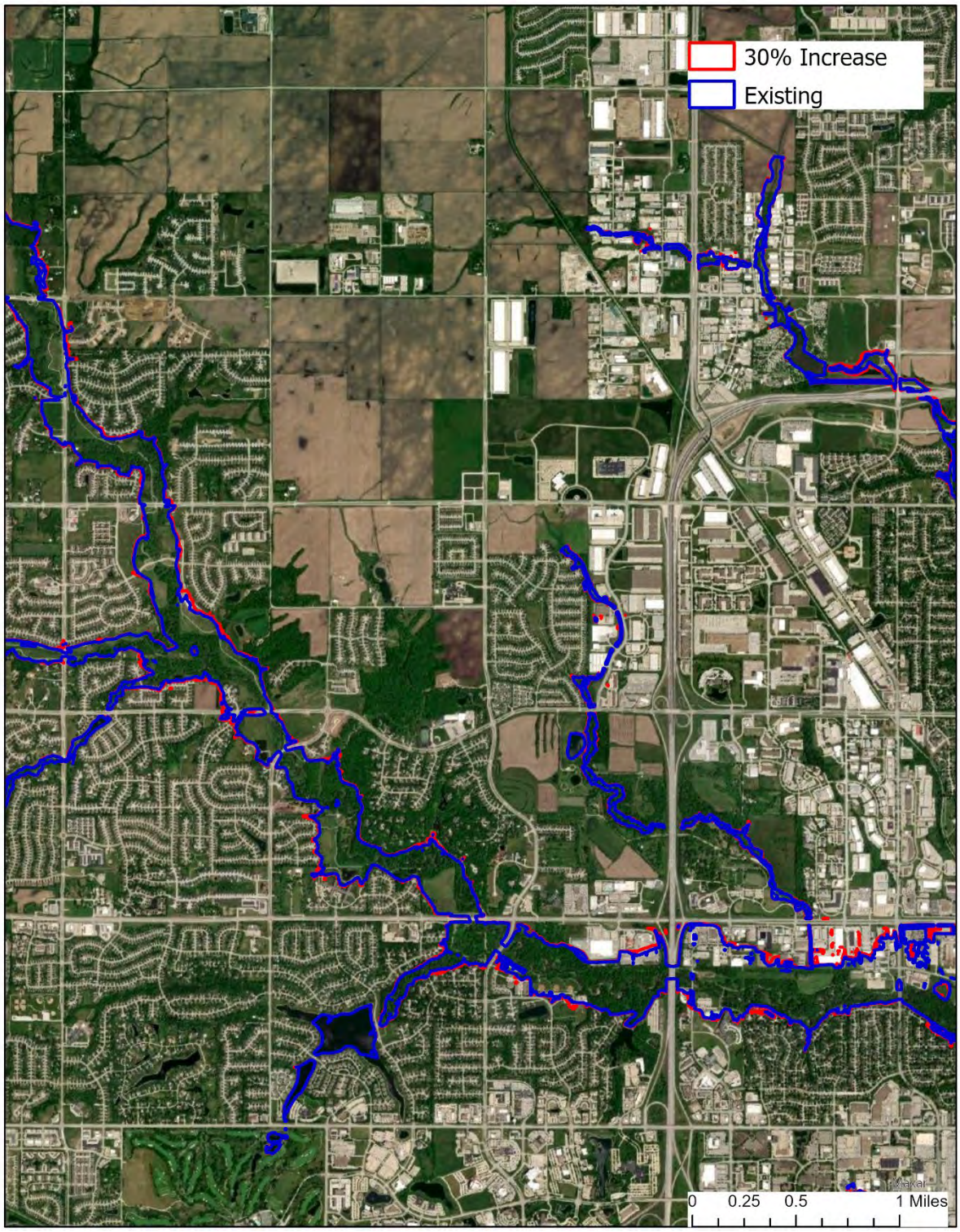

Figure 5-14: 30% Increase vs. Existing 100-Year Streamflow Middle Section

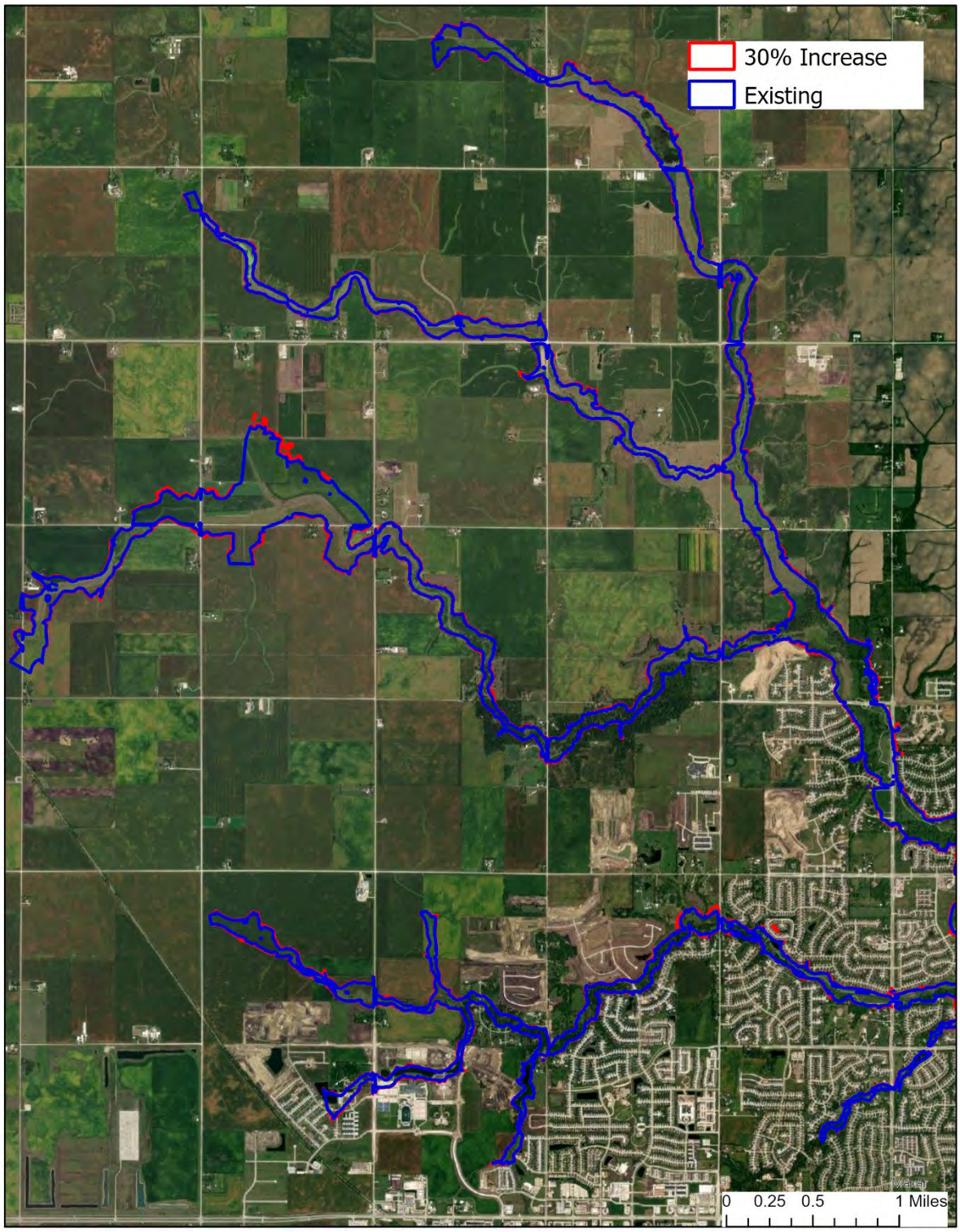

Figure 5-15: 30% Increase vs. Existing 100-Year Streamflow Western Section

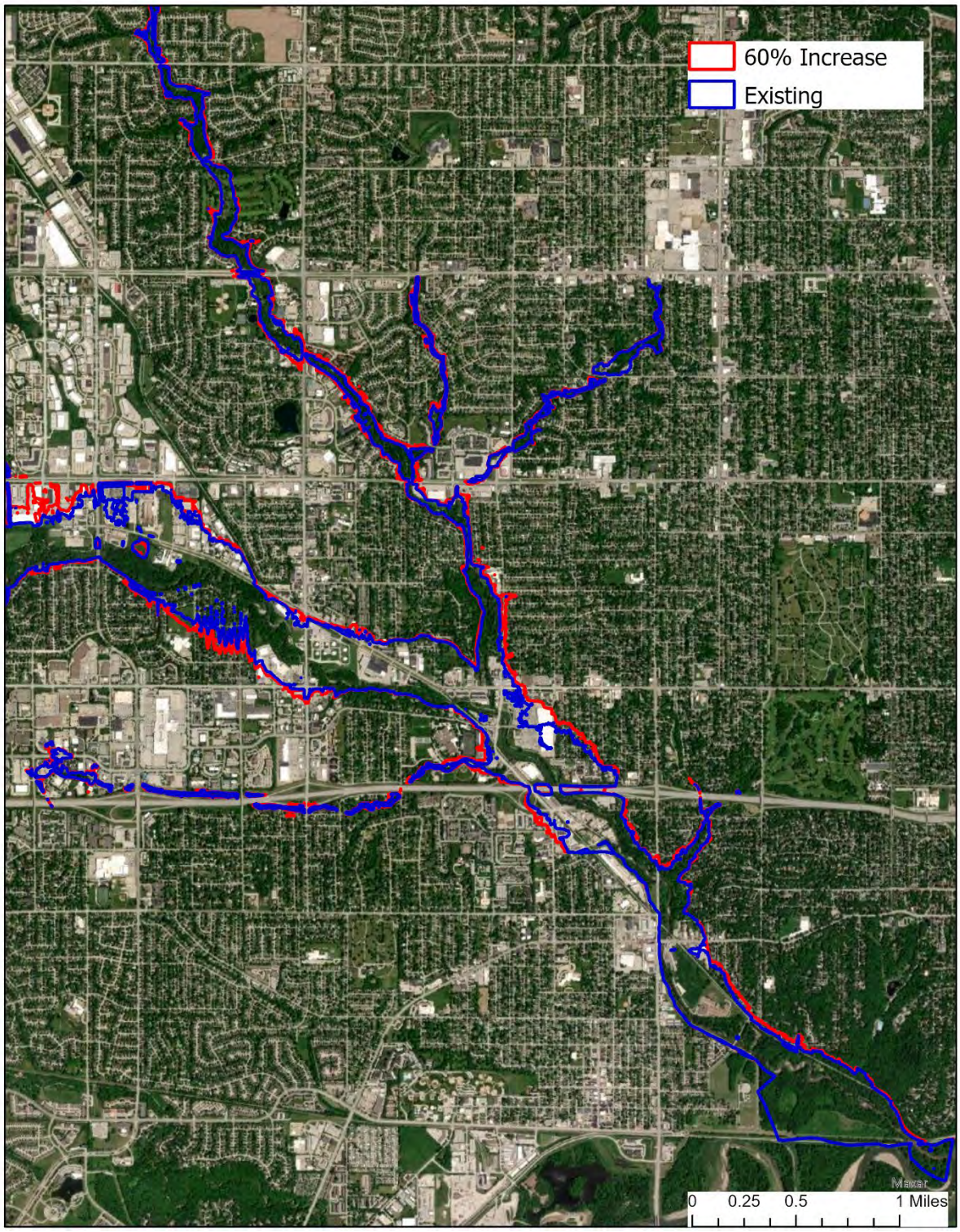

Figure 5-16: 60% Increase vs. Existing 100-Year Streamflow Southern Section

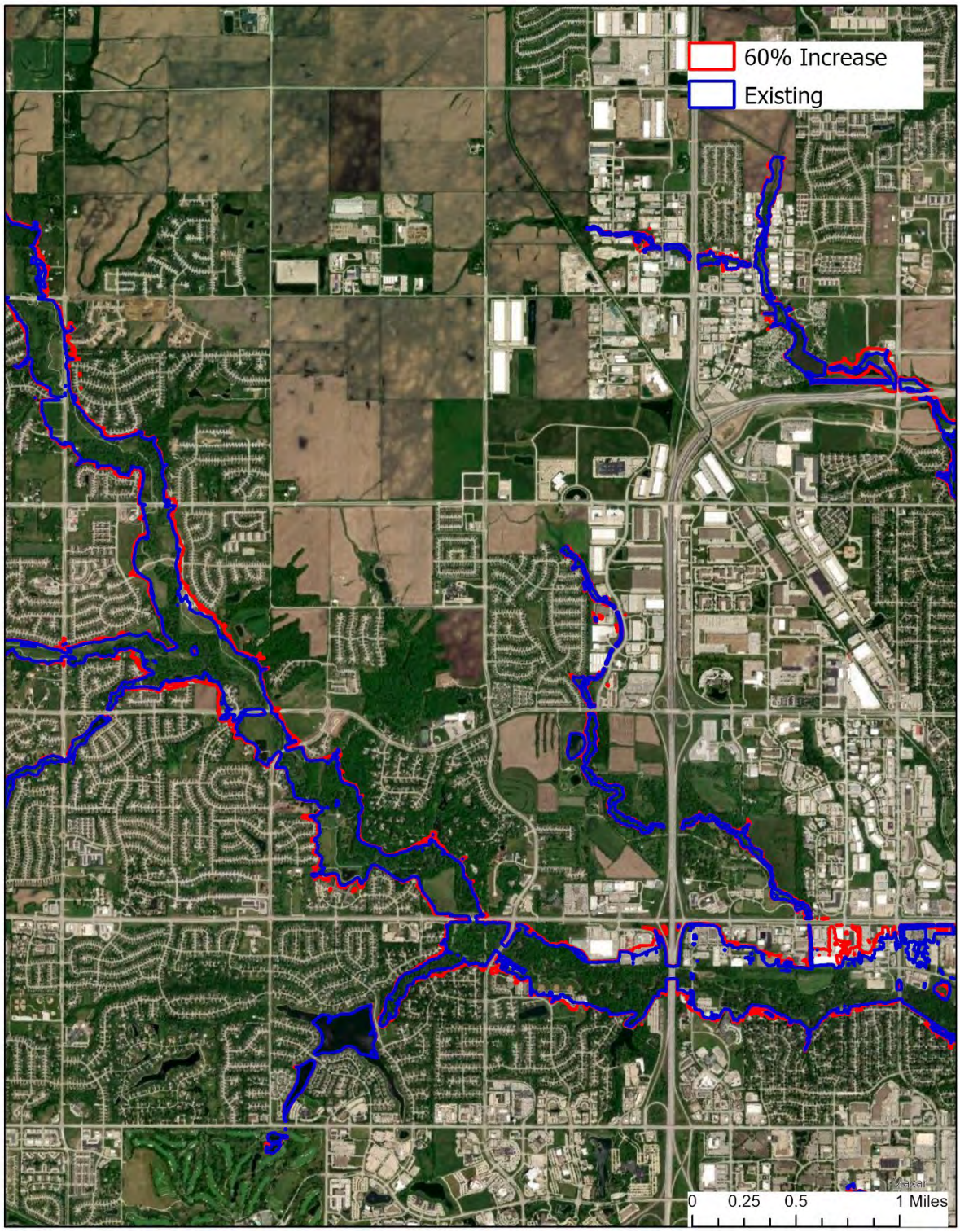

Figure 5-17: 60% Increase vs. Existing 100-Year Streamflow Middle Section

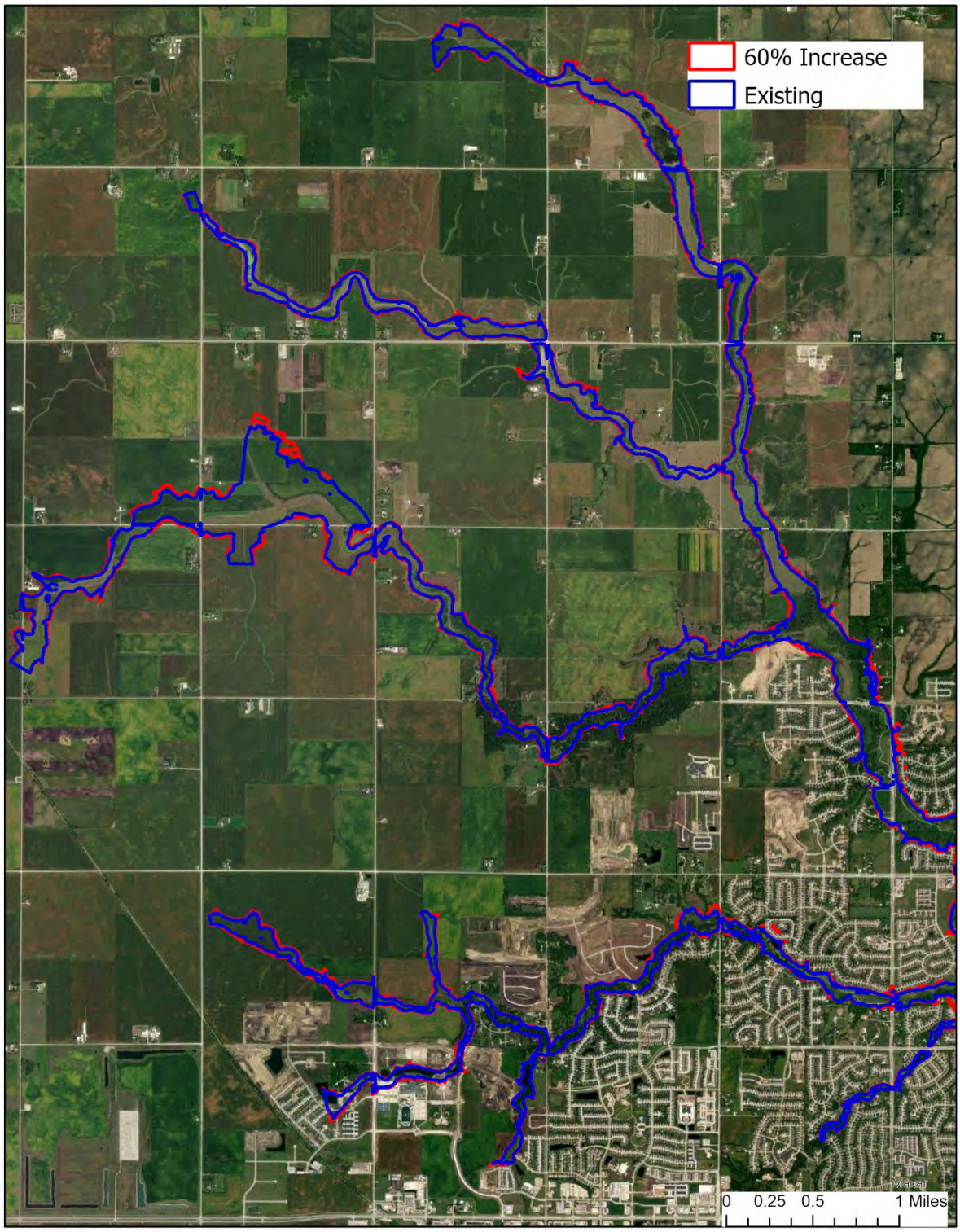

Figure 5-18: 60% Increase vs. Existing 100-Year Streamflow Western Section

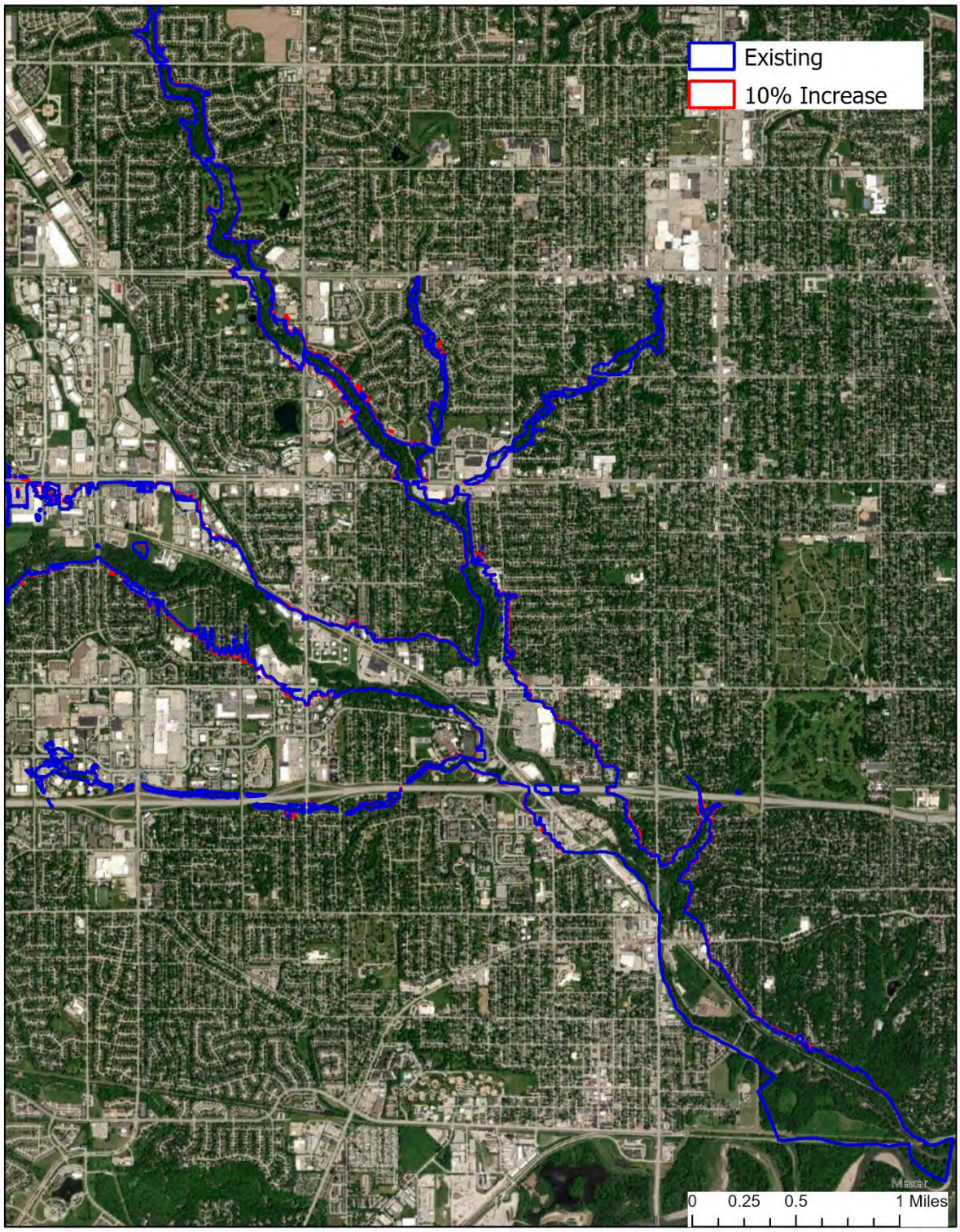

Figure 5-19: 10% Increase vs. Existing 1000-Year Streamflow Southern Section

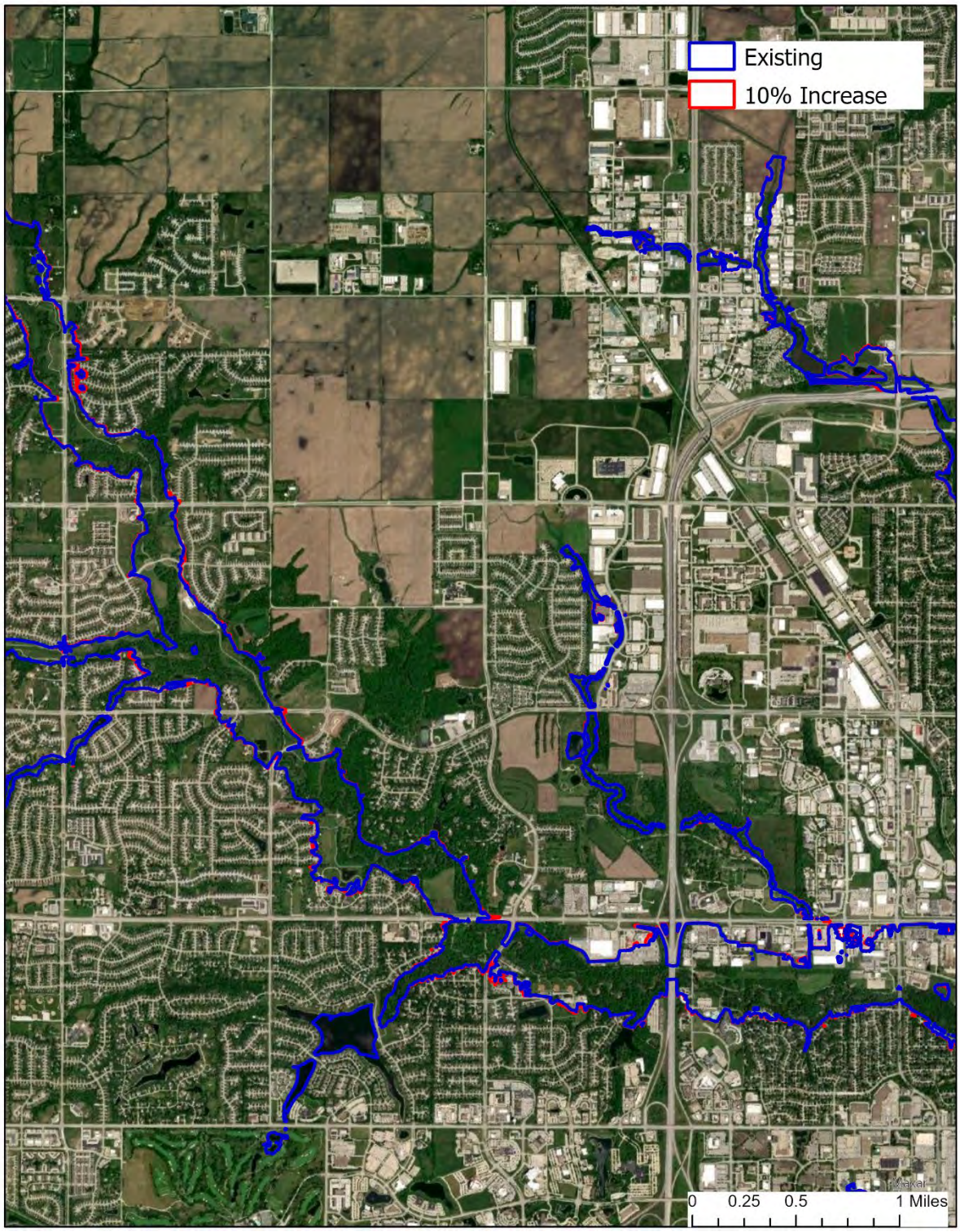

Figure 5-20: 10% Increase vs. Existing 1000-Year Streamflow Middle Section

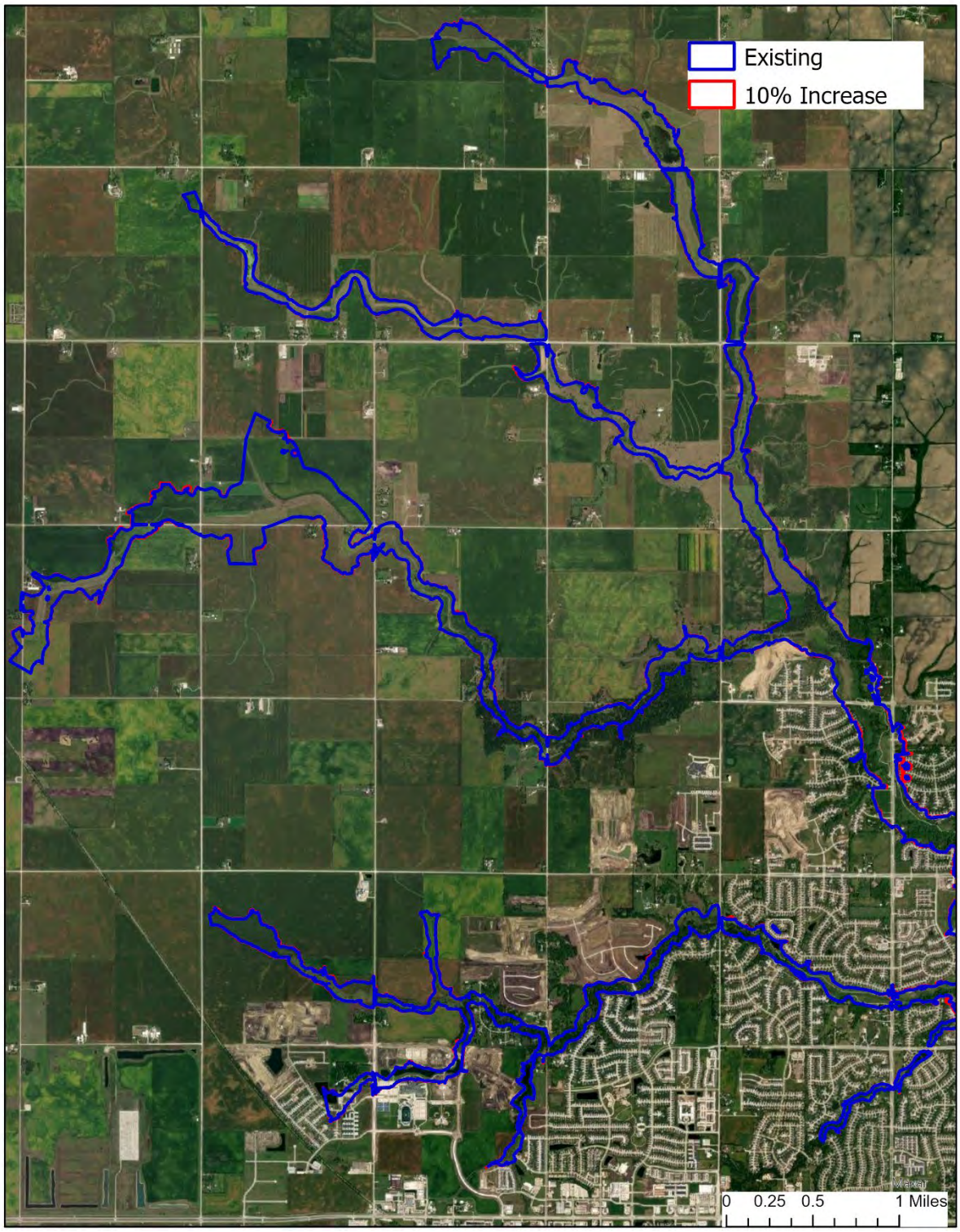

Figure 5-21: 10% Increase vs. Existing 1000-Year Streamflow Western Section

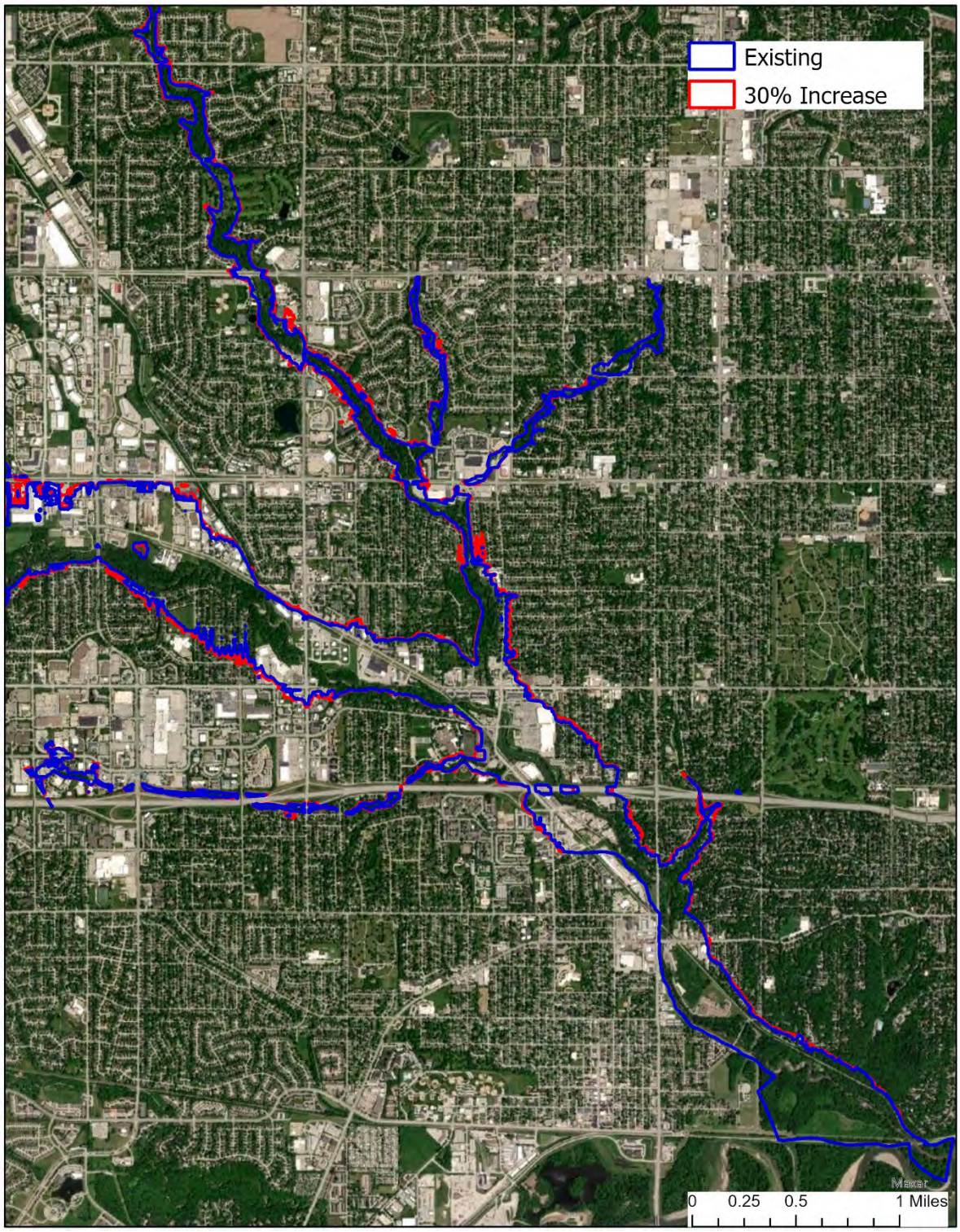

Figure 5-22: 30% Increase vs. Existing 1000-Year Streamflow Southern Section

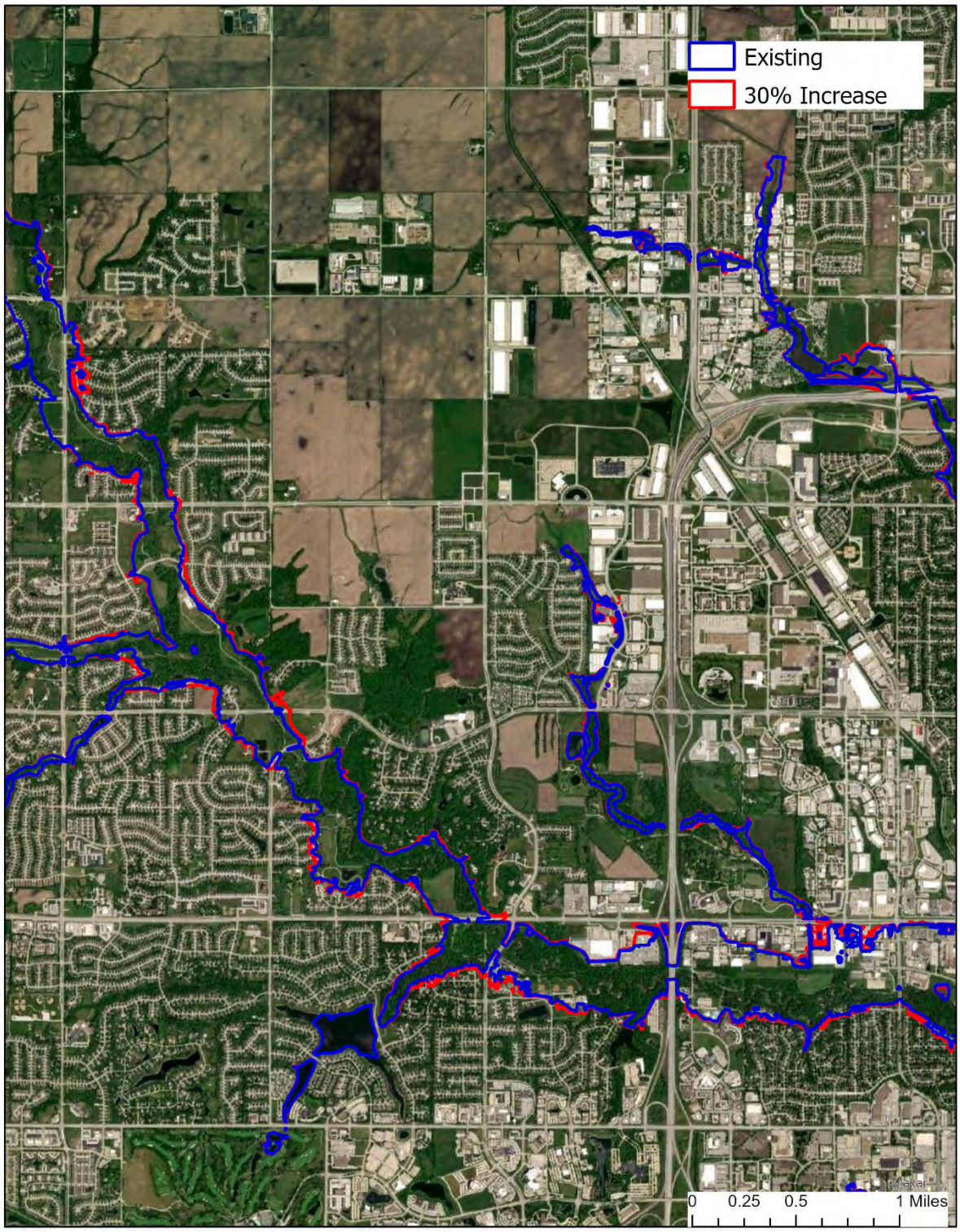

Figure 5-23: 30% Increase vs. Existing 1000-Year Streamflow Middle Section

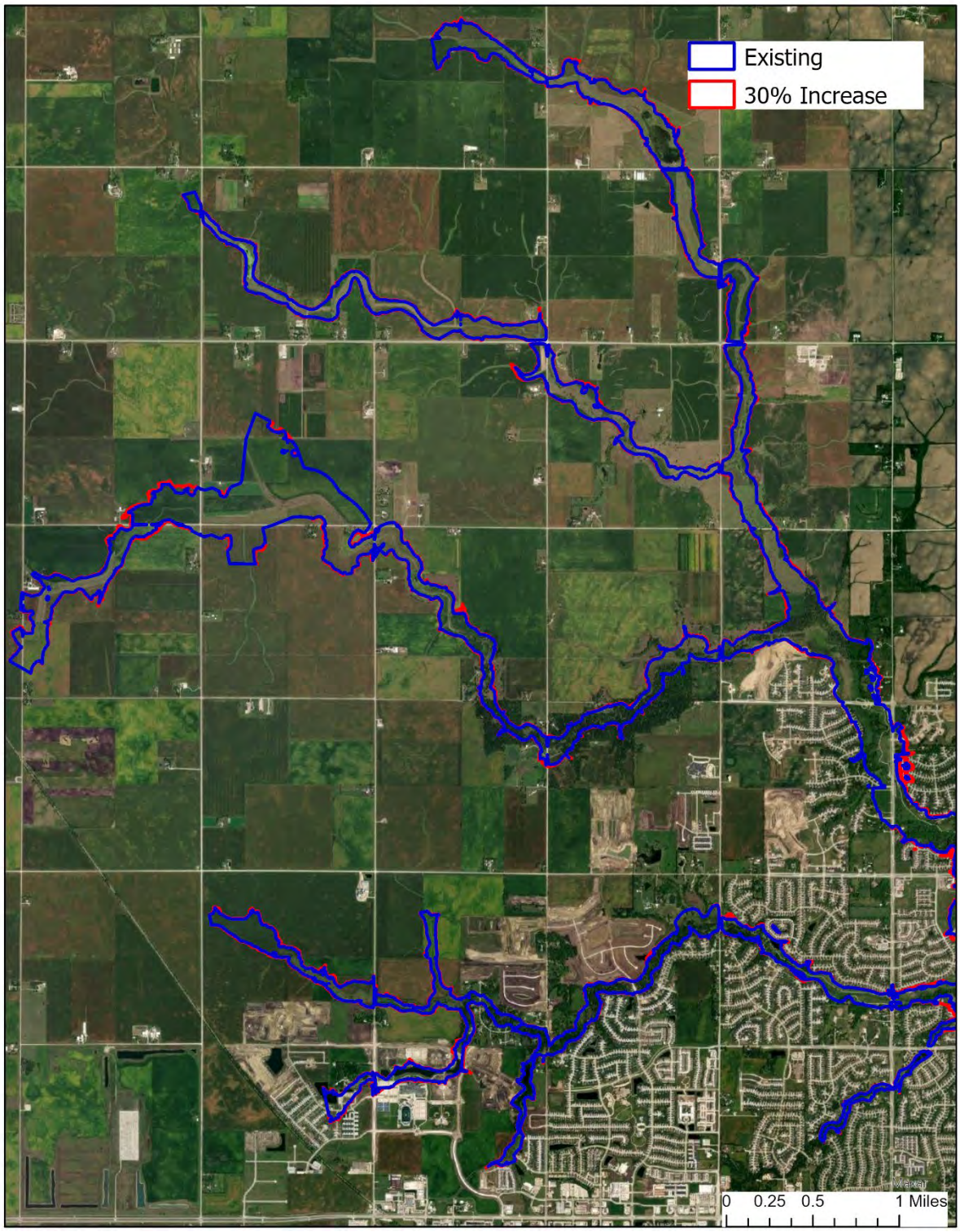

Figure 5-24: 30% Increase vs. Existing 1000-Year Streamflow Western Section

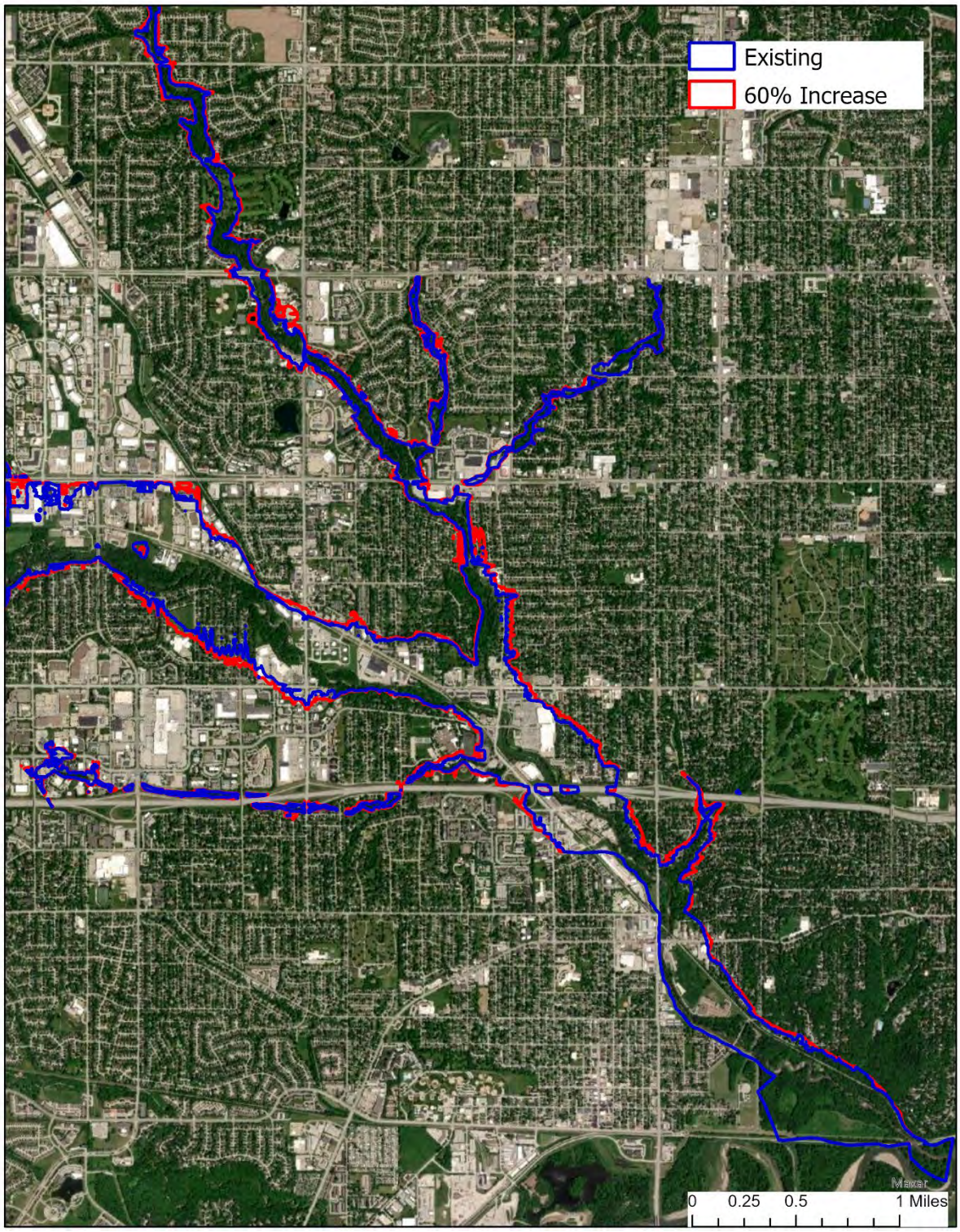

Figure 5-25: 60% Increase vs. Existing 1000-Year Streamflow Southern Section

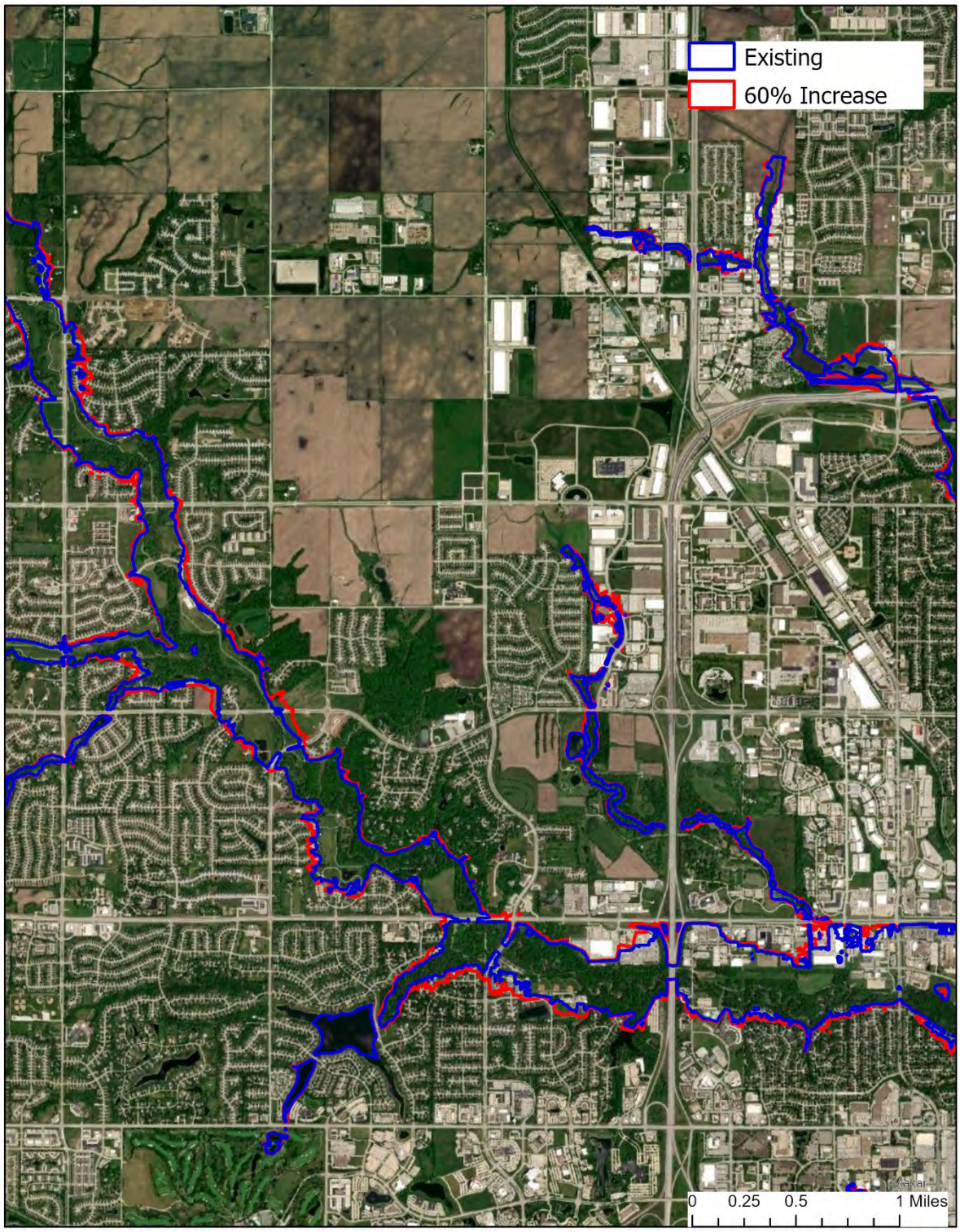

Figure 5-26: 60% Increase vs. Existing 1000-Year Streamflow Middle Section

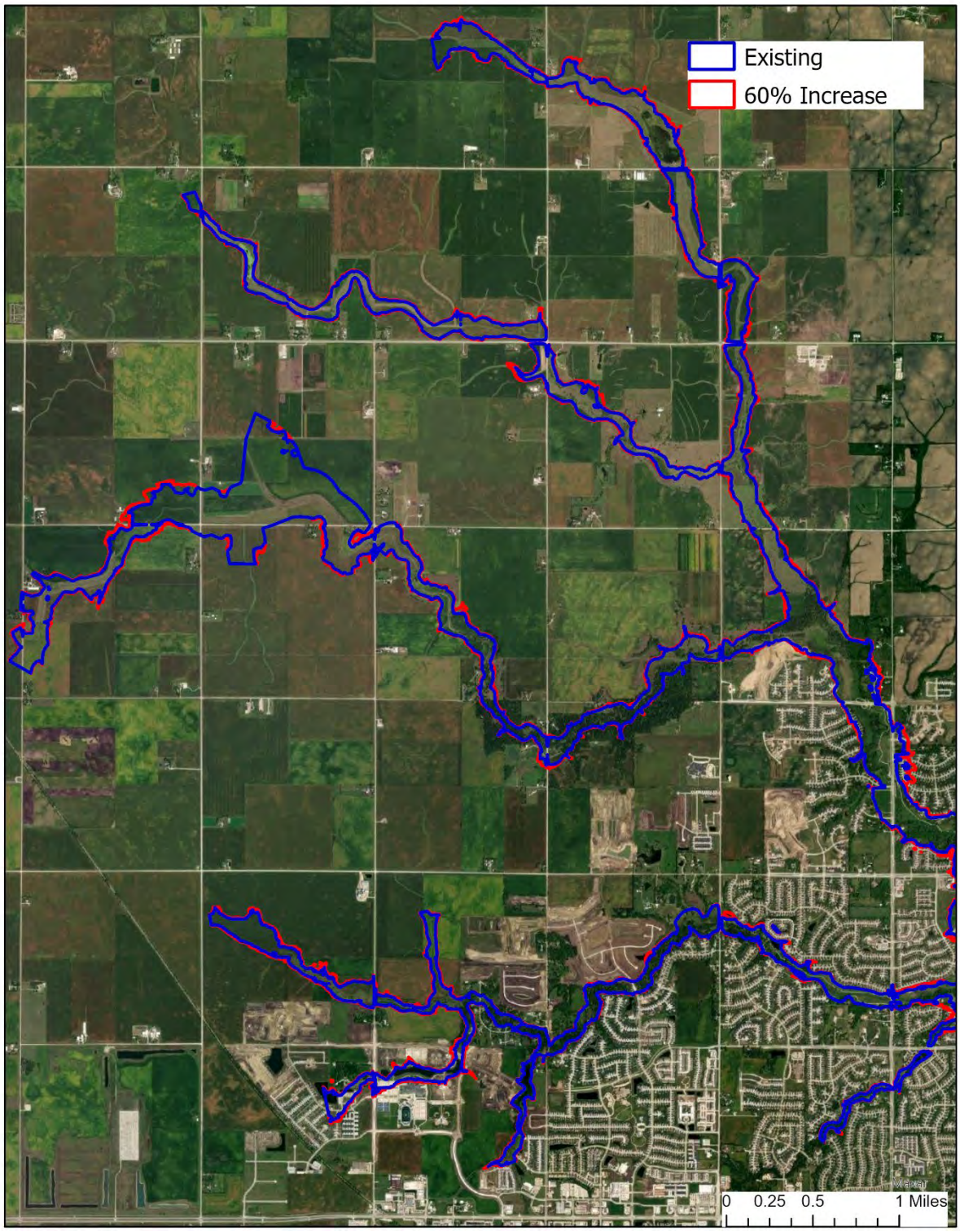

Figure 5-27: 60% Increase vs. Existing 1000-Year Streamflow Western Section

Appendix A: Qualitative Assessment References

Archfield, S.A., R.M. Hirsch, A. Viglione, and G. Bloschl (2016). Fragmented patterns of flood change across the United States. Geophysical Research Letters 43, 10,232-10,239.

Cai X, Wang D, Laurent R. (2009). *Impact of climate change on crop yield: A case study of rainfed corn in central Illinois.* Journal of Applied Meteorology and Climatology 48:1868-1881.

Chapman, JL. (2018). *Iowa Growing in Population Thanks to Urbanization.* School of Journalism and Mass Communications. University of Iowa. September 21, 2018.

Döll P, Zhang J. (2010). *Impact of climate change on freshwater ecosystems: a global-scale analysis of ecologically relevant river flow alterations.* Hydrol. Earth Syst. Sci. Discuss. 7:1305-1342.

Duan Q, Schaake J, Andreassian V, Franks S, Goteti G, Gupta HV, Gusev YM, Habets F, Hall A, Hay L, Hogue T, Huang M, Leavesley G, Liang X, Nasonova ON, Noilhan J, Oudin L, Sorooshian S, Wagener T, Wood EF. (2006). *Model Parameter Estimation Experiment. (MOPEX): An overview of science strategy and major results from the second and third workshops.* Journal of Hydrology 320: 3-17.

Eller, D. (2015). *Farming 101: What you need to know about tiling runoff.* Des Moines Register September 14, 2015.

Gao Y, Fu JS, Drake JB, Liu Y, Lamarque JF. (2012). *Projected changes of extreme weather events in the eastern United States based on a high resolution climate modeling system.* Environmental Research Letters 7.

Grundstein A. (2009). *Evaluation of climate change over the continental United States using a moisture index.* Climatic Change 93:103-115.

Hagemann S, Chen C, Clark DB, Folwell S, Gosling SN, Haddeland I, Hanasaki N, Heinke J, Ludwig F, Voss F, Wiltshire AJ. (2013). *Climate change impact on available water resources obtained using multiple global climate and hydrology models.* Earth System Dynamics 4:129-144.

Jha M, Arnold JG, Gassman PW, Giorgi F, Gu RR. (2006). *Climate change sensitivity assessment on Upper Mississippi River Basin streamflows using SWAT.* Journal of the American Water Resources Association 42:997-1016.

Joetzjer E, Douville H, Delire C, Ciais P, Decharme B, Tyteca S. (2013). *Hydrologic benchmarking of meteorological drought indices at interannual to climate change timescales: A case study over the Amazon and Mississippi river basins.* Hydrology and Earth System Sciences 17:4885-4895.

Johnson SL, Stefan HG. (2006). *Indicators of climate warming in Minnesota: Lake ice covers and snowmelt runoff.* Climatic Change 75:421-453.

Kunkel KE, Liang X-Z, Zhu J. (2010). *Regional climate model projections and uncertainties of U.S. summer heat waves.* Journal of Climate 23:4447-4458.

Mauget SA. (2004). *Low frequency streamflow regimes over the central United States: 1939-1998.* Climatic Change 63:121-144.

McRoberts DB, Nielsen-Gammon JW. (2011). *A new homogenized climate division precipitation dataset for analysis of climate variability and climate change.* Journal of Applied Meteorology and Climatology 50:1187-1199.

Norvell K. (2016). *D.M. metro is Iowa's fastest-growing urban area.* Des Moines Register March 24, 2016.

Palecki MA, Angel JR, Hollinger SE. (2005). *Storm precipitation in the United States. Part I: Meteorological characteristics.* Journal of Applied Meteorology 44:933-946.

Pryor SC, Howe JA, Kunkel KE. (2009). *How spatially coherent and statistically robust are temporal changes in extreme precipitation in the contiguous USA?* International Journal of Climatology 29:31-45.

Pryor, S. C., D. Scavia, C. Downer, M. Gaden, L. Iverson, R. Nordstrom, J. Patz, and G. P. Robertson. (2014). Ch. 18: Midwest. *Climate Change Impacts in the United States: The Third National Climate Assessment*, J. M. Melillo, Terese (T.C.). Richmond, and G. W. Yohe, Eds., U.S. Global Change Research Program, 418-440. doi:10.7930/J0J1012N.

Qian T, Dai A, Trenberth KE. (2007). *Hydroclimatic trends in the Mississippi River basin from 1948 to 2004.* Journal of Climate 20:4599-4614.

Scherer M, Diffenbaugh N. (2014). *Transient twenty-first century changes in daily-scale temperature extremes in the United States.* Climate Dynamics 42:1383-1404.

Schmidt M. (2020). *Modernizing Agricultural Drainage Law in Iowa.* Iowa Environmental Council. https://www.iaenvironment.org/webres/File/Modernizing%20Ag%20Drainage%20Law%20in%20Iowa.pdf

Schuster ZT, Potter KW, Liebl DS. (2012). *Assessing the effects of climate change on precipitation and flood damage in Wisconsin.* Journal of Hydrologic Engineering 17:888-894.

Schwartz MD, Ault TR, Betancourt JL. (2013). *Spring onset variations and trends in the continental United States: Past and regional assessment using temperature-based indices.* International Journal of Climatology 33:2917-2922.

Tebaldi C. (2006). *Going to the Extremes: An Intercomparison of Model-Simulated Historical and Future Changes in Extreme Events.* Climate Change 79:185-211. 2006

U.S. Army Corps of Engineers. (June 2000). Upper Mississippi River and Illinois Waterway Cumulative Effects Study, Volume I: Geomorphic Assessment.

(2015). *Recent US Climate Change and Hydrology Literature Applicable to US Army Corps of Engineers Missions – Water Resources Region 07, Upper Mississippi*. Civil Works Technical Report, CWTS-2015-13, Washington, DC.

(2017). Engineering Technical Letter 1100-2-3: *Guidance for Detection of Nonstationarities in Annual Maximum Discharges*.

(2018). Engineering and Construction Bulletin 2018-14: *Guidance for Incorporating Climate Change Impacts to Inland Hydrology in Civil Works Studies, Designs, and Project*s.

USACE Climate Hydrology Assessment Tool
http://corpsmapu.usace.army.mil/cm_apex/f?p=313:2:0::NO

USACE Non-Stationarity Detection Tool http://corpsmapu.usace.army.mil/cm_apex/f?p=257:2:0::NO

USACE Time Series Toolbox https://climate-test.sec.usace.army.mil/tst_app/

USACE Vulnerability Assessment Tool https://maps.crrel.usace.army.mil/apex/f?p=201

Villarini G, Smith JA, Vecchi GA. (2013). *Changing Frequency of Heavy Rainfall over the Central United States.* Journal of Climate 26:351-357.

Wang D, Hejazi M, Cai X, Valocchi AJ. (2011). *Climate change impact on meteorological, agricultural, and hydrological drought in central Illinois.* Water Resources Research 47.

Wang H, Schubert S, Suarez M, Chen J, Hoerling M, Kumar A, Pegion P. (2009). *Attribution of the seasonality and regionality in climate trends over the United States during 1950-2000.* Journal of Climate 22:2571-2590.

Wang J, Zhang X. (2008). *Downscaling and projection of winter extreme daily precipitation over North America.* Journal of Climate 21:923-937.

Westby RM, Lee Y-Y, Black RX. (2013). *Anomalous temperature regimes during the cool season: Long-term trends, low-frequency mode modulation, and representation in CMIP5 simulations.* Journal of Climate 26:9061-9076.

Wilson CO, Weng Q. (2011). *Simulating the impacts of future land use and climate changes on surface water quality in the Des Plaines River watershed, Chicago Metropolitan Statistical Area, Illinois.* Science of the Total Environment 409:4387-4405.

Wu Y, Liu S, Abdul-Aziz OI. (2012). *Hydrological effects of the increased CO2 and climate change in the Upper Mississippi River Basin using a modified SWAT.* Climatic Change 110:977-1003.

Appendix B: Climate Models Precipitation Data

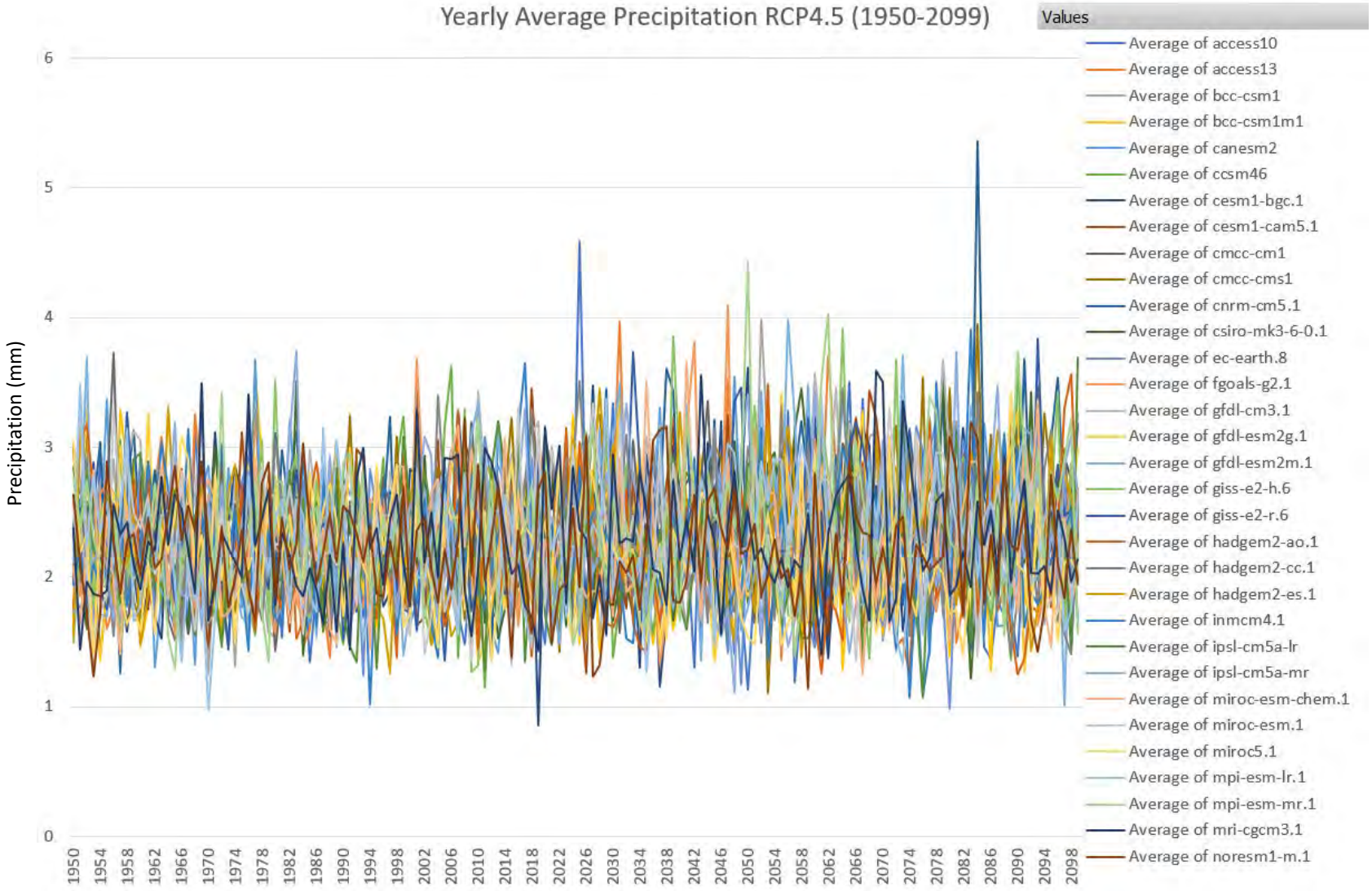

Figure B-1: Yearly Average Precipitation RCP 4.5 (1950-2099)

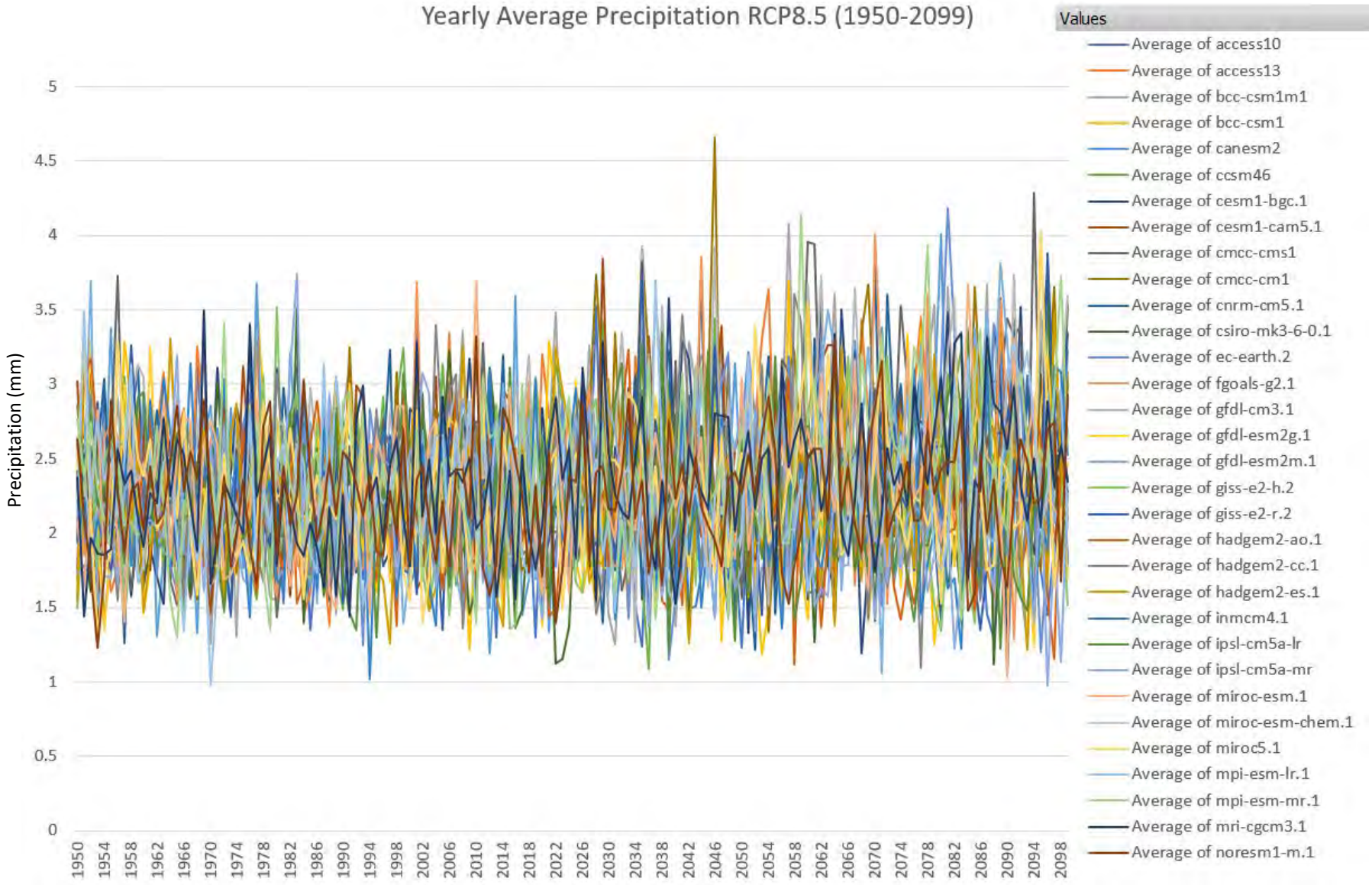

Figure B-2: Yearly Average Precipitation RCP 8.5 (1950-2099)

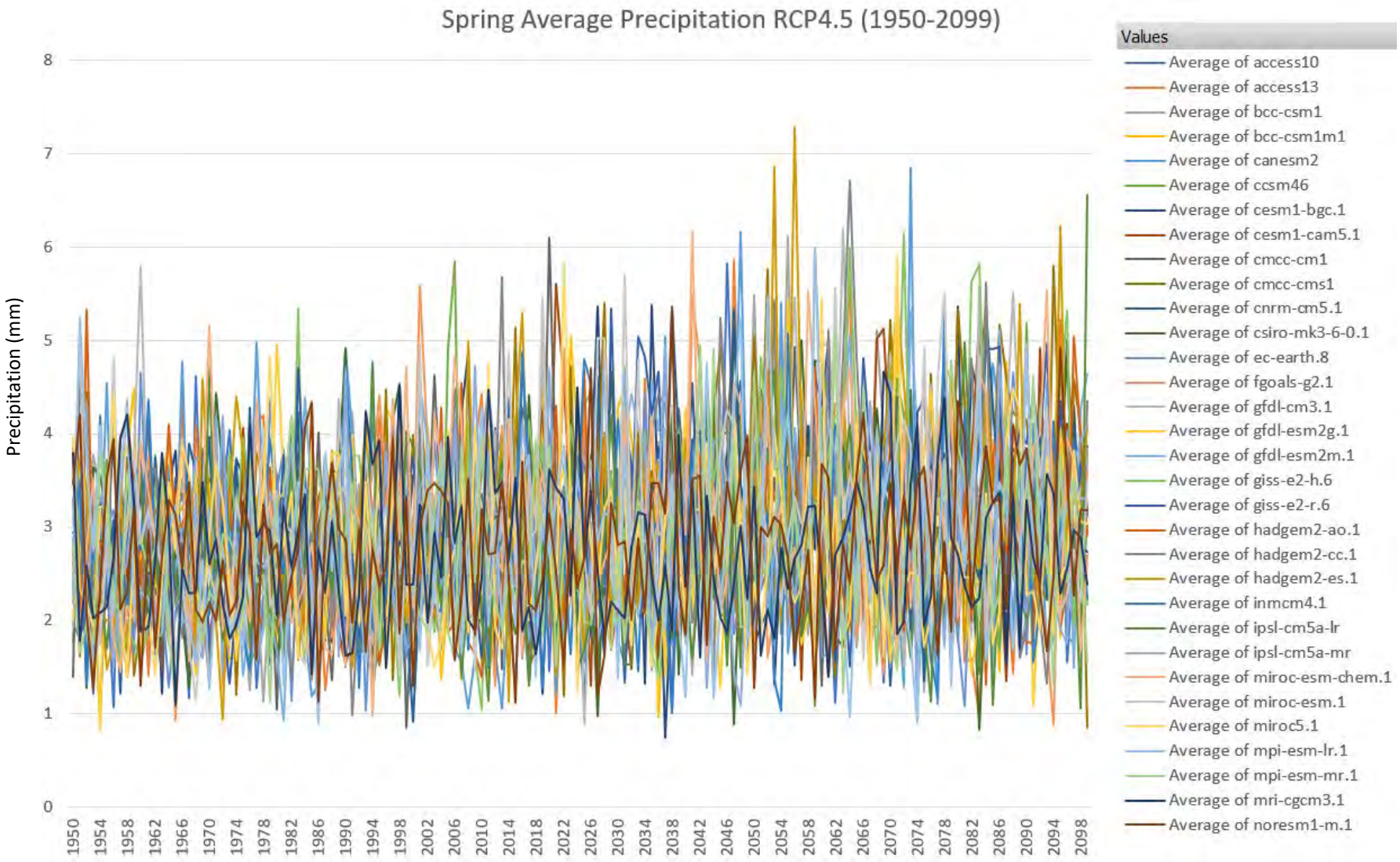

Figure B-3: Spring Average Precipitation RCP 4.5 (1950-2099)

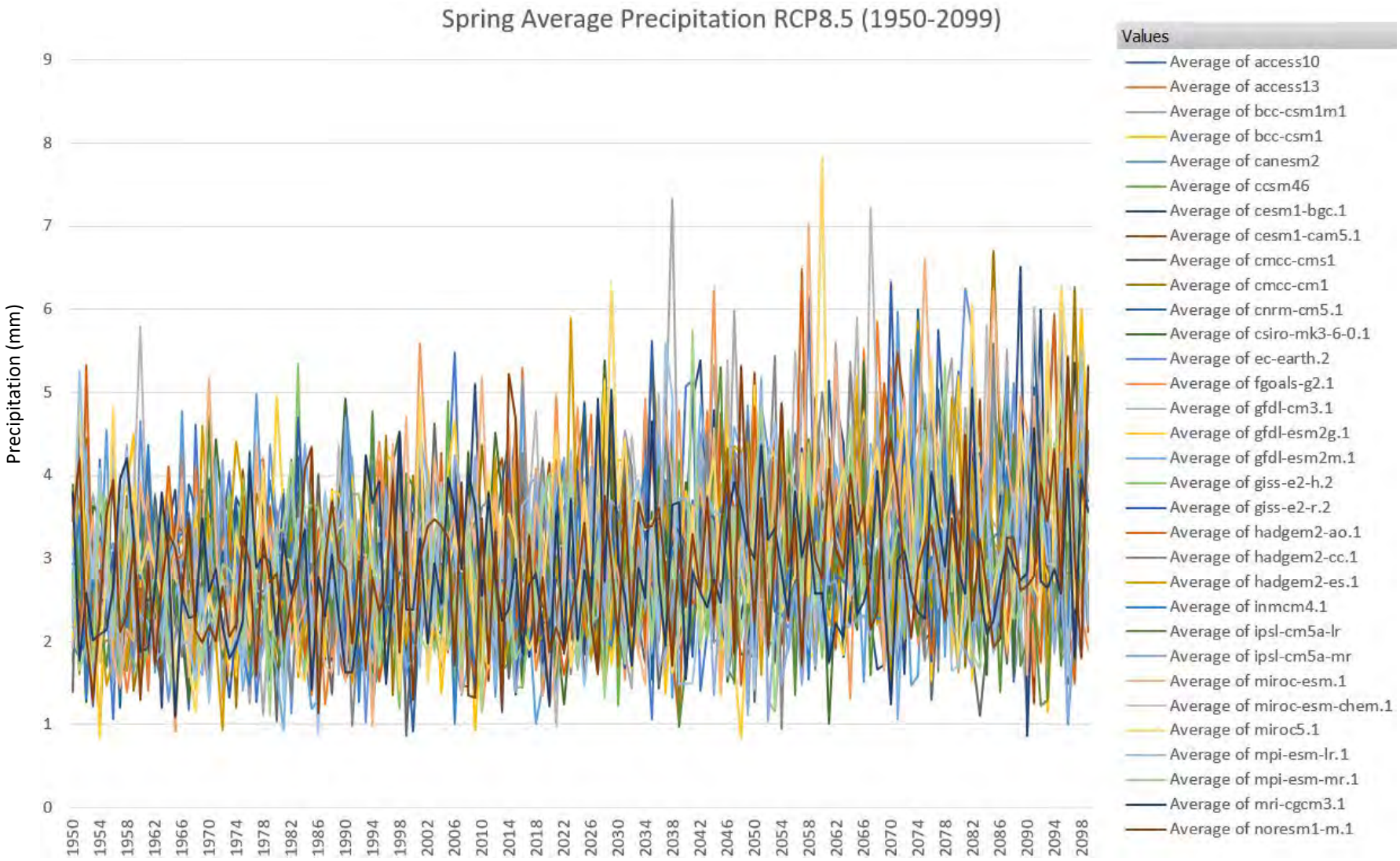

Figure B-4: Spring Average Precipitation RCP 8.5 (1950-2099)

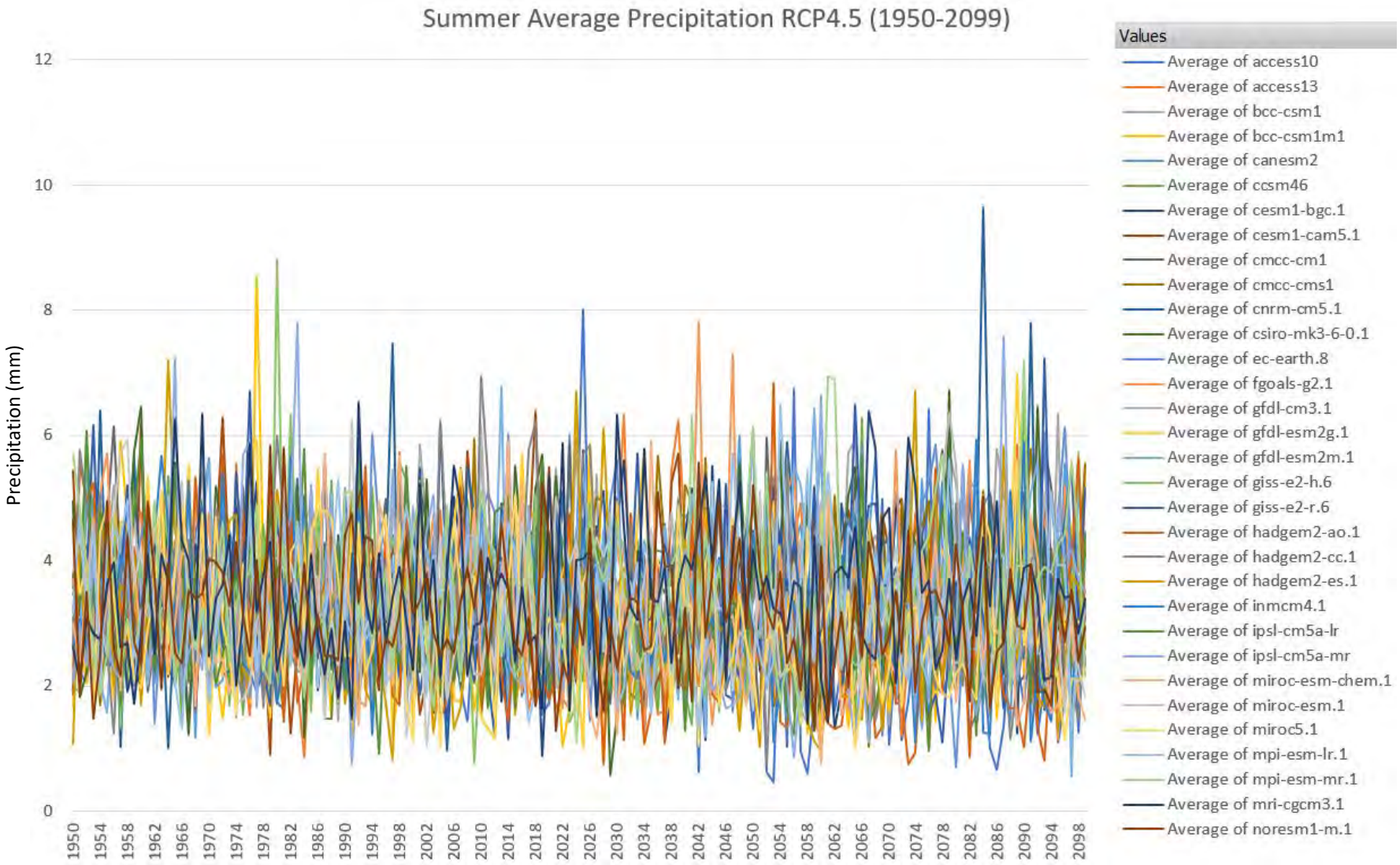

Figure B-5: Summer Average Precipitation RCP 4.5 (1950-2099)

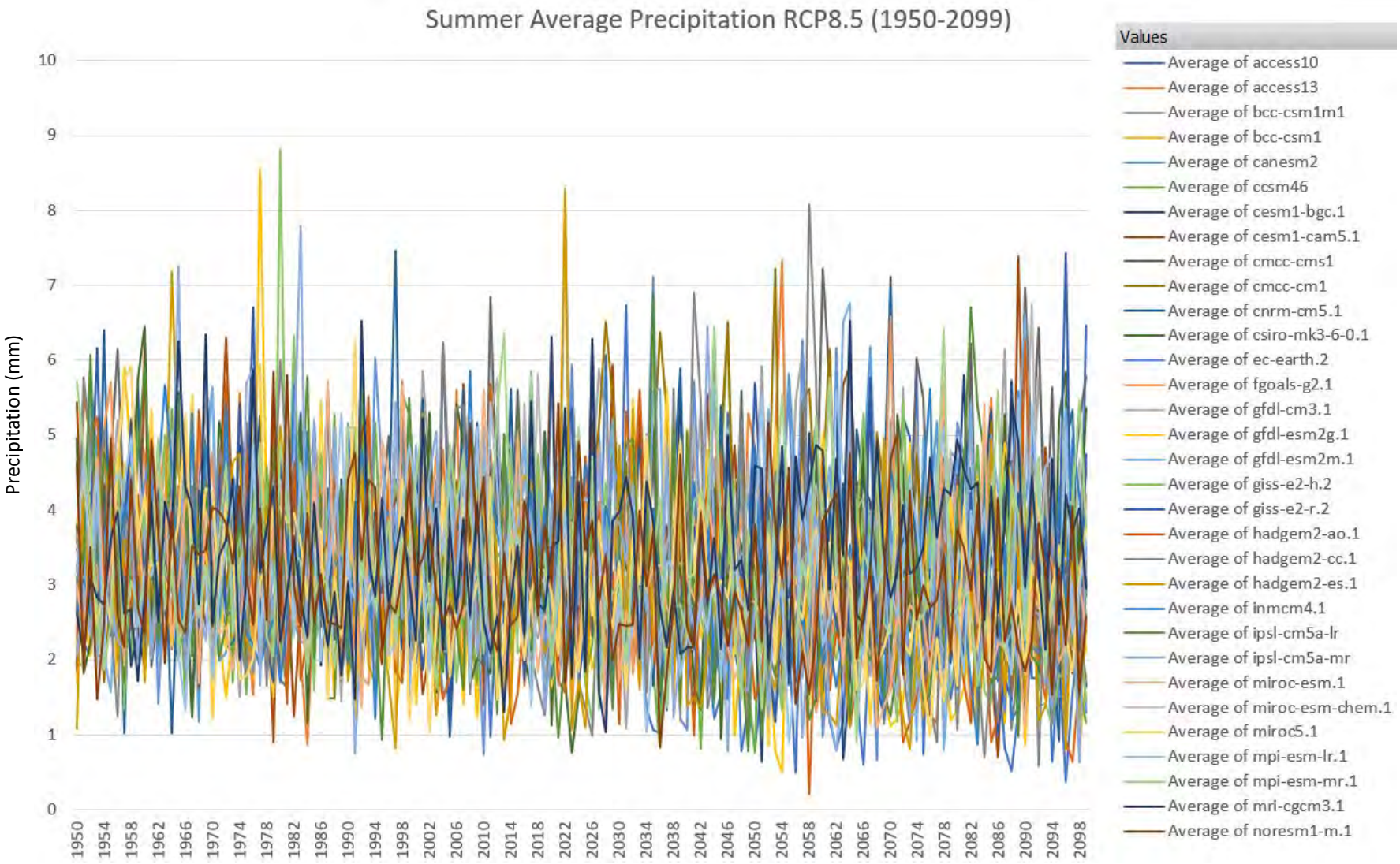

Figure B-6: Summer Average Precipitation RCP 8.5 (1950-2099)

Appendix C: Model Results

The results for each model for each RCP were taken and plotted both individually and as a composite plot. The following sections will discuss the results for the composite plots and trends seen for five individual models. These models were selected based on accuracy compared to observed streamflow data that was used during the calibration process. This dataset ranges from October 1, 1971 to July 8, 2021. Model accuracy was determined using Nash-Sutcliffe efficiency, percent bias, and Root Mean Square Error (RMSE) standard deviation. Using these statistics, the models with the highest performance for RCP 4.5 are ACCESS1-0, ACCESS1-3, CanESM2, CNRM-CM5, and MIROC-ESM.1 and the models with the highest performance for RCP 8.5 are MIROC5.1, MIROC-ESM.1, HadGEM2-AO, FGOALS-g2.1, CCSM46.

To get a better understanding of trends, the yearly average and seasonal averages were taken and plotted for each model and each RCP output.

C.1 RCP 4.5 Composite Results

The RCP 4.5 yearly average streamflow (cfs) results for every model were plotted together to look for trends between models (Figure C-1). There is a high amount of variability between models and it difficult to discern any significant trends. Variability between models increases through the end of the century.

The RCP 4.5 seasonal average streamflow for spring and summer were plotted together to find trends between models during seasons where streamflow due to precipitation is the highest (Figure C-2 and C-3). Similar to the yearly averages, it's difficult to see much of a trend due to significant variability between models and an increase in variability between models through the end of the century. This is the case for both spring and summer.

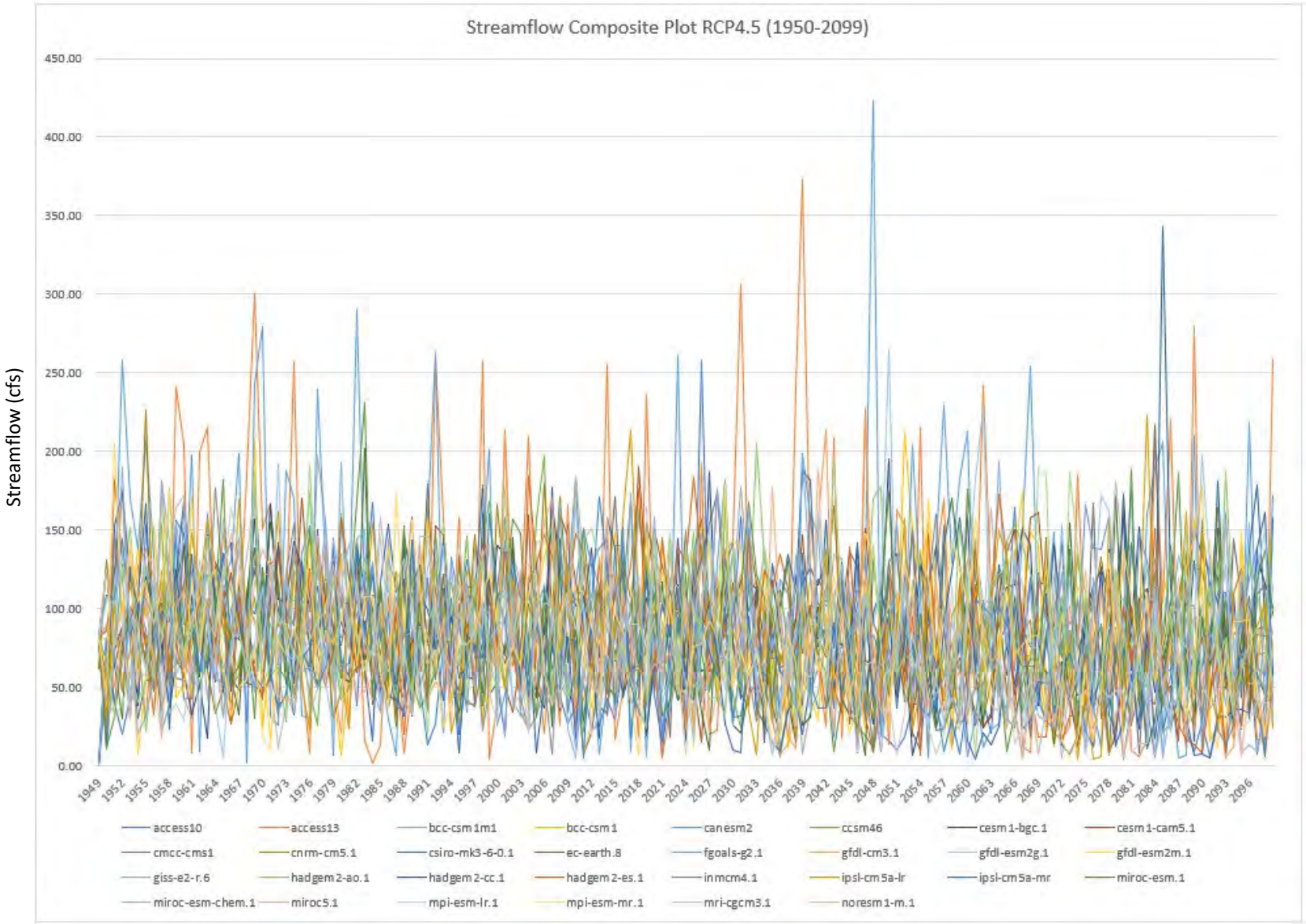

Figure C-1: Streamflow Composite Plot RCP 4.5 (1950-2099)

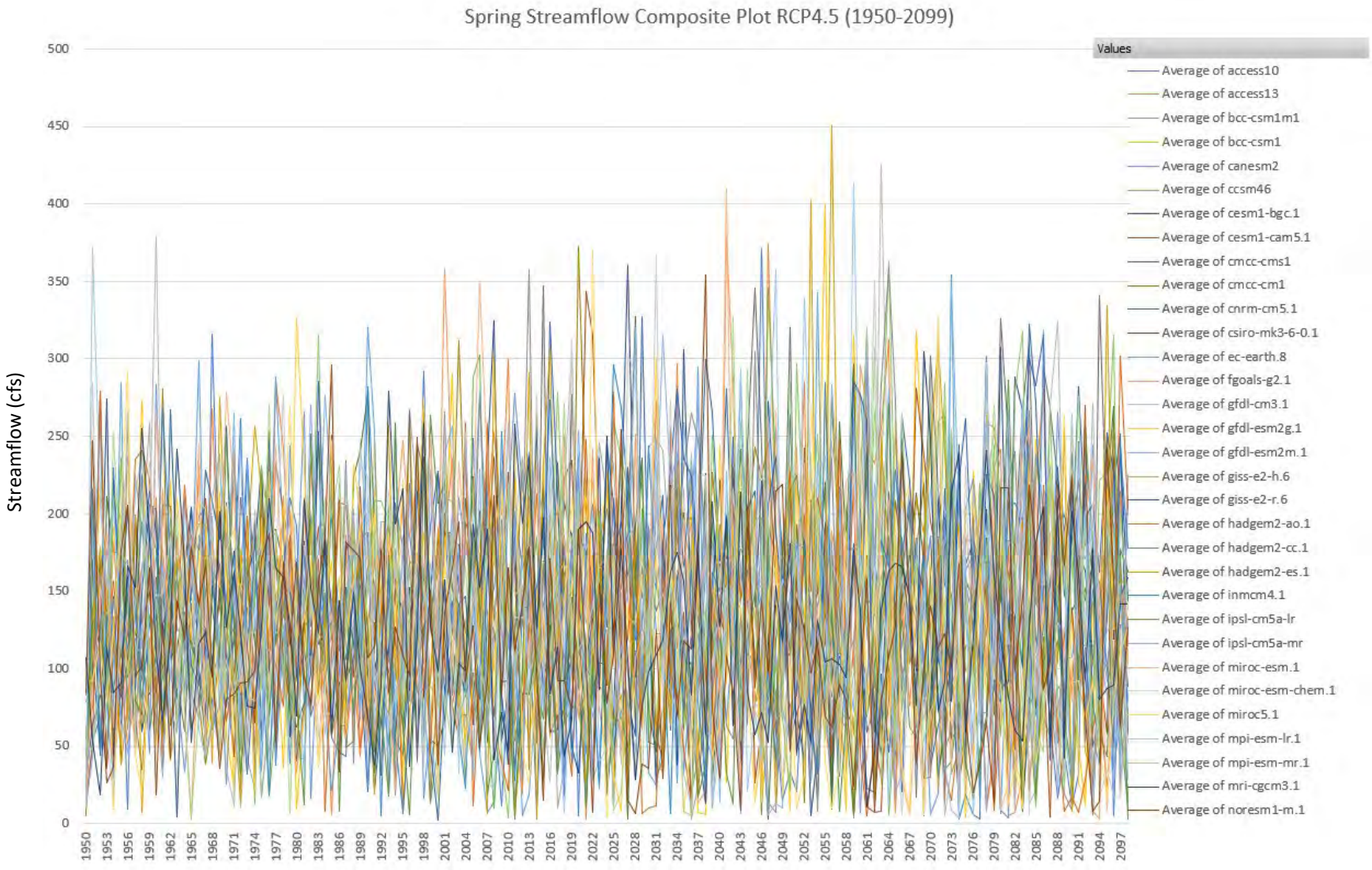

Figure C-2: Spring Streamflow Composite Plot RCP 4.5 (1950-2099)

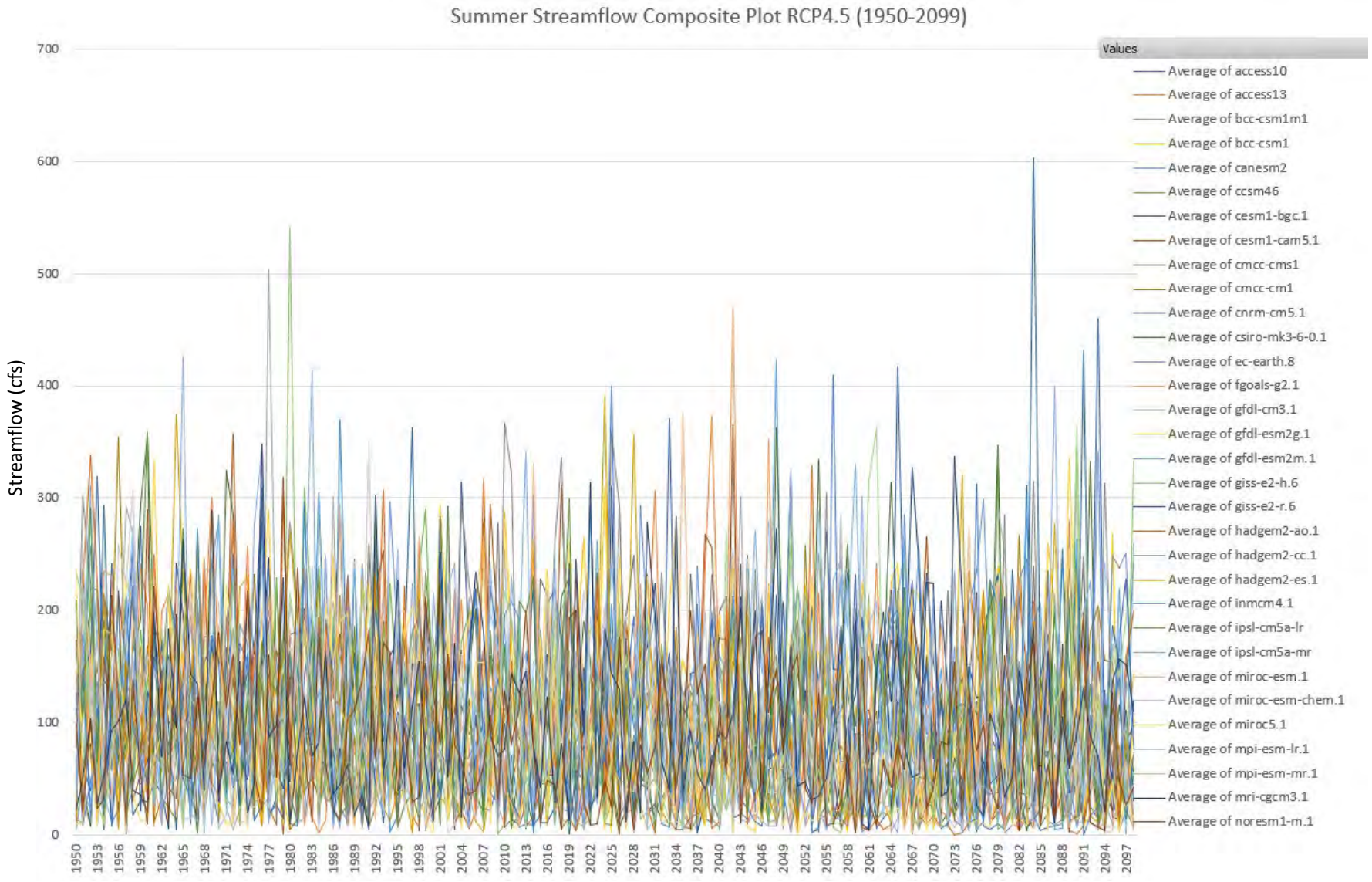

Figure C-3: Summer Streamflow Composite Plot RCP 4.5 (1950-2099)

C.2 RCP 8.5 Composite Results

The RCP 8.5 yearly average streamflow results for every model were plotted together to look for trends between models (Figure C-4). There is a high amount of variability between models and it difficult to discern any significant trends. Variability between models increases through the end of the century.

The RCP 8.5 seasonal average streamflow for spring and summer were plotted together to find trends between models during seasons where streamflow due to precipitation is the highest (Figure C-5 and C-6). For spring, there is a slight increase in streamflow values, however there is still significant variability between models and this variability increases through the end of the century. For summer, it's difficult to see much of a trend due to significant variability between models and an increase in variability between models through the end of the century.

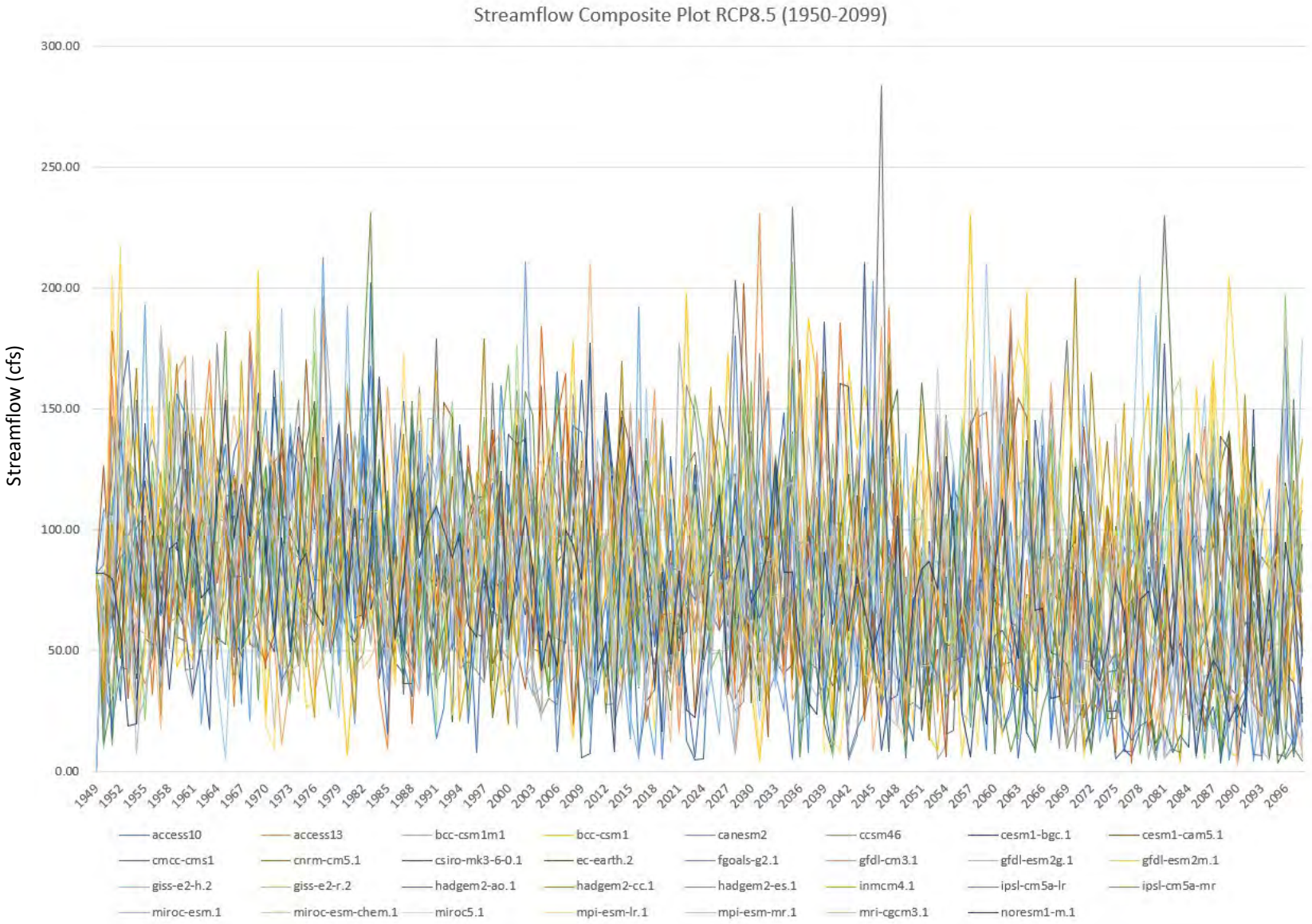

Figure C-4:Streamflow Composite Plot RCP 8.5 (1950-2099)

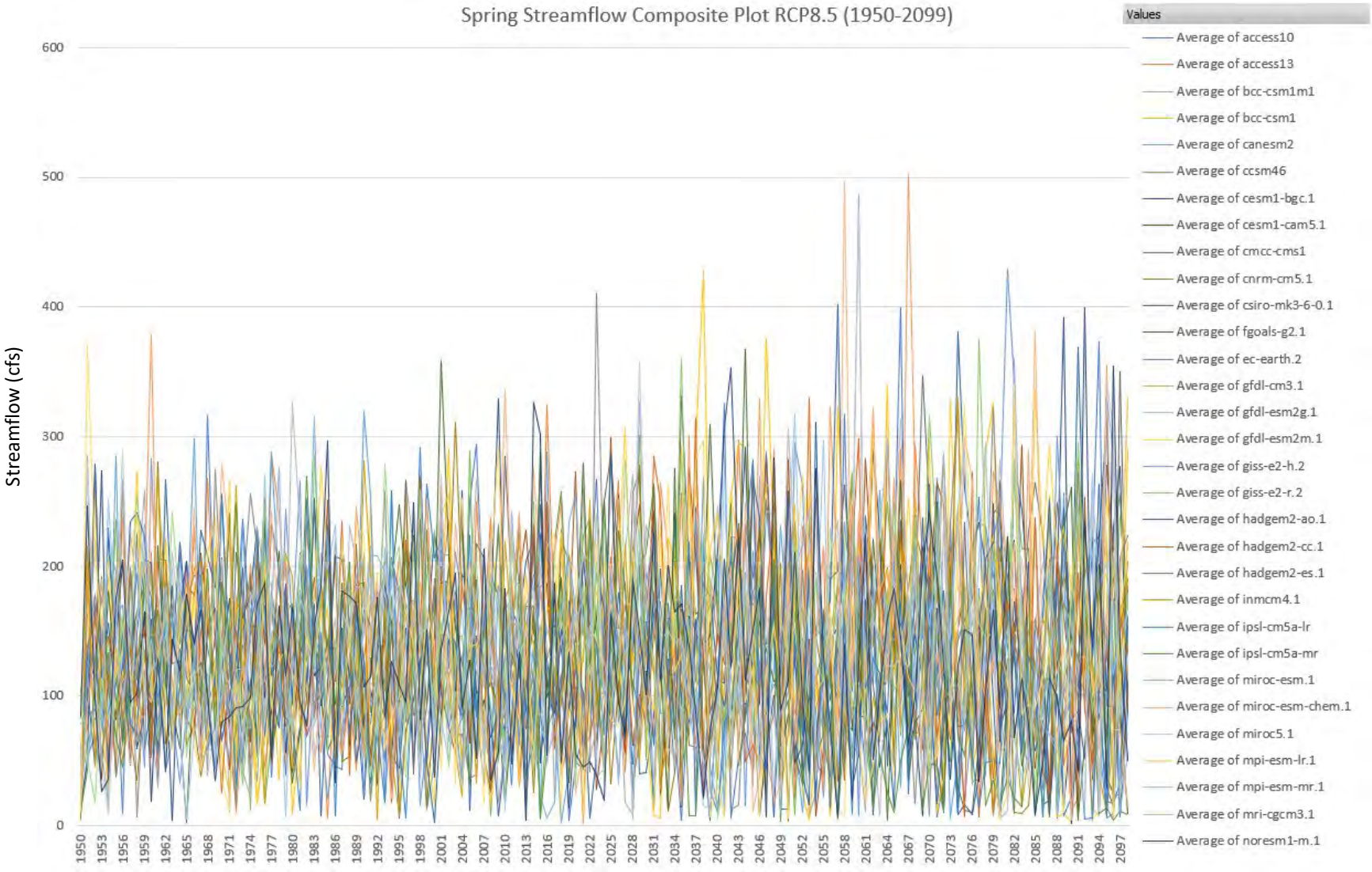

Figure C-5: Spring Streamflow Composite Plot RCP 8.5 (1950-2099)

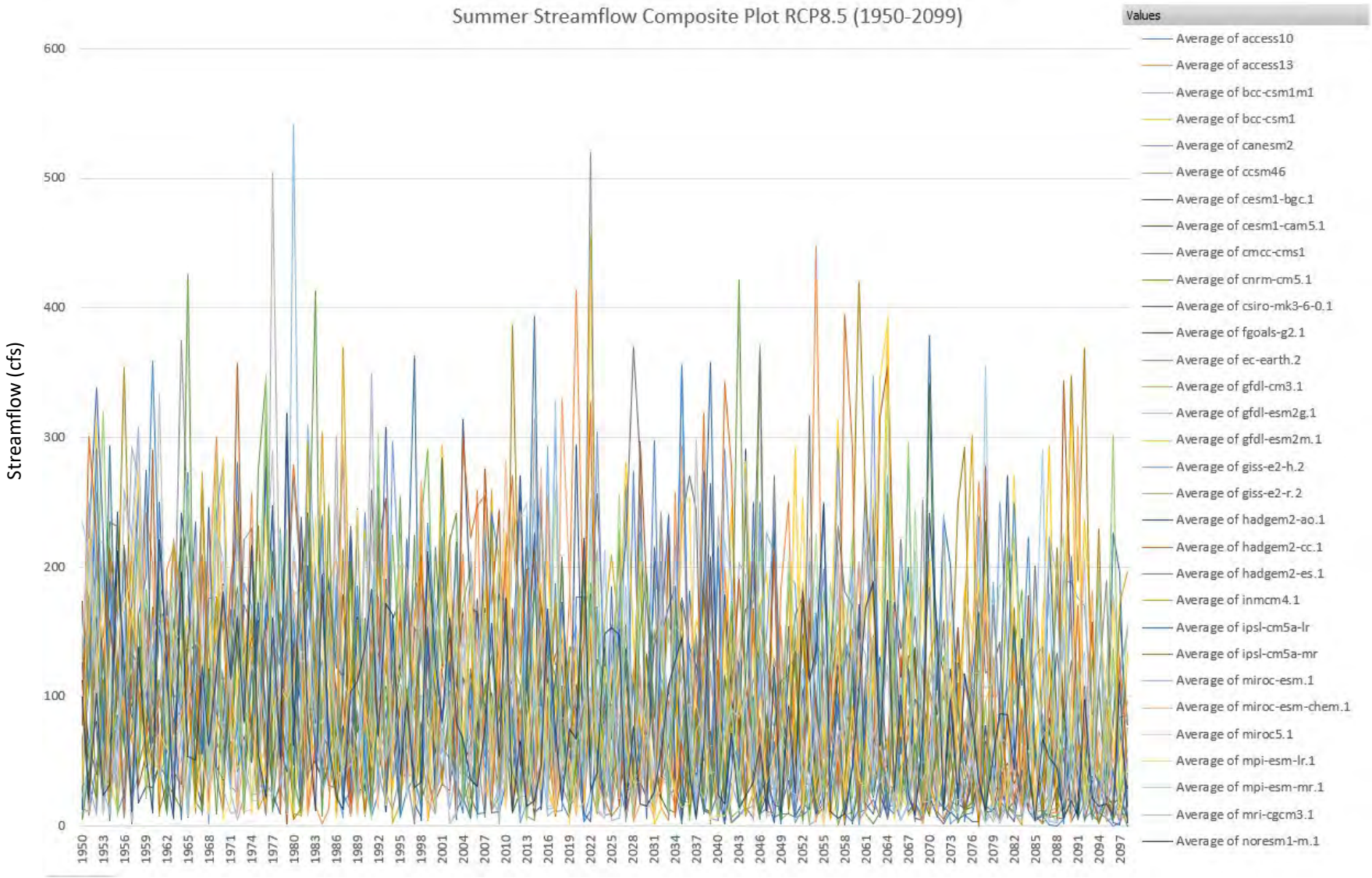

Figure C-6: Summer Streamflow Composite Plot RCP 8.5 (1950-2099)

C.3 RCP 4.5 Individual Model Results

Of the models 32 models, five were selected based on model accuracy, which was determined using Nash-Sutcliffe efficiency, percent bias, and Root Mean Square Error (RMSE) standard deviation. Table C-1 shows these statistics for the five models that were selected for this analysis. The yearly average streamflow results for each model are shown in Figures C-7 through C-11. A majority of these models show a decrease in the streamflow overtime, with the exception being CNRM-CM5.1, which shows a slight increase in average streamflow. These are surprising results considering the precipitation data for these models indicates an increasing trend in yearly average precipitation. To get a better understanding of projected trends, the seasonal averages for spring and summer were also analyzed for these five models in Figures C-13 through C-21.

Table C-1: Nash-Sutcliffe Efficiency, Percent Bias, and RMSE Standard Deviation for the 5 best performing models

Model	RMSE Std Dev	Nash-Sutcliffe	Percent Bias
ACCESS10	1.2	-0.531	14.60%
ACCESS13	1.2	-0.514	18.93%
CANESM2	1.2	-0.501	18.93%
CNRM-CM5.1	1.2	-0.553	22.43%
MIROC-ESM.1	1.3	-0.563	23.23%

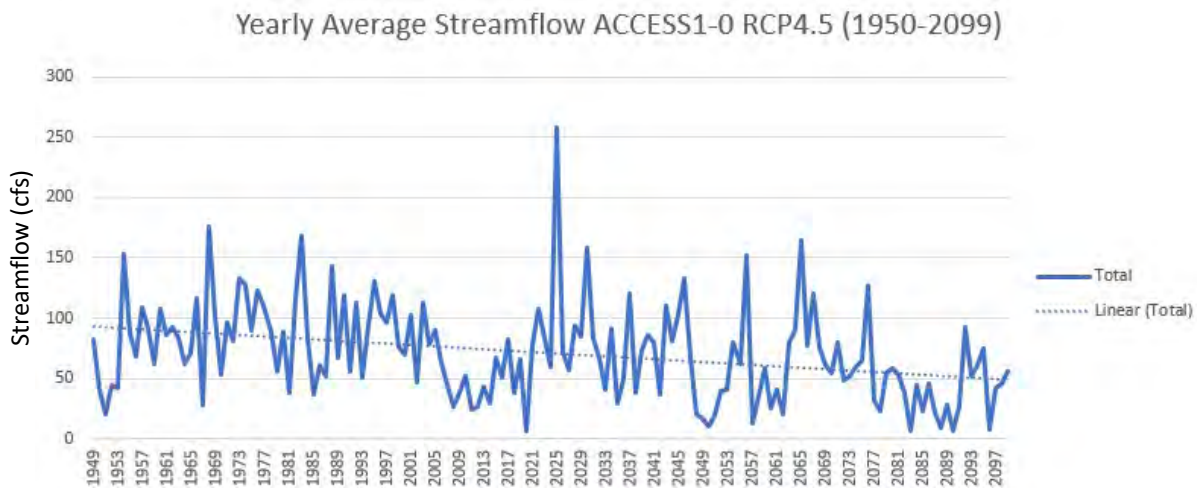

Figure C-7: Yearly Average Streamflow ACCESS1-0 RCP 4.5 (1950-2099)

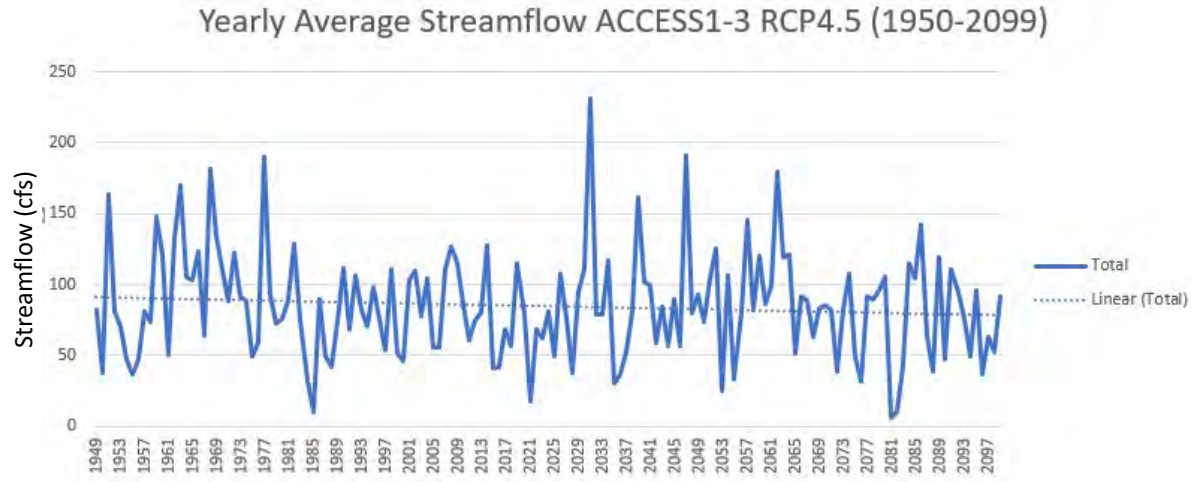

Figure C-8: Yearly Average Streamflow ACCESS1-3 RCP 4.5 (1950-2099)

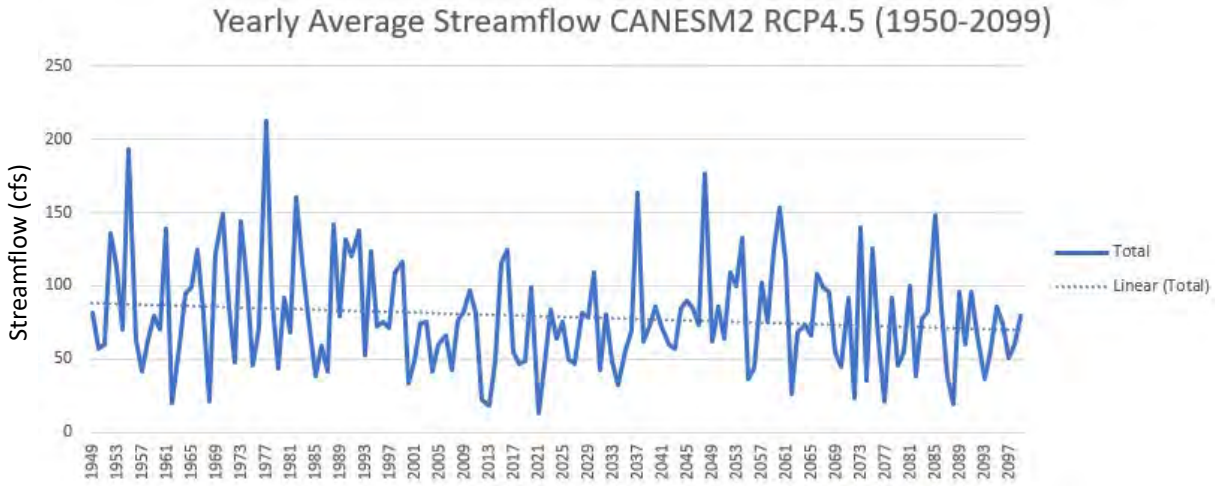

Figure C-9: Yearly Average Streamflow CANESM2 RCP 4.5 (1950-2099)

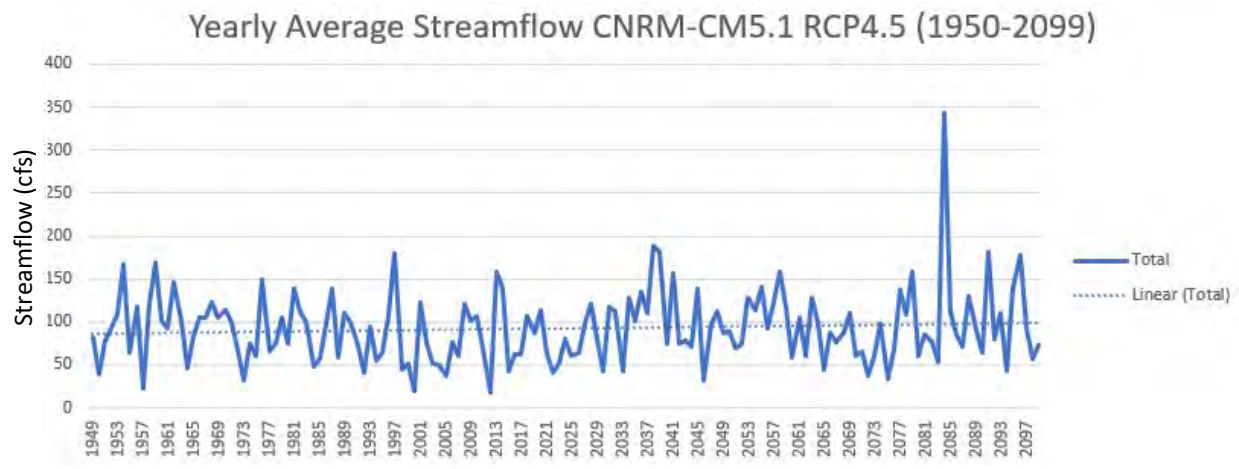

Figure C-10: Yearly Average Streamflow CNRM-CM5.1 RCP 4.5 (1950-2099)

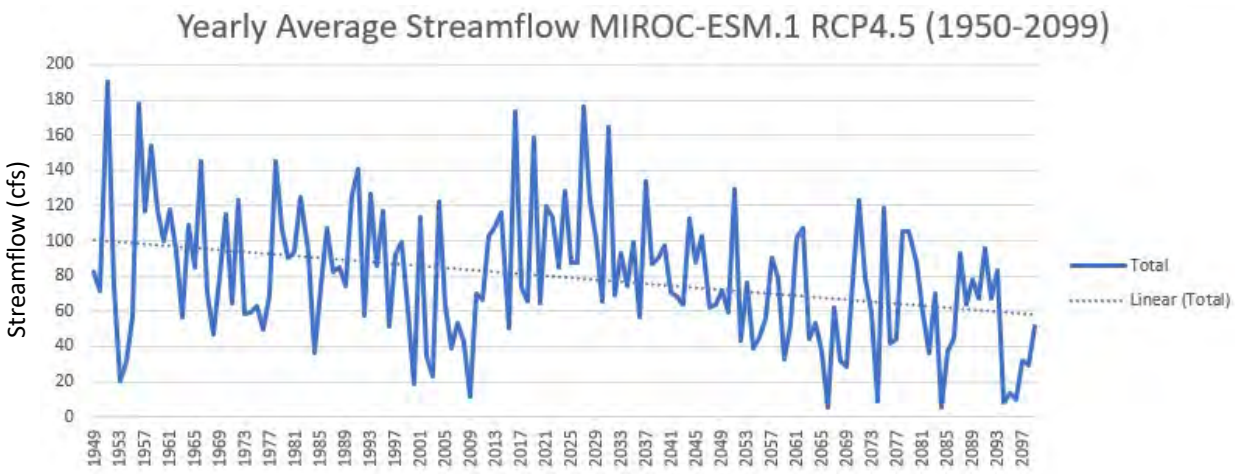

Figure C-11: Yearly Average Streamflow MIROC-ESM.1 RCP 4.5 (1950-2099)

Results vary greatly between model and season. For the spring results, two of the five models show an increase in streamflow, two show a clear decrease in streamflow, and one model doesn't show a significant change. For the summer results, four of the five models show a decrease in streamflow and one model shows an increase. Based on these results this indicates there will most likely be a decrease in streamflow for summer months and there is too much variability in spring months for a clear trend. In general, there is a lot of variability between models and due to uncertainties mentioned in previous sections, it's difficult to determine if these trends are reliable.

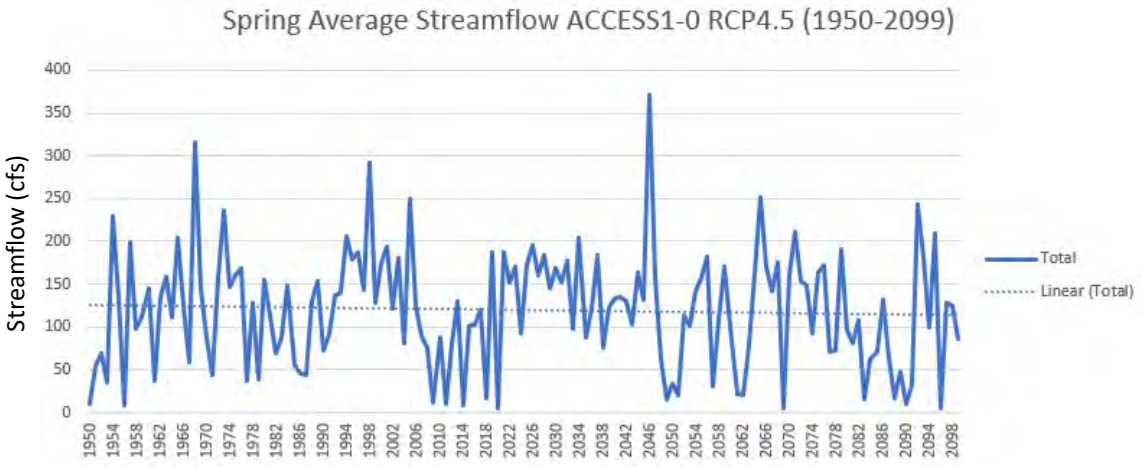

Figure C-12: Spring Average Streamflow ACCES1-0 RCP 4.5 (1950-2099)

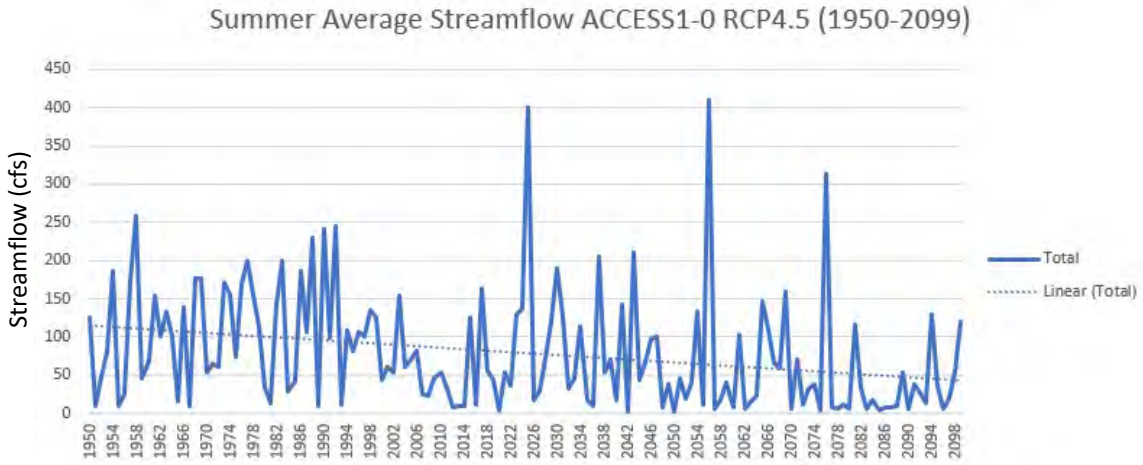

Figure C-13: Summer Average Streamflow ACCES1-0 RCP 4.5 (1950-2099)

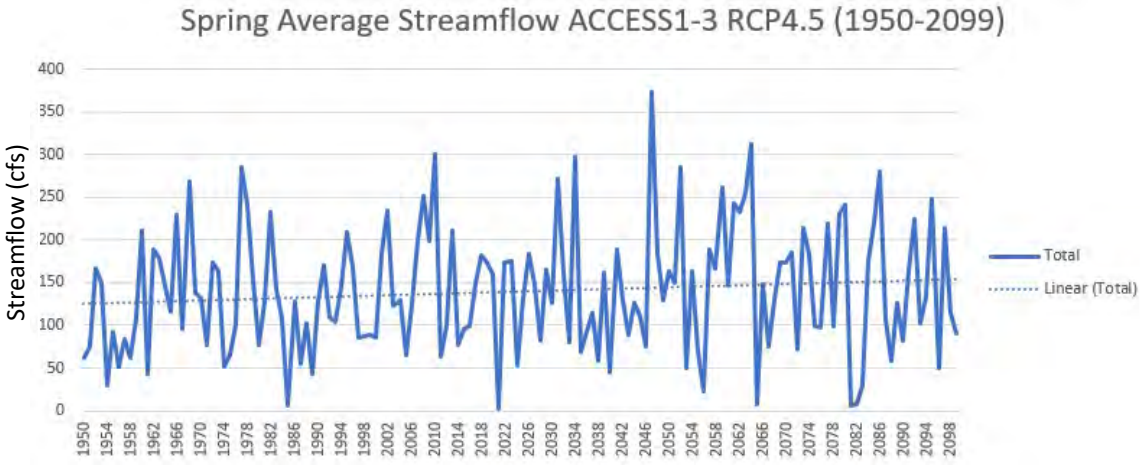

Figure C-14: Spring Average Streamflow ACCESS1-3 RCP 4.5 (1950-2099)

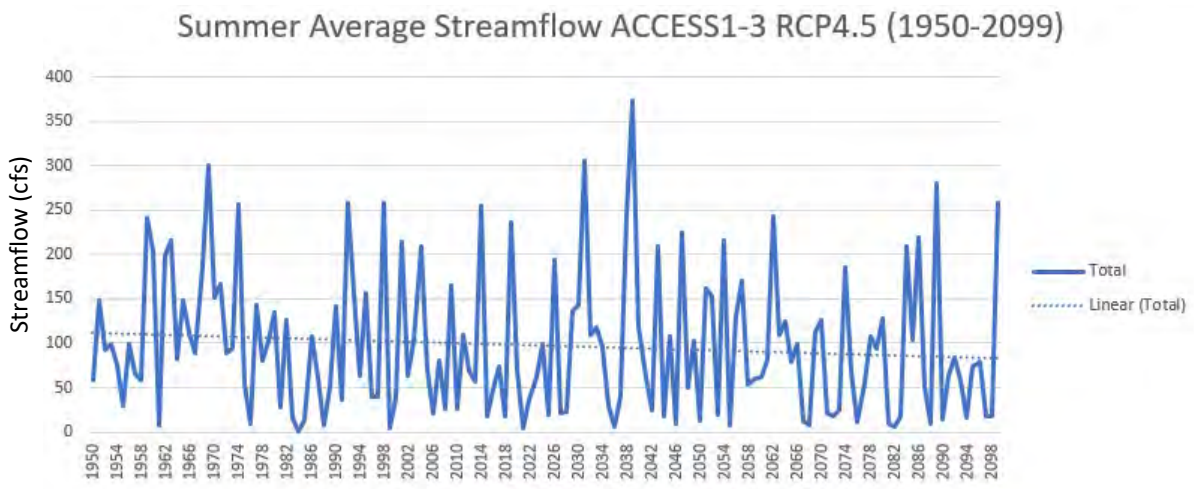

Figure C-15: Summer Average Streamflow ACCES1-3 RCP 4.5 (1950-2099)

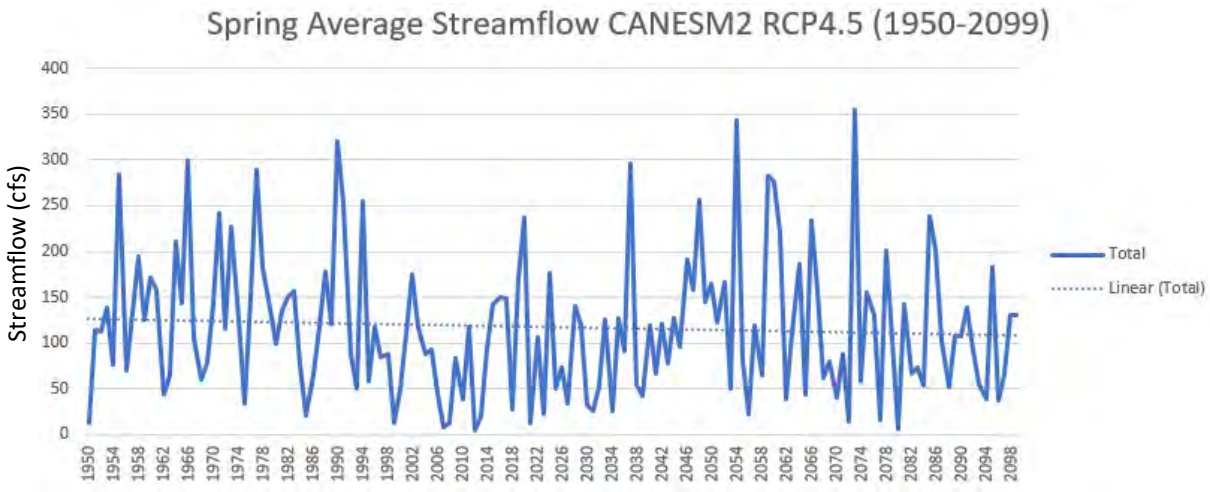

Figure C-16: Spring Average Streamflow CANESM2 RCP 4.5 (1950)

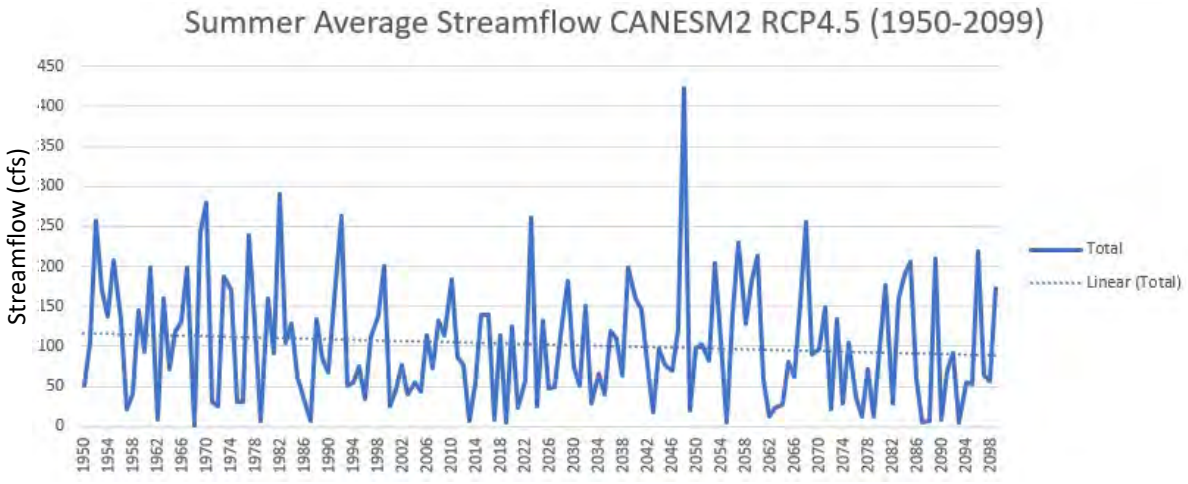

Figure C-17: Summer Average Streamflow CANESM2 RCP 4.5 (1950-2099)

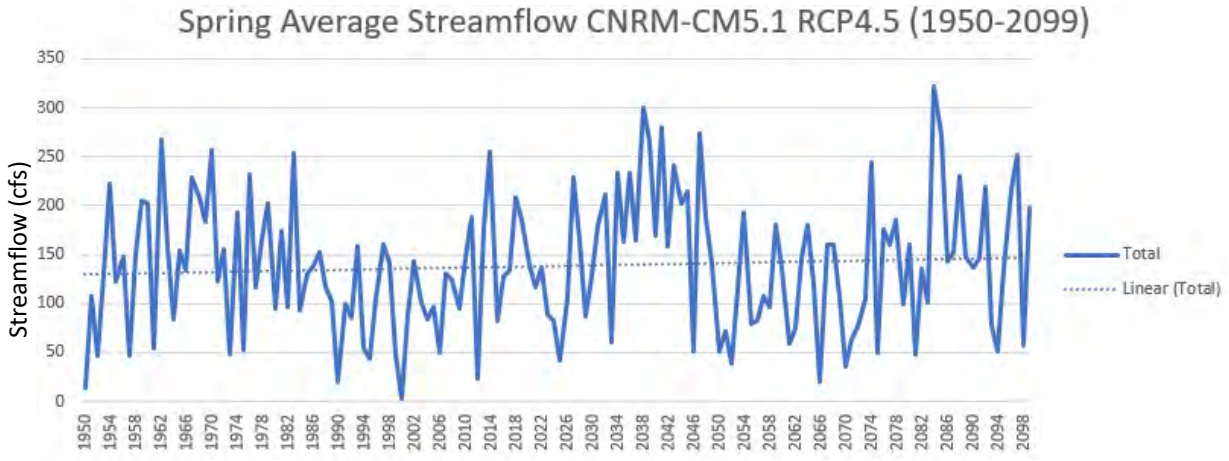

Figure C-18: Spring Average Streamflow CNRM-CM5.1 RCP 4.5 (1950-2099)

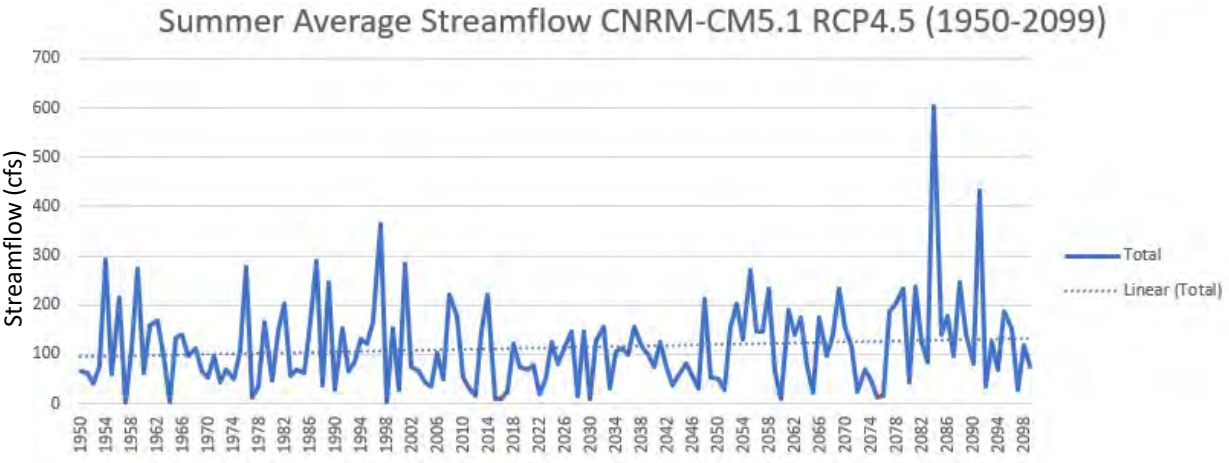

Figure C-19: Summer Average Streamflow CNRM-CM5.1 RCP 4.5 (1950-2099)

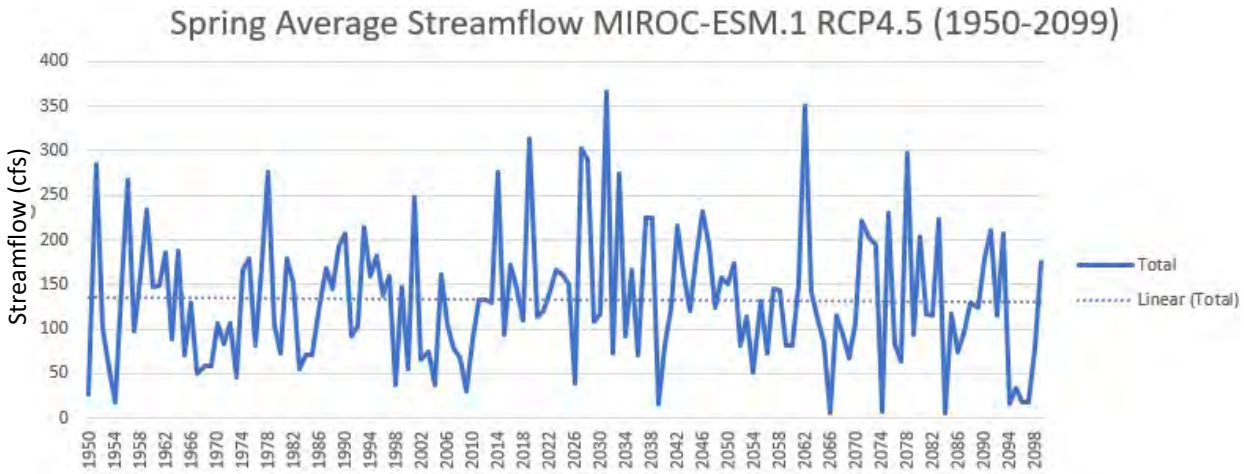

Figure C-20: Spring Average streamflow MIROC-ESM.1 RCP 4.5 (1950-2099)

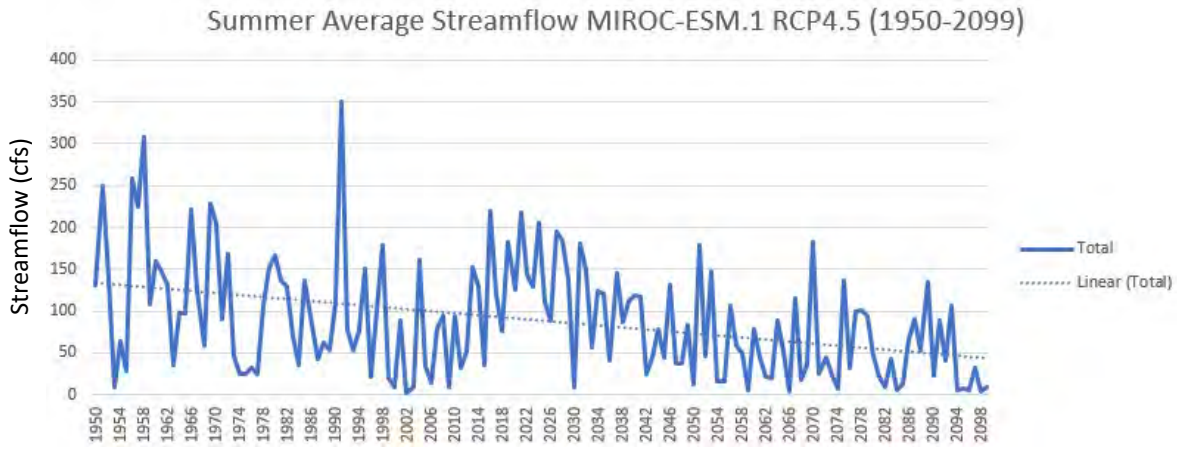

Figure C-21: Summer Average Streamflow MIROC-ESM.1 RCP 4.5 (1950-2099)

C.4 RCP 8.5 Individual Model Results

Of the models 32 models, five were selected based on model accuracy, which was determined using Nash-Sutcliffe efficiency, percent bias, and Root Mean Square Error (RMSE) standard deviation. Table C-2 shows these statistics for the five models that were selected for this analysis. The yearly average streamflow results for each model are shown in Figures C-22 through C-26. All five models show a decrease in the streamflow overtime. These are surprising results considering the precipitation data for these models indicates an increasing trend in yearly average precipitation. To get a better understanding of projected trends, the seasonal averages for spring and summer were also analyzed for these five models in figures C-27 through C-36.

Table C- 2: Nash-Sutcliffe Efficiency, Percent Bias, and RMSE Standard Deviation for the 5 best performing models

Model	RMSE Std Dev	Nash-Sutcliffe	Percent Bias
MIROC5	1.2	-0.516	19.85%
MIROC-ESM.1	1.2	-0.521	20.95%
HADGEM2-AO.1	1.3	-0.577	19.99%
FGOALS-G2	1.3	-0.574	21.71%
CCSM4.6	1.3	-0.57	21.94%

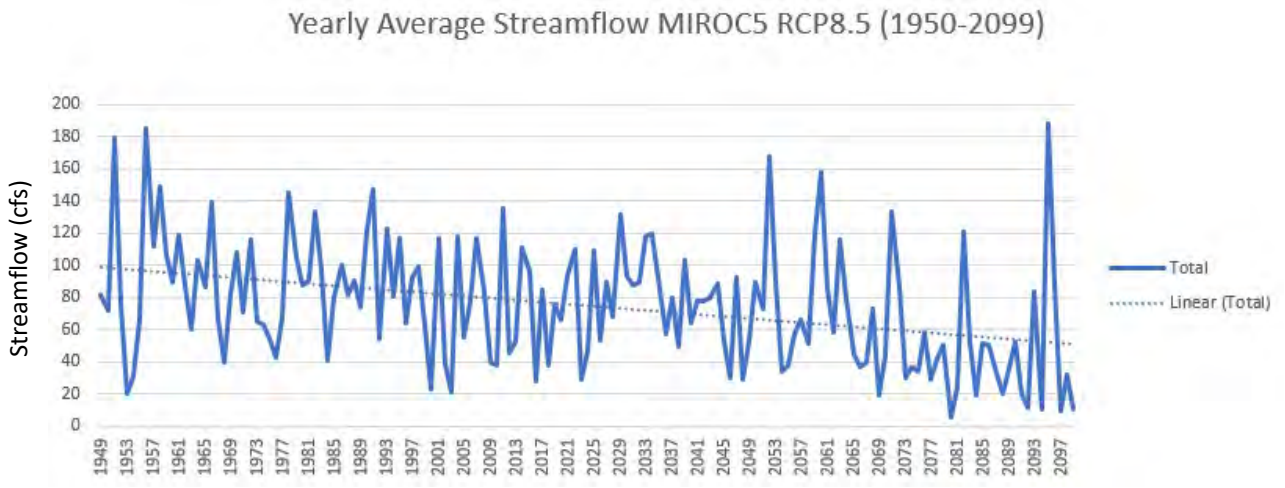

Figure C-22: Yearly Average Streamflow MIROC5 RCP 8.5 (19850-2099)

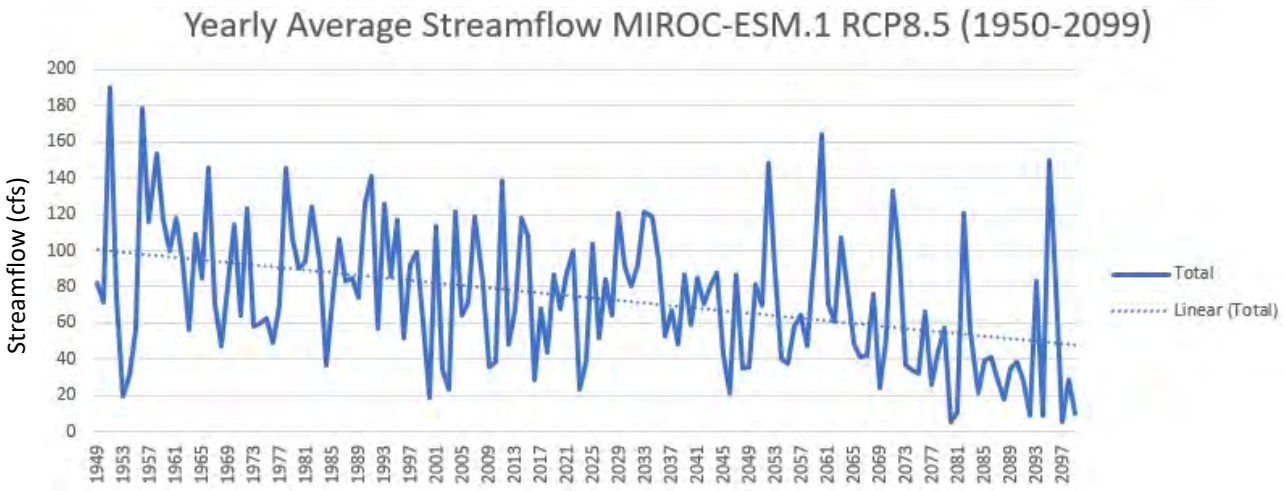

Figure C-23: Yearly Average Streamflow MIROC-ESM.1 RCP 8.5 (1950-2099)

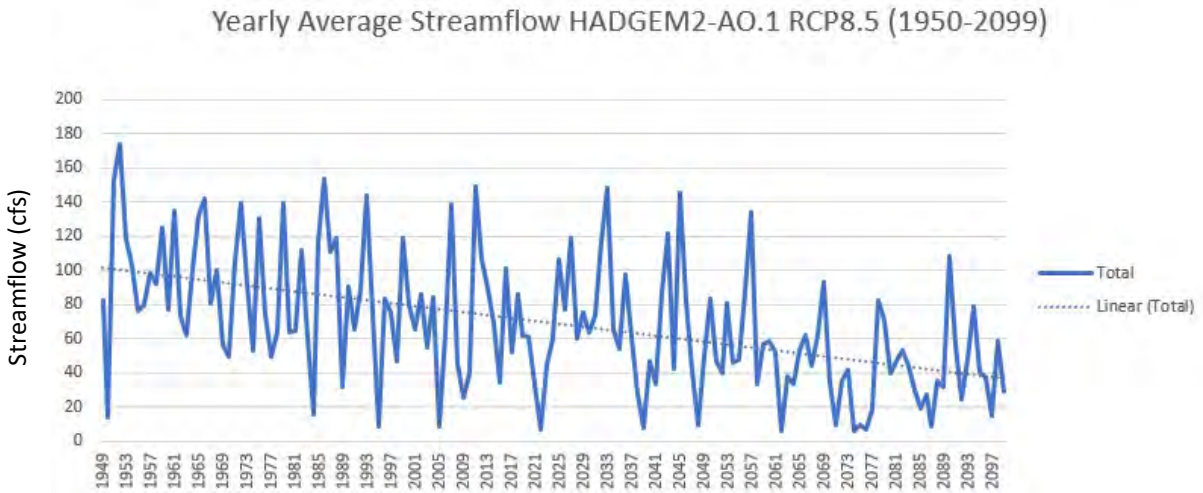

Figure C-24: Yearly Average Streamflow HADGEM2-AO.1 RCP 8.5 (1950-2099)

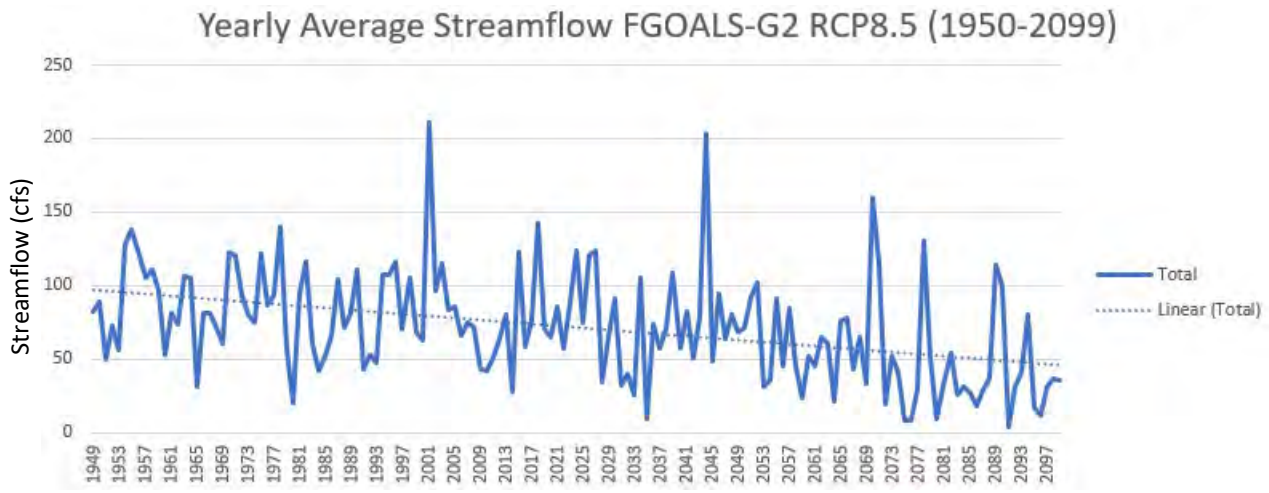

Figure C-25: Yearly Average Streamflow FGOALS-G2 RCP 8.5 (1950-2099)

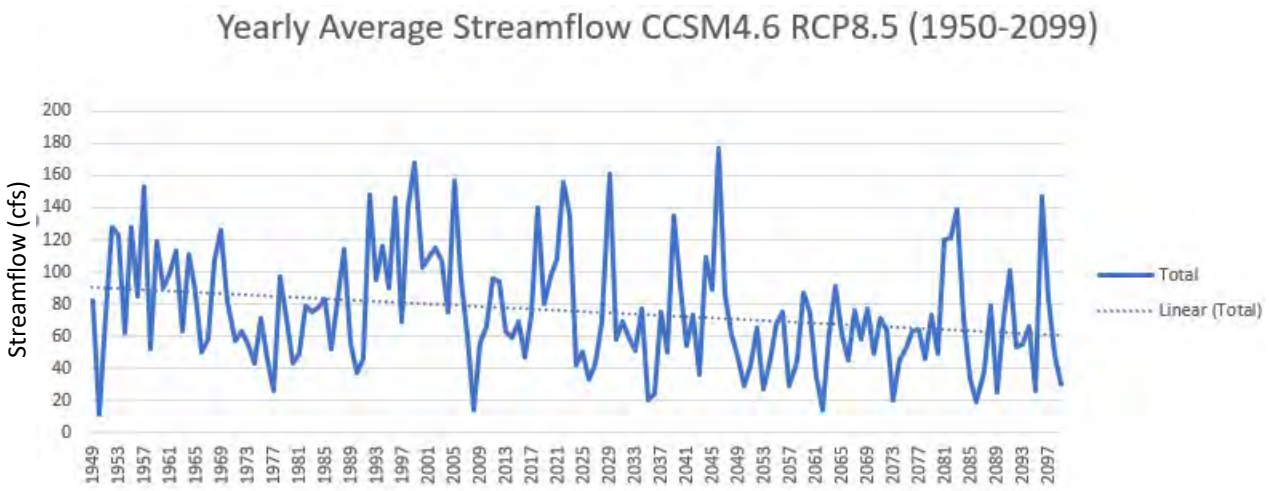

Figure C-26: Yearly Average Streamflow CCSM4.6 RCP 8.5 (1950-2099)

Results vary greatly between model and season. For the spring results, two of the five models show an increase in streamflow, one shows a clear decrease in streamflow, and two models don't show a significant change. For the summer results, all five models show a decrease in streamflow. Based on these results this indicates there will most likely be a decrease in streamflow for summer months and there is too much variability in spring months for a clear trend. In general, there is a lot of variability between models and due to uncertainties mentioned in previous sections, it's difficult to determine if these trends are reliable.

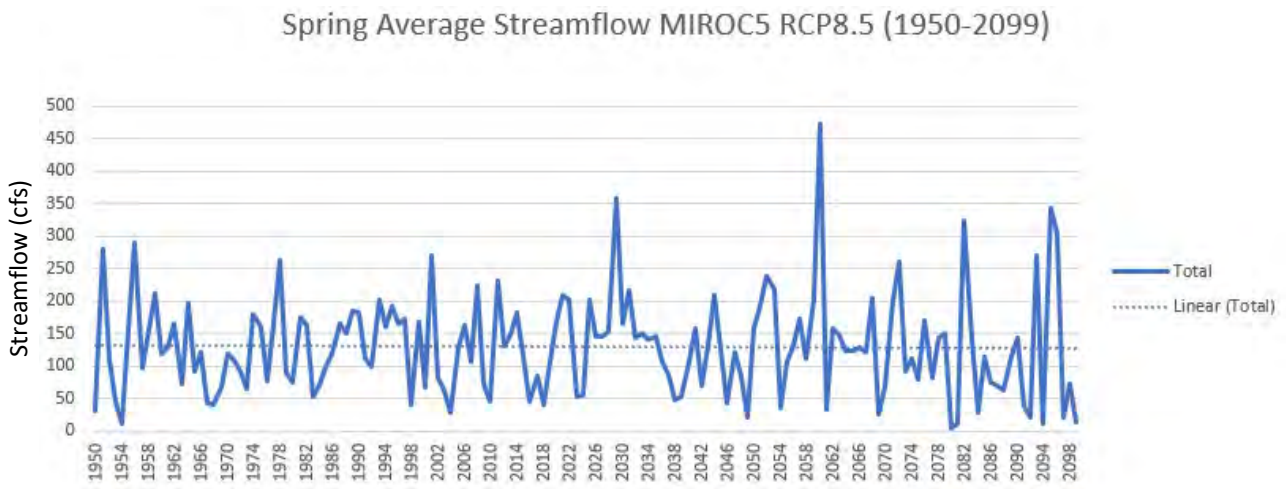

Figure C-27: Spring Average Streamflow MIROC5 RCP 8.5 (1950-2099)

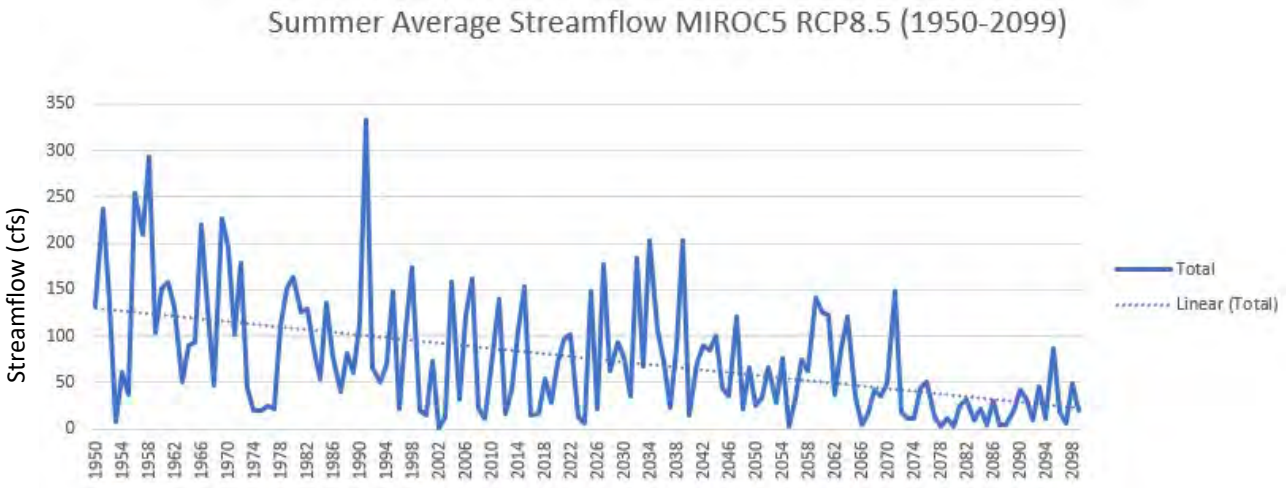

Figure C-28: Summer Average Streamflow MIROC5 RCP 8.5 (1950-2099)

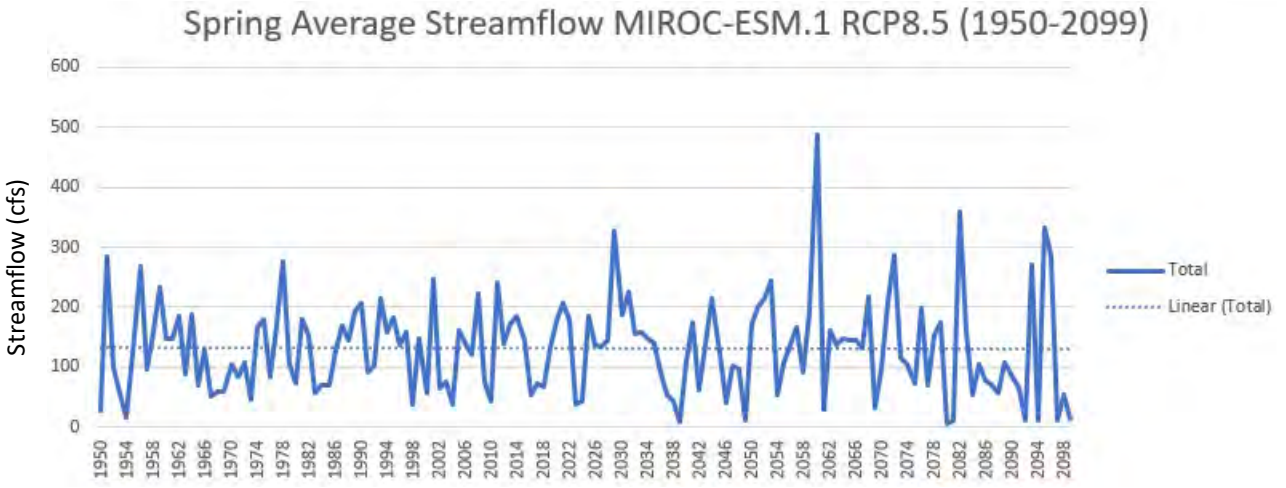

Figure C-29: Spring Average Streamflow MIROC-ESM.1 RCP 8.5 (1950-2099)

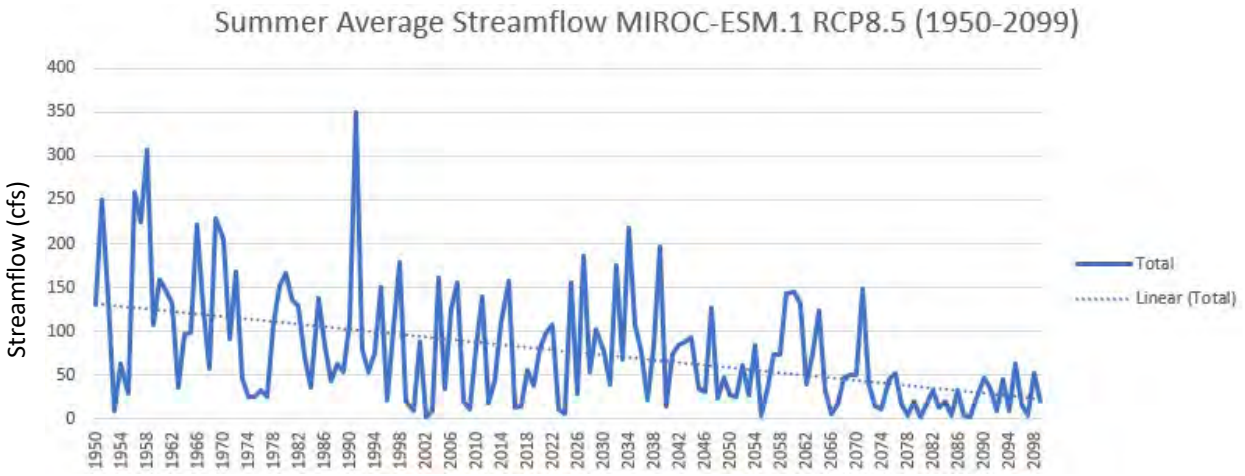

Figure C-30: Summer Average Streamflow MIROC-ESM.1 RCP 8.5 (1950-2099)

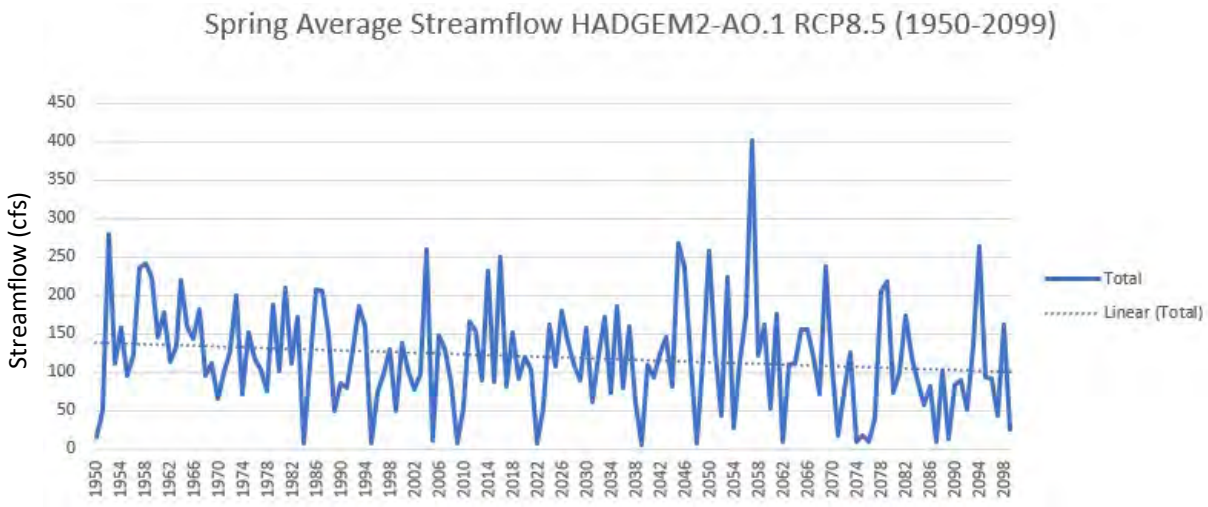

Figure C-31: Spring Average Streamflow HADGEM2-AO.1 RCP 8.5 (1950-2099)

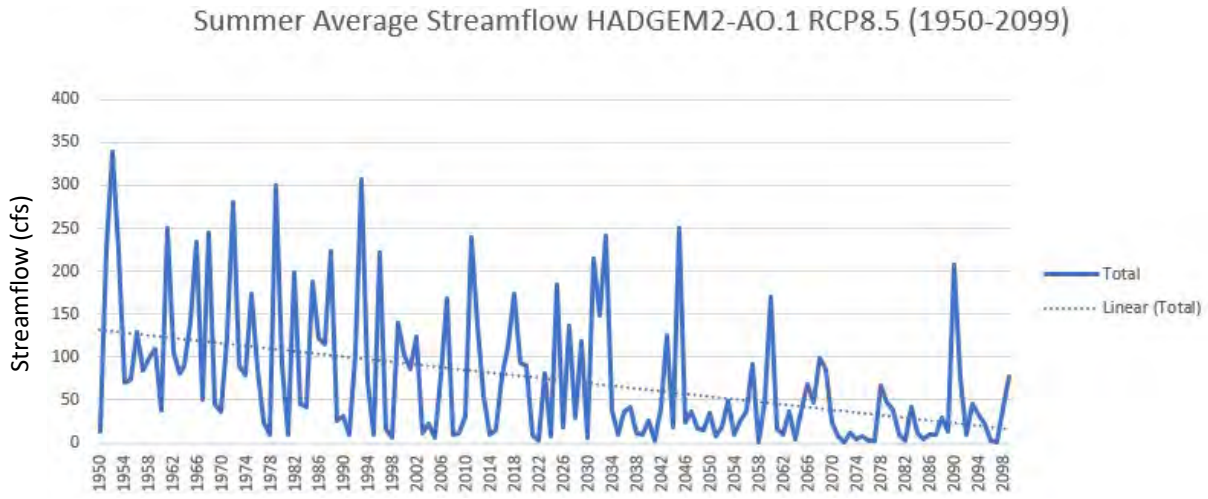

Figure C-32: Summer Average Streamflow HADGEM2-AO.1 RCP 8.5 (1950-2099)

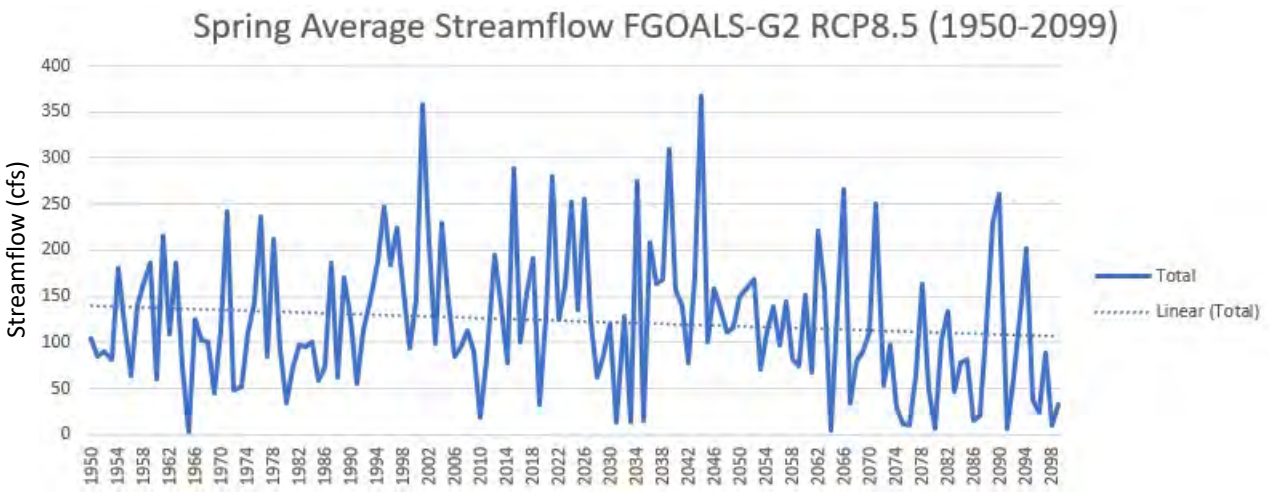

Figure C-33: Spring Average Streamflow FGOALS-G2 RCP 8.5 (1950-2099)

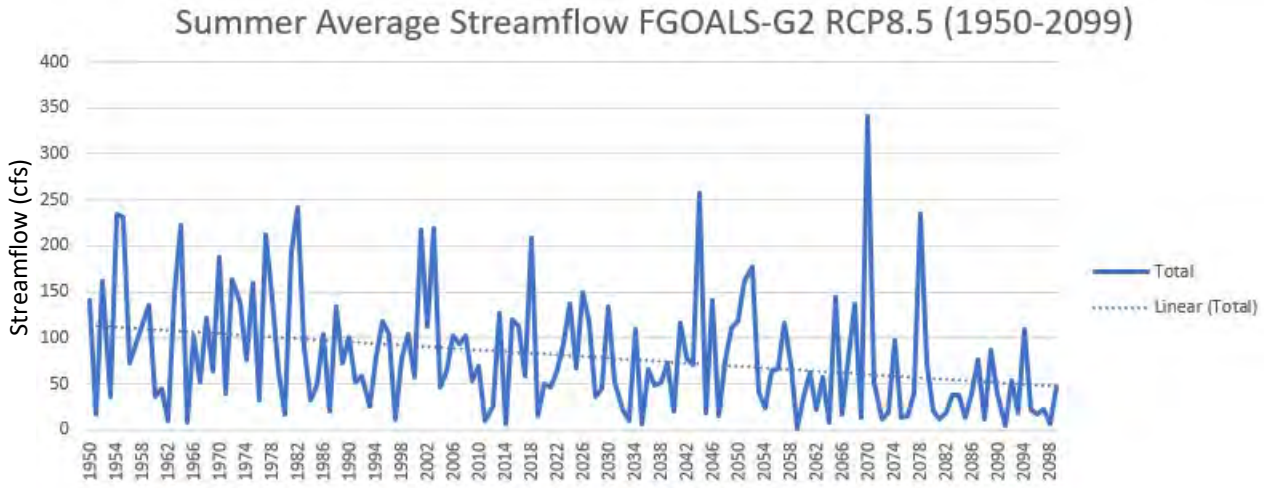

Figure C-34: Summer Average Streamflow FGOALS-G2 RCP 8.5 (1950-2099)

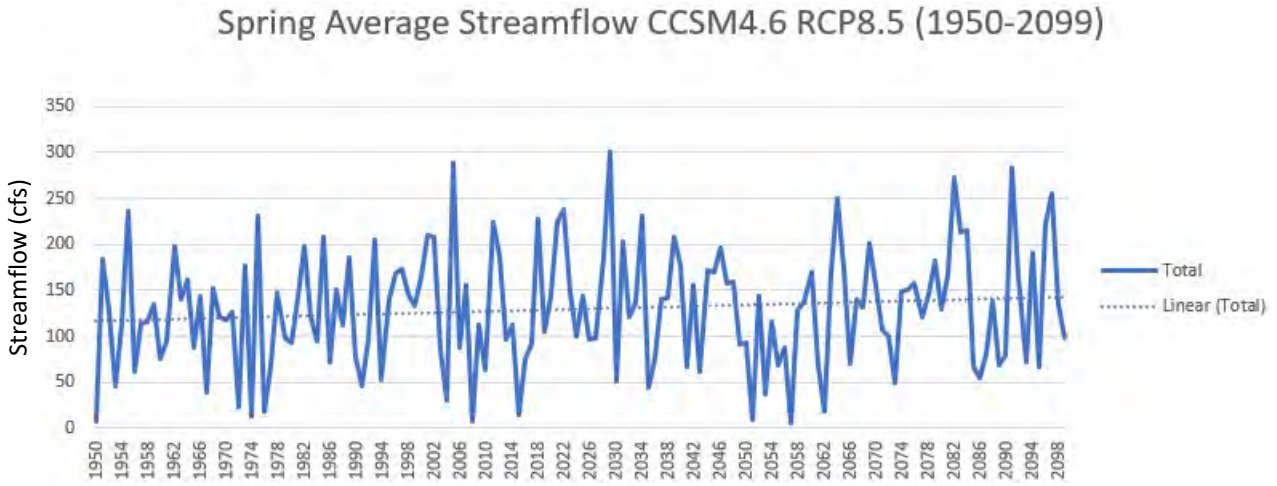

Figure C-4: Spring Average Streamflow CCSM4.6 RCP 8.5 (1950-2099)

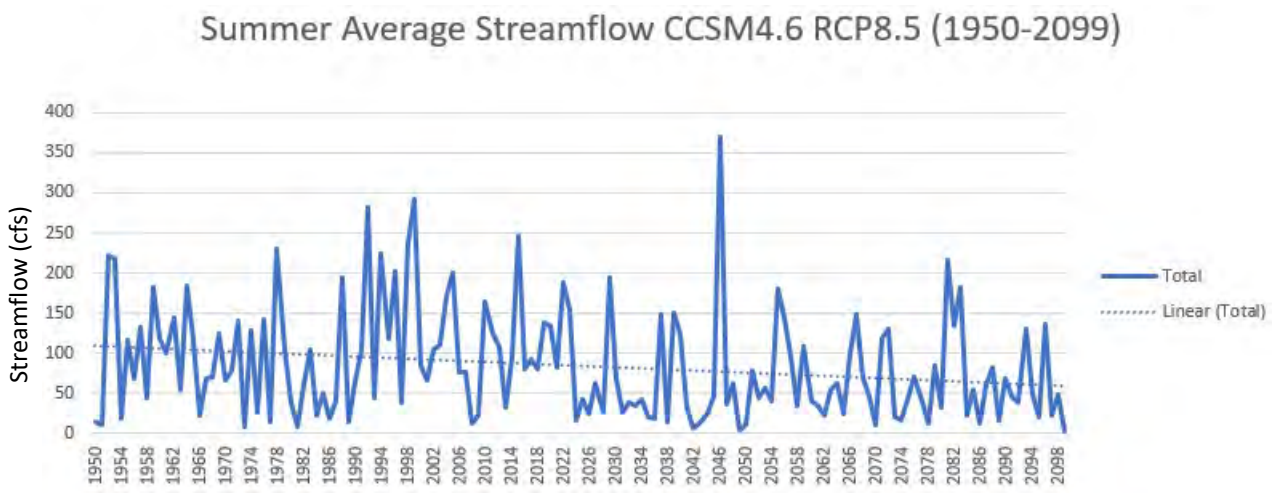

Figure C-5: Summer Average Streamflow CCSM4.6 RCP 8.5 (1950-2099)